INVESTIGATIONS OF SPONTANEOUS PAIN AND MODULATION WITH SPINAL CORD STIMULATION

A Dissertation
Presented to
The Academic Faculty

By

Shaquia L. Idlett-Ali

In Partial Fulfillment
of the Requirements for the Degree
Doctor of Philosophy in the
Wallace H. Coulter Department of Biomedical Engineering

Georgia Institute of Technology

May 2020

INVESTIGATIONS OF SPONTANEOUS PAIN AND MODULATION WITH SPINAL CORD STIMULATION

Approved by:

Dr. Shawn Hochman, Advisor
Department of Physiology
Emory University School of Medicine

Dr. Robert Butera
School of Electrical and Computer Engineering
Department of Biomedical Engineering
Georgia Institute of Technology and Emory University School of Medicine

Dr. Lena Ting
Department of Biomedical Engineering
Georgia Institute of Technology and Emory University School of Medicine

Dr. Sandra Garraway
Department of Physiology
Emory University School of Medicine

Dr. Timothy Cope
School of Biological Sciences
Department of Biomedical Engineering
Georgia Institute of Technology and Emory University School of Medicine

Date Approved: March 23, 2020

My mission in life is not merely to survive, but to thrive; and to do so with some passion, some compassion, some humor, and some style

Maya Angelou

To Hisham, Saleem, and Kai the Pitty

ACKNOWLEDGEMENTS

I would first like to thank my advisor Dr. Shawn Hochman. It has been an honor to work with and learn from you. I firmly believe that my scientific development and confidence grew to new levels under your support and guidance. Thank you for your dedication, time, and willingness to foster my independent curiosity.

To Mike, Mallika, Makalele, and Drs. Michael McKinnon, Heidi Kloefkorn, and Celia Li of the Hochman Lab, you all are awesome and helped make the difficult reality of academic research feel less isolating. I could not imagine having better colleagues and consider you to be great friends.

To my thesis committee members: Drs. Robert Butera, Lena Ting, Tim Cope, and Sandra Garraway, thank you for your commitment to me and the betterment of my work. Thank you for creating space for discussions of my work and my professional goals anytime Ive asked. Additionally, I would like to thank Dr. Garraway, Dr. Donald Noble and Karmarcha for helping to expand my sphere of knowledge in surgical techniques and behavioral assays of pain in contusion rodent models. Chapter 2 of my dissertation would not have been possible without you.

To Pamela Idlett, my mom, you are the most resilient and determined person I have ever met. It is a privilege to have been raised by you and to continue to witness all the ways you are amazing. You are my inspiration.

To Hisham Ali, my husband, I love you with all of my heart and I am so glad we found each other. You are brilliant, dedicated, and kind. Thank you for the sacrifices you have made and will make in the future for the benefit of me and our family. Thank you for the

all-nighter to help me compile my dissertation. Thank you for leaving in a pandemic to find a tripod for my remote defense. Thank you for supporting my sometimes-crazy goals and helping me attain them. Thank you for always working to find a way in no way situations. You are some of the things I am and a lot of the things I am not. I am lucky to have you and so is Saleem.

This work was supported by the National Science Foundation Graduate Research Fellowship Grant (DGE-1650044), the National Institutes of Health Computational Neuroscience Training Grant (5T90DA032466), Boston Scientific Neuromodulation, and the Alfred P. Sloan Foundation. Thank you.

TABLE OF CONTENTS

LIST OF TABLES

LIST OF FIGURES

LIST OF ABBREVIATIONS

(a)CSF (artificial) cerebrospinal fluid

4-AP 4-aminopyridine

5-HT serotonin, 5-hydroxytryptamine

BIC bicuculline

CNS central nervous system

CPP conditioned place preference

CRPS complex regional pain syndrome

CV conduction velocity

DC dorsal column

DH dorsal horn

DLF dorsal lateral funiculus

DR dorsal root

DREZ dorsal root entry zone

DRG dorsal root ganglia

DRP dorsal root potential

DRR dorsal root reflex

EF electric field

EFP extracellular field potential

FBSS failed back surgery syndrome

FEM finite element model

FFT fast Fourier transform

GABA gamma aminobutyric acid

Kv voltage gated potassium channel

LT Lissauers Tract

LTMR low threshold mechanoreceptor

LTP Long-term potentiation

MoT motor threshold

Nav voltage gated sodium channel

NS nociceptive specific projection neuron

PAD primary afferent depolarization

PNI peripheral nerve injury

PSDC postsynaptic dorsal column tract cells

PWT paw withdrawal threshold

REM rapid eye movement

RR respiratory rate

RRV respiratory rate variability

SA spontaneously active

SC spinal cord

SC-DRG spinal cord-dorsal root ganglia preparation

SCI spinal cord injury

SCS spinal cord stimulation

$\mathbf{T}_{DC}$ dorsal column threshold

$\mathbf{T}_{DR}$ dorsal root threshold

TTX tetrodotoxin

VR ventral root

WDR wide dynamic range projection neuron

SUMMARY

Chronic pain is the leading cause of long-term disability. It is a condition that affects the quality of life for its sufferers because it is frequently comorbid with anxiety, depression, and sleep deprivation. Heterogeneity in etiology and manifestation of neuropathic pain contribute to difficulties finding broadly effective pain management strategies. In cases where pharmacological treatment has failed to provide relief, epidural spinal cord stimulation (SCS) has emerged as an alternative intervention for intractable pain. This technology has been in clinical use for over 50 years, yet efficacy rates have remained stagnant and etiology-dependent. A barrier to improved efficacy is an absence of knowledge identifying the mechanism by which SCS can selectively inhibit chronic, spontaneous pain. The gate control theory presents a theoretical framework of the therapy's mechanism of action, but the true mechanisms remain unclear. This is further complicated by the absence of spontaneous pain models and metrics for quantifying them.

The objective of this dissertation was to generate knowledge that leads to a better understanding of both spontaneous neuropathic pain and SCS pain relief. To do this, I first establish links between spontaneous sensory hyperexcitability and stimulus-independent physio-behavioral indices of pain, using a contusion model of spinal cord injury (SCI). I hypothesized that greater spontaneous primary afferent activity would be observed in the SCI model of neuropathic pain, and that it would occur alongside development of respiratory and sleep dysfunction. My results identify functional shifts in sleep, respiration and sensory function after SCI. Next, I used an ex vivo adult mouse spinal cord preparation to assess axonal recruitment with SCS. A computational model was utilized to inform parameter selection for examining clinically-analogous SCS with our model system. I hypothesized that dorsal column and dorsal root axons would be recruited at the same threshold—indicative of Aβ axons being the first recruited population with SCS. These experiments successfully

characterized the recruitment thresholds for afferents in the lumbar dorsal column, dorsal roots, and Lissauer's tract. A key finding was that the lowest threshold DC axons are not primary afferent collaterals, but possibly postsynaptic dorsal column tract cell. Finally, I tested the gate control theory by examining SCS modulation in *ex vivo* model of spontaneous pain. For these studies, I extended the spinal cord preparation to include intact dorsal root ganglia from multiple lumbar segments and characterized spontaneous activity in primary afferents and spinal nociceptive circuits. I hypothesized that SCS would reduce spontaneous activity in nociceptive circuitry during, and after SCS. Results indicated that antidromic afferent recruitment was not sufficient to replicate prolonged modulation of spontaneous nociceptive activity with SCS.

Together, these findings provide greater insight into the development and identification of spontaneous neuropathic pain and the underlying mechanisms leading to pain relief with SCS.

CHAPTER 1
INTRODUCTION

Spinal cord stimulation **(SCS)** is a form of electrical neuromodulation implemented to alleviate neuropathic pain resistant to traditional methods of treatment. Though it has been in clinical use for over 40 years, we still lack critical understanding of how it induces pain relief [1][2]. This lack of understanding has been identified as a contributor to its limited improvement in efficacy[2][3], which has resulted in the development of various preclinical studies aiming to expand knowledge of its underlying mechanisms of action[4][2]. The goal of this dissertation is to delineate how axonal recruitment with SCS contributes to modulation of spontaneous activity in the spinal cord. Below, I first describe the classification and organization of afferents in the dorsal spinal cord, to lay a foundation for understanding the potential source of aberrant sensory signaling and the potential targets of SCS. Next, I present clinical and preclinical evidence demonstrating the role of peripheral and spinal sensory circuit hyperexcitability in the development of chronic pain, with emphasis on spontaneous activity. I then describe the clinical application of SCS as a therapeutic for neuropathic pain, followed by a summary of preclinical studies contributing to our current understanding of its mechanism of action. I close this chapter with a discussion of remaining limitations and knowledge gaps relevant to the field; and include an outline of aims designed to address these limitations and gaps.

1.1 Organization of Afferents in the Dorsal Spinal Cord

The spinal cord is the locus of transition between the peripheral and central nervous systems. Primary afferents of the peripheral nervous system transmit somatosensory information about the state of our body and our environment to the spinal cord. These incoming sensory signals are then processed in the spinal cord and transmitted to the brain via

higher-order neurons and afferents. Neural processing at the cortical region of the brain gives meaning to the peripheral stimuli, as the Morse cord of neuronal spiking is translated to perceptions such as temperature, touch, and pain and their associated location of occurrence. The output of cortical processing permits interactions with our environment by initiating signals transmitted to the ventral spinal cord by pathways including direct descending corticospinal efferents. Activation of ventral neurons elicit a motor response by exciting or inhibiting an effector, such as a muscle cell.

While the spinal cord is typically regarded as a critical relay center of incoming sensory and outgoing motor information to and from the brain, it also serves as integrative center capable of modifying sensory encoding and as a processing center that permits rapid responsive interactions that generate the various reflex motor responses. Dysfunction of primary afferents and their consequent actions in neuronal circuits in the spinal cord have been associated with various etiologies of chronic pain, thus serving as a target for therapeutic interventions. Understanding the potential mechanisms underlying the effects of such therapeutics requires knowledge of the system organization and function along with understanding of the aberrant shifts that occur following injury or disease.

1.1.1 Peripheral branches of primary afferents

Primary afferents are the first-order neurons of sensory processing. These pseudo-unipolar cells have specialized dendrites called nerve endings that selectively transduce mechanical, chemical, or thermal information from its receptive field. The collective cell bodies of primary afferents from peripheral nerves within a dermatome, a specific cutaneous region of the body **(see Figure 1.1)** , reside in a single dorsal root ganglion **(DRG)** and have axons that travel to the spinal cord via the dorsal root **(DR)** of a segmental spinal nerve ([5]; **see Figure 1.2**) . This organization is conserved across the 8 cervical, 12 thoracic, 5 lumbar, and 5 sacral spinal cord segments.

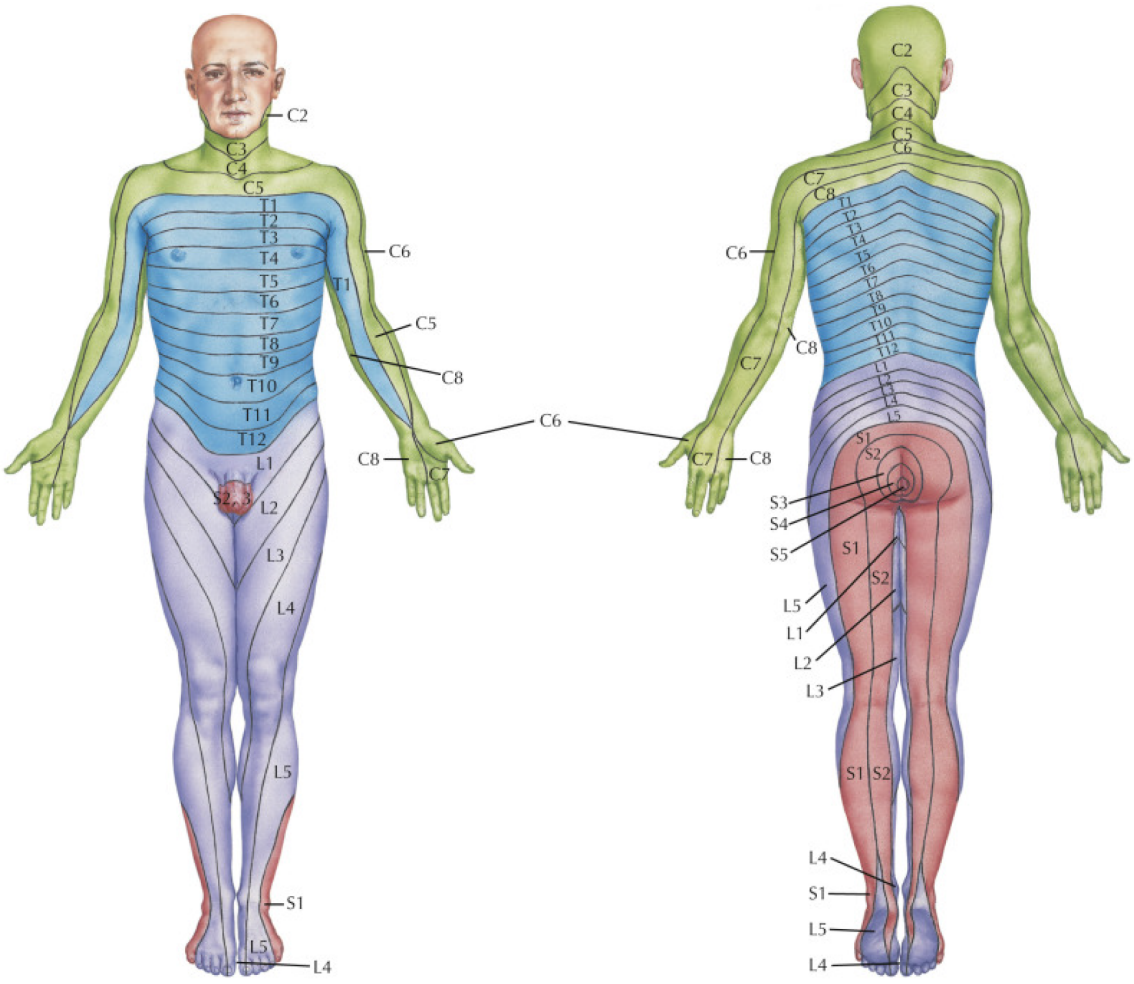

Figure 1.1: Somatotopic diagram of dermatomes and associated spinal nerves.

A dermatome is a cutaneous region of the body that receives sensory innervation from primary afferents residing in a single segmental dorsal root. Cervical roots innervate regions the arms, neck, and head. Thoracic roots innervation regions of the arms and trunk. Lumbar and sacral roots innervate regions of the lower back and legs. Figure from: Felten 2016 [5].

Perceptual discrimination of stimulus-types, such as the difference between pressure and pain, is aided by the division of somatosensory transduction across different classes of afferents. Cutaneous primary afferents have historically been classified by their axon diameter and degree of myelination (i.e. speed of impulse conduction) along with their functional specialization (i.e. the type of stimuli producing activation). The main classifications are myelinated A fibers (Aα, Aβ, Aδ–in decreasing order of myelination) and unmyelinated C fibers. Large diameter, densely myelinated Aα/β fibers have the fastest

conduction of the cutaneous afferents, with speeds $>$ 17 m/s, in rats [6]. While these fibers are typically unimodal low-threshold mechanoreceptors **(LTMRs)** transducing proprioceptive and mechanosensitive information about the body, a portion of fibers have been identified with Aβ conduction speeds yet transduce noxious (i.e. painful) stimuli [7]. Thinly myelinated, smaller diameter Aδ fibers have speeds ranging from 1.8-17 m/s [6], and transduce both noxious and innocuous stimuli from touch, temperature, and pain modalities. Unmyelinated, small diameter C fibers can be unimodal or polymodal in their transduction of noxious stimuli, with 0.3-1.3 m/s conduction speeds [6]. Aδ and C fibers transmitting noxious information from the periphery are called nociceptors. Though nociceptors comprise a large portion of fibers with Aδ and C conduction speeds, recent work has identified the presence of Aδ-LTMR and C-LTMR transmitting non-noxious mechanical information to the spinal cord [7][8][9][10]. The heterogeneity of sensory fiber functions surpasses the complexity of conduction speed-based classifications, thus molecular/genetic markers of afferent subclasses has been the focus of recent work and has enable selective targeting for imaging and identification using genetically-encoded fluorescent markers and optogenetic and chemogenetic approaches to control their activity [7].

1.1.2 Dorsal axon tracts

Primary afferents from one dermatome enter the spinal cord through a single segmental DR. Upon entering the cord, the axon trifurcates with one branch terminating in the dorsal horn of the spinal segment and the other branches entering a dorsal axon tract, projecting axon collaterals to the dorsal horn of spinal segments rostral and caudal to the segment of entry. Short range projections of C fibers and long-range projections of Aδ fibers travel to other segments via Lissauers tract **(LT)**. While LT consists mostly of C fibers traveling one segment rostral and caudal to the site of entry, it also contains Aδ collaterals projecting up to 7 segments rostral [11], and the axons of interneurons. LT laterally borders the dorsal column **(DC)** of the medial lemniscus pathway (see **Figure 1.2**).

The DC is a collection of ascending afferents transmitting proprioceptive and mechanosensitive information to the dorsal column nuclei of the brainstem; eventually leading to encoding and perception at the sensory cortex. While this tract consists mostly of collaterals from Aα and Aβ fibers, it also contains visceral C fibers and the axons of neurons with cell bodies in the dorsal horn called postsynaptic dorsal column tract cells **(PSDCs)** [12][13][14][15][16]. PSDCs are mostly located in lumbar and cervical regions of the spinal cord [13]. These cells receive multi-convergent synaptic inputs from various primary afferents and account for 30% of cells projecting to the gracile nucleus of the brainstem [17][13]. Interestingly, anatomical studies suggest that these cells also have intraspinal axon collaterals located in the same dorsal horn as their cell bodies, indicating a possible role in altering sensory processing at the spinal cord.

The DC is smallest at sacral segments and gets larger when more axons enter the tract at lumbar, thoracic, and cervical regions. Branches of Aα/β fibers are shifted medially in the DC as they ascend and join branches from other spinal segments **(see Figure 1.3)**. This attributes to the somatotopic organization of the DC in rostral spinal cord regions. In the cervical cord, the lateral cuneate fascicle transmits information from the neck, arms, and upper trunk while the medial gracile fascicle sends signals from the lower trunk and legs [18]. Recent evidence suggests that the receptive field-based somatotopic map model co-exists, with a modality-specific segregation of ascending DC afferents. In the modality-based organization, long-range mechanoreceptors project medially in the DC while shorter-range proprioceptors project laterally [19]. Studies also indicate that as Aα/β fibers ascend in the dorsal column, their conduction speed decreases with each subsequent collateralization of rostral spinal segments [20][21]; suggesting an associated decrease in axon diameter with each bifurcation.

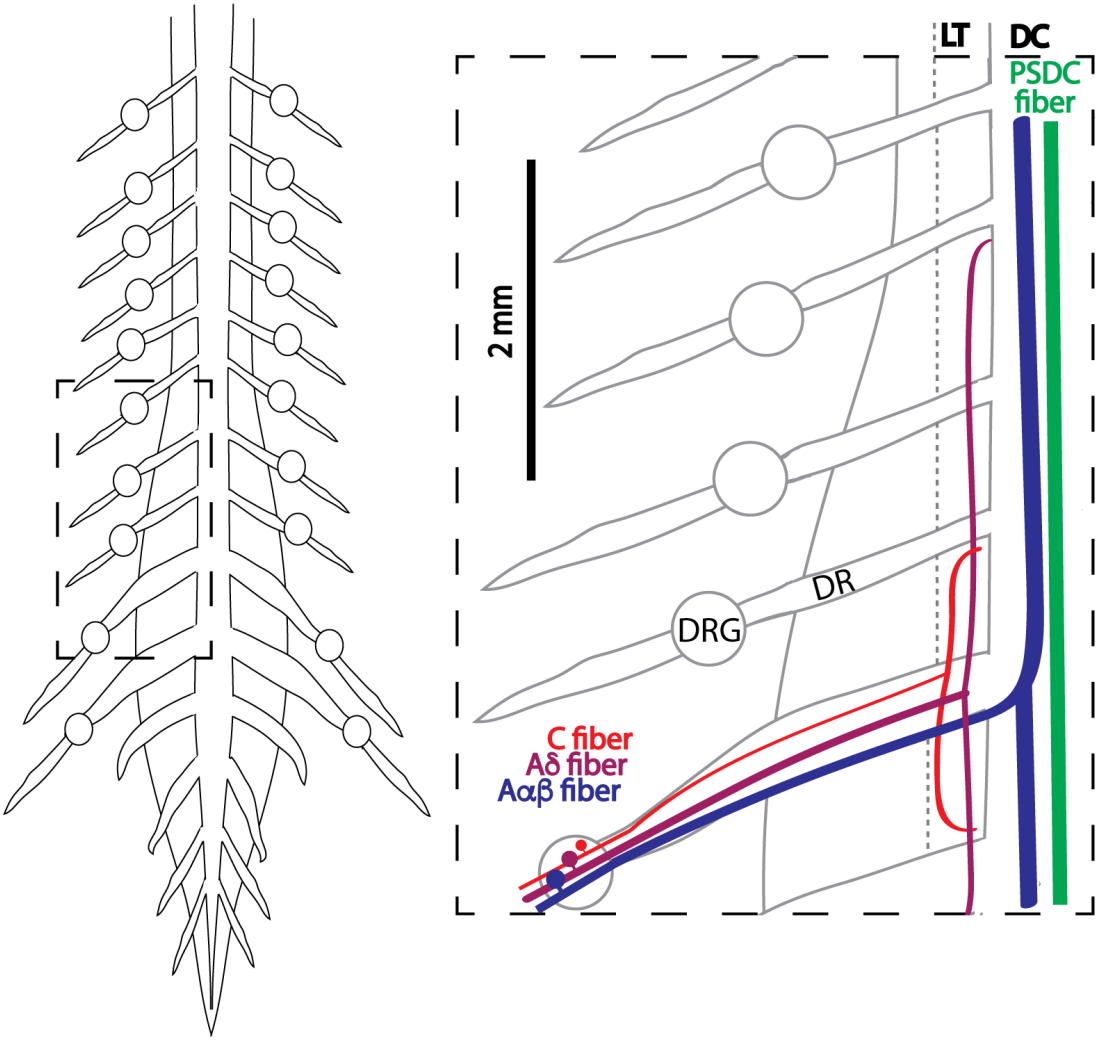

Figure 1.2: Schematic of dorsal axon tracts and primary afferent projections.

Primary afferents from a single dermatome have cell bodies that reside in dorsal root ganglion (DRG). These axons enter the spinal cord via the dorsal root (DR) and trifurcate sending one collateral into the dorsal horn, one collateral rostral, and another on caudal. Both Aδ and C fibers have collaterals in Lissauers tract (LT). A$\alpha\beta$ fibers travel to the dorsal column nuclei, along side postsynaptic dorsal column cells (PSDCs), via the neighboring dorsal column (DC).

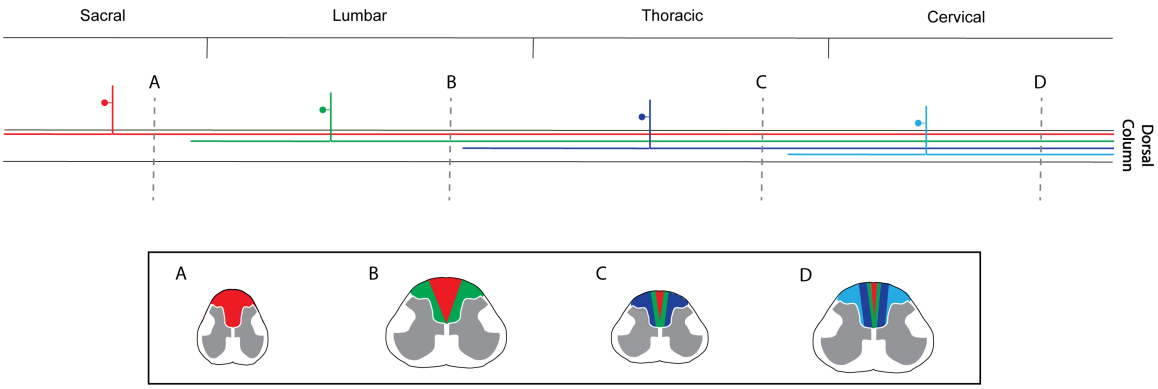

Figure 1.3: Somatotopic organization of the dorsal column.

The dorsal column has a somatotopic arrangement that differs, depending on the level of observation. Sacral afferents (red) compose most of the DC at sacral segments of the spinal cord, but as they ascend and issue collaterals, the axons are presumed to decrease in diameter and shift more medial at lumbar (B), thoracic (C), and cervical (D) segments. This phenomenon is conserved across regions of the spinal cord such that at the cervical DC (D), sacral (red) and lumbar (green) afferents are most medial while thoracic (dark blue) and cervical (light blue) afferents are more lateral.

1.1.3 Dorsal horn terminations

Laminar terminations of afferent presynaptic terminals in the dorsal horn of the spinal cord, all of which release the excitatory neurotransmitter glutamate, are subtype-specific **(see Figure 1.4)**. While Aδ and C fibers tend to terminate in the superficial dorsal horn of lamina I-II, Aβ typically terminates in the deeper lamina III-V [22][23]. Synapses with dorsal horn interneurons serve to integrate and process incoming sensory information, with projection neurons sending the signals to supraspinal centers of the brain. Projection neurons transmitting pain and temperature information have axons that travel to the brainstem via the ventrolateral (anterolateral) tract, commonly referred to as the spinothalamic tract [23]. Nociceptive-specific **(NS)** projection neurons of lamina I receive excitatory input from Aδ and C fibers encoding noxious temperature, mechanical, and chemical information from the periphery [23]. Lamina V wide dynamic range **(WDR)** neurons receive multimodal, convergent input from nociceptors and Aβ mechanoreceptors [23].

Many therapeutics intended to induce analgesia (i.e. pain-relief) aim to inhibit nociceptive transmission to or from the spinal cord; with targets including primary afferents

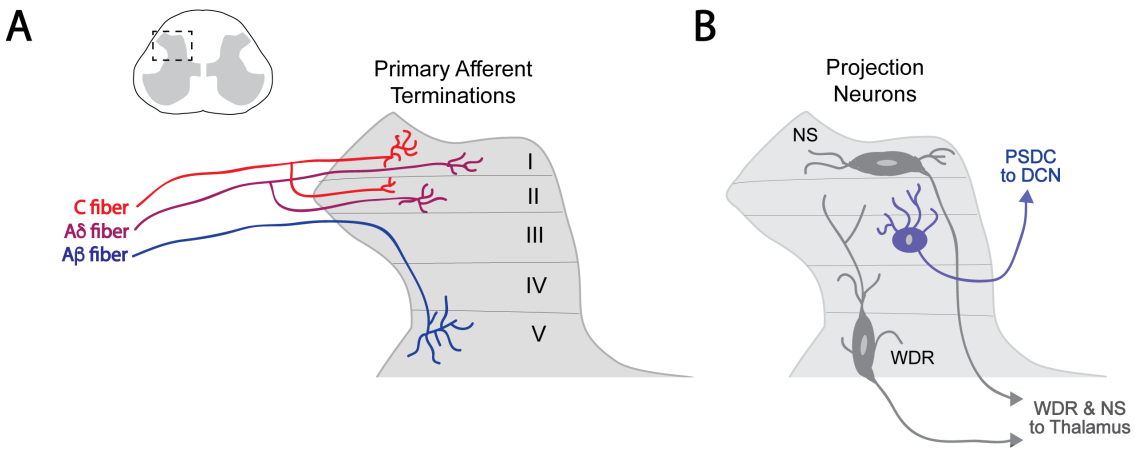

Figure 1.4: Laminar terminations of primary afferents.

Primary afferents have distinct regions of dorsal horn termination. **A)** Aδ and C fibers tend to have monosynaptic connections with interneurons in the superficial dorsal horn (lamina I/II), while Aβ fibers typically terminate in the deeper dorsal horn (lamina IV/V). **B)** The signals traveling via these afferents are sent to brain via nociceptive-specific (NS), wide dynamic range (WDR), or postsynaptic dorsal column (PSDC) neurons.

(peripheral nerves and DRGs) and the projection neurons of the dorsal horn. In the next section I review evidence demonstrating the contribution of peripheral and spinal sensory circuit hyperexcitability to the development and maintenance of pain, with emphasis on its role in persistent, spontaneous pain. **Table 1.1** provides definitions (as it relates to this dissertation) for key pain-related terminology.

1.2 Persistent Pain: The Role of Peripheral and Spinal Hyperexcitability

Persistent pain is the leading cause of long-term disability, with few available and effective treatments. Approximately 3% of the world population is plagued with neuropathic pain resulting from various forms of injury or disease [24]. It is a condition that affects the quality of life for its sufferers not solely due to the burden of pain, but because it is frequently comorbid with anxiety, depression, and sleep deprivation.

Table 1.1: *Definitions for pain-related terminology.*

Term	Definition
nociceptor	*pain encoding primary afferents, typically Aδ and C primary afferents*
nociception/nociceptive activity	*refers to the transmission of signals from pain encoding/processing fibers and spinal circuits*
sensory (circuit)	*for the purpose of this dissertation, refers to primary afferents and dorsal horn circuitry*
hypersensitivity	*increased sensitivity to sensory stimuli, can refer to evoked behavior or neural responses*
hyperexcitability	*refers to a reduced excitation threshold for sensory circuits, which can manifest as spontaneous activity or a greater sensitivity to stimuli*
spontaneous	*a stimulus-independent state of neural activity or pain*
evoked	*a stimulus-dependent state of neural activity or pain*
chronic/persistent pain	*pain that lasts for months or years*
neuropathic pain	*a chronic/persistent pain state typically occurring alongside nervous system injury or disease*
hyperalgesia	*increased sensitivity to pain*
allodynia	*perception of pain from typically non-painful stimuli*
analgesia	*relief/depression of pain*

1.2.1 Hyperexcitability

Hyperexcitability in neuronal circuits refers to the presence of aberrant spontaneous activity and/or greater sensitivity to a stimulus-evoked response. Hyperexcitable responses to stimulation include lower excitation thresholds and the generation of doublet or burst firing in response to stimulation that would typically elicit a single spike. Sensory circuit hyperexcitability has been associated with neuronal changes after peripheral and central nervous system injury or disease, contributing to the emergence of abnormal sensory conditions including persistent neuropathic pain. Below I summarize clinical and preclinical evidence implicating sensory hyperexcitability as a driver of persistent spontaneous pain. Though there are many possible origins of pain in the sensory circuit, the content of this dissertation focuses on the *peripheral* and *spinal* aspects.

1.2.2 Clinical evidence of peripheral hyperexcitability

Peripheral contributions to neuropathic pain were examined in patients with polyneuropathy, using microneurographya technique permitting examination of single-unit impulse trains, including those of unmyelinated C-fibers [25]. Peripheral hyperexcitability manifested as reduced receptor threshold (i.e. hypersensitivity), spontaneous activity in C nociceptors, and/or amplified nociceptor stimulus-evoked responses [26][27]. Receptor hypersensitivity is associated with behavioral indications of allodynia, where normally innocuous stimulation (mechanical or thermal) is perceived as noxious. Spontaneous C fiber activity demonstrates stimulus-independent activation of nociceptors, an occurrence perceived in patients as spontaneous burning pain [27]. Hyperalgesia encompasses amplified responses to noxious stimuli, suggesting an increased sensitivity to pain.

Hyperalgesia resulting from thermal and mechanical stimuli have been linked to reduced polymodal C-fiber thresholds [28][27] in patients with chronic pain. While single impulses are typical responses to electrical stimulation of C fibers [29][30][31] in normal subjects, double or triple spikes have been observed in painful neuropathy patients [32][33][27] and this amplified response can coincide with spontaneous activity in the same nociceptors [33]. Significant differences in mechanoinsensitive C-nociceptors have been observed in polyneuropathy patients, with those experiencing pain demonstrating a higher proportion of spontaneously active fibers than those with non-painful neuropathy [34][35]. This evidence, combined with observations that local anesthetic block of peripheral nerves from painful cutaneous foci abolishes allodynia and spontaneous pain [36][37], implicates ongoing C fiber input as a persistent driver of nociceptive central processing and subsequent perceptions of pain.

1.2.3 Preclinical evidence of sensory hyperexcitability

Early evidence of spinal contributions to evoked hypersensitivity was defined by observations of activity-dependent plasticity in dorsal horn circuits, frequently referred to as central sensitization **(see Figure 1.5)**. Experiments demonstrated that repetitive nociceptive stimulation led to a progressive increase in dorsal horn output. This was observed as increases in spike frequency [38] or amplitudes of dorsal horn field potentials [39][40], phenomena now referred to as wind up and spinal long-term potentiation **(LTP)**. Electrophysiological manifestations of central sensitization include reduced thresholds for activation, larger responses to stimulation, increased receptive field size and persistent stimulus-independent firing [39][40][41]. These occurrences are said to underlie neuropathic pain conditions like allodynia, hyperalgesia, and spontaneous pain, observed in patients and animal models.

Peripheral nerve injury models

Models of peripheral nerve injury **(PNI)**, including spinal nerve ligation and chronic constriction sciatic injury, have been used to explore both stimulus-evoked and stimulus-independent manifestations of neuropathic pain. Ipsilateral hind paw sensitivity, manifesting as mechanical allodynia or hyperalgesia, was observed in conjunction with hyperexcitable responses in dorsal horn neurons [42][43][44]. Studies suggest that stimulus-evoked hyperexcitability could be caused by factors including WDR spine remodeling [42], injury-induced activation of substance P receptor (SPR) -expressing neurons [45], or disruption of the glycinergic feed-forward inhibitory circuit [44]. Though peripherally-driven activation of dorsal horn neurons forms the basis of most observation of central contributions to neuropathic pain, studies conducted in animals with dorsal root transections suggest that in the absence of peripheral input, ectopic firing can develop in the dorsal horn neurons and thereby contribute to neuropathic pain [46].

The emergence of stimulus-independent, spontaneous activity in peripheral branches of

primary afferents has been implicated as a major driver to maladaptive plasticity in spinal circuits, leading to the development of persistent neuropathic pain. Local nerve blockade after PNI, prevented the development of spontaneous primary afferent activity and permanently inhibited the develop of hyperalgesia and allodynia [47]. Dorsal root transections, proximal to the DRG, eliminated observations of centrally conducting spontaneous activity [48][49]. This was not observed with transections of the peripheral nerve [48][49]. Combined, this evidence identifies primary afferent somata as the source of spontaneous activity.

Additionally, investigations conducted with models of PNI implicate DRGs associated with the dermatome of injury, as the driver of subsequent neuropathic pain [50] [49] [51] [52] [53] [54]. While most studies observed spontaneously active somata of myelinated A fibers after injury [50][49][51][52][54]; a few studies have also observed hyperexcitability in C fibers, emerging as spontaneous activity or double-spiking evoked by mechanical stimulation [55][35]. This somatal activity manifests as irregular or burst firing [51][52][53], and can correspond with enhanced sensitivity to mechanical stimuli, observed electrophysiologically [53][52] and behaviorally [50][51][54].

Spinal cord injury models

In spinal cord injury **(SCI)** models of neuropathic pain, hyperexcitability of dorsal horn neurons were observed rostral and caudal to level of injury [56]. Lower thresholds and greater firing frequencies for responses evoked by mechanical and thermal stimuli were observed in wide dynamic range **(WDR)** and nociceptive specific **(NS)** neurons of the dorsal horn [56][57]. While upregulated Nav1.3 membrane expression in neurons has been identified as a potential contributor to these observed responses [57], decreased astrocyte expression of the GLT1 glutamate transporter has been attributed to increased persistent activation of dorsal horn neurons, after injury [58].

In a contusion model of SCI, selective recording of small diameter primary afferent somata (presumed Aδ and C fibers) identified an increased incidence of spontaneously active and repetitively spiking DRG neurons below the level of injury. This activity corresponded with behavioral indicators of hypersensitivity to mechanical and thermal stimuli [48][59]. In primary afferent somata, upregulation of Nav1.8 surface expression has been implicated as a mechanism contributing to the emergence of spontaneous activity [60], while down-regulation of Kv3.4 surface expression is suggested to underlie multi-spiking phenomena, after SCI [59].

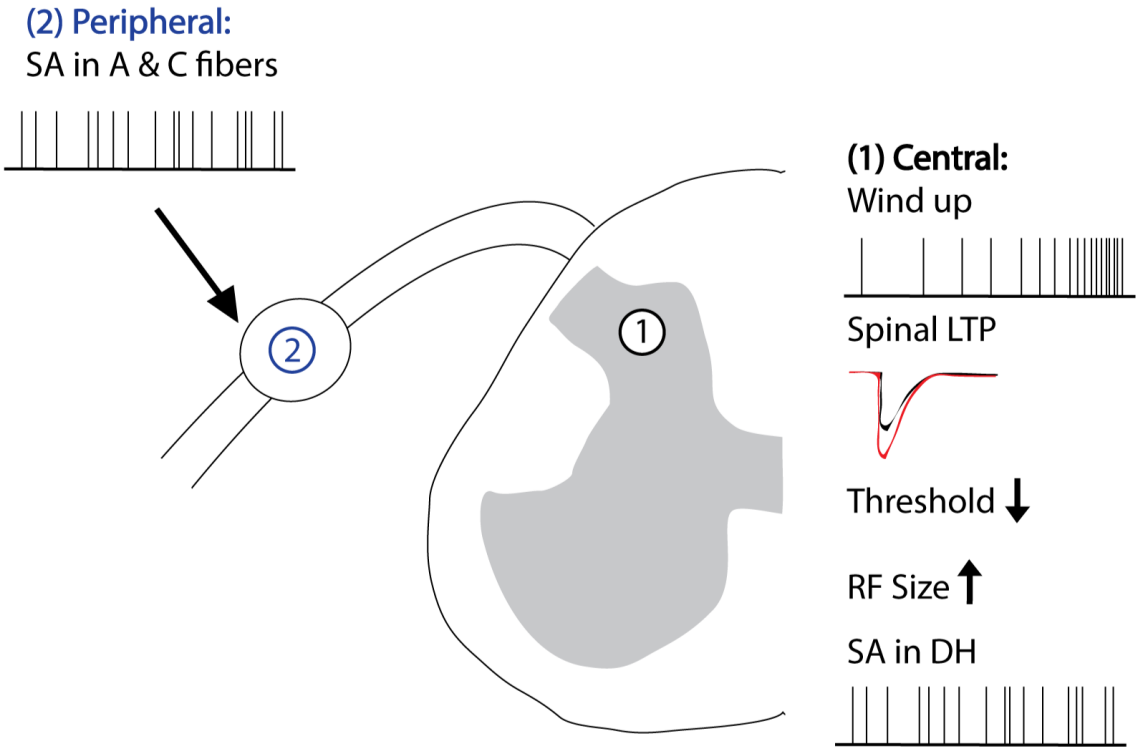

Figure 1.5: Summary of peripheral and central components of sensory circuit hyperexcitability.

The evidence presented suggests that neuropathic pain resulting from sensory circuit hyperexcitability can have either central or peripheral origins. 1) Hyperexcitability in central circuits can manifest as wind up, spinal LTP, decreases in recruitment threshold, increases in receptive field size, and spontaneous activity in dorsal horn neurons. 2) Spontaneous activity in A and C primary afferents has been identified as a driver of maladaptive plasticity in central circuits. Figure adapted from West 2015[61].

1.3 Pain Control: Clinical Spinal Cord Stimulation

Pharmacological treatments aim to quell sensory hyperexcitability and subsequent pain through systemic application of compounds that alter the excitability of target cells. This can occur via functional activation or inhibition of membrane-associated channels or receptors. The ubiquity of many receptors and channels throughout differing regions of body, along with the systemic nature of the drug application can lead to off-target side effects. Some patients are averse to these side effects or experience pain that is resistant to traditional pharmacological treatment. Thus, electrical neuromodulation has emerged as an alternative therapeutic.

The spinal cord is a prime target for therapeutics aimed at blocking the transmission of pain signals, as it is the interface of ascending and descending information to and from the brain. Spinal cord stimulation (SCS) is a form of electrical neuromodulation that has been used clinically to inhibit aberrant signaling in cases of refractory pain, for over 40 years. This is implemented via electrodes inserted into the epidural space and chronically placed over the dorsal surface of the spinal cord for continuous stimulation. Compared to those receiving pharmacological treatment alone, patients receiving SCS have reported greater pain relief and higher quality of life as outcomes of the therapy [62][63]. Details regarding its clinical implementation are described below, including the parameters utilized and its efficacy for various pain etiologies.

1.3.1 Stimulation parameters

SCS systems are fully-implantable devices that consist of multi-contact paddle or percutaneous arrays positioned in the epidural space and rechargeable pulse generators that can deliver controlled-voltage or controlled-current pulses [64]. While the enhanced surface area of paddle electrodes enables larger arrays of electrode contacts and thereby greater

ability to shape the stimulation field, they require surgical laminectomies for placement. The advent of percutaneous leads facilitated a reversible surgical procedure with lower associated morbidity [24]. Epidural placement complicates the goal of neural selectivity, as the layer of cerebrospinal fluid **(CSF)** serves as a dampening barrier for applied electric fields. Thus, technological improvements related to electrode geometry and stimulation parameters have been implemented with the goal of minimizing off-target stimulation.

Important parameter considerations for the application of SCS include segmental electrode placement, stimulation amplitude, stimulation frequency, and waveform pulse duration; factors that determine the target of stimulation. SCS is commonly used to treat chronic leg and/or back pain. For this, electrodes are typically placed over the caudal thoracic cord (T8-T11) in order to activate medial dorsal column fibers ascending from lumbar segments [64]. Stimulation amplitude and pulse duration are critical parameters determining if SCS is sub-threshold, therapeutic threshold, or supra-threshold (discomfort threshold); along with determining the distribution of activation across multiple dermatomes [64][65]. For traditional SCS, therapeutic threshold is associated with patients perception of a tingling/buzzing sensation, or paresthesia. Paresthesia is a sensation said to result from orthodromic propagation of impulses from dorsal column axons, to the brain. It is a side-effect of SCS that has been useful for helping to determine appropriate electrode placement and stimulation parameters **(see Figure 1.6)** [64]; as concordance of the paresthesia focus with pain has been identified as a predictor of relief [24]. Paresthesias have been deemed necessary, but not sufficient for obtaining lasting pain relief with traditional SCS [66][24][67][68][69]. Aversion to the paresthesia has resulted in some patients deciding to opt out of the treatment, despite obtaining pain relief [70]. As a result, exploration of methods to obtain relief with sub-threshold (paresthesia-free) amplitudes have produced the clinical application of new waveforms and frequencies.

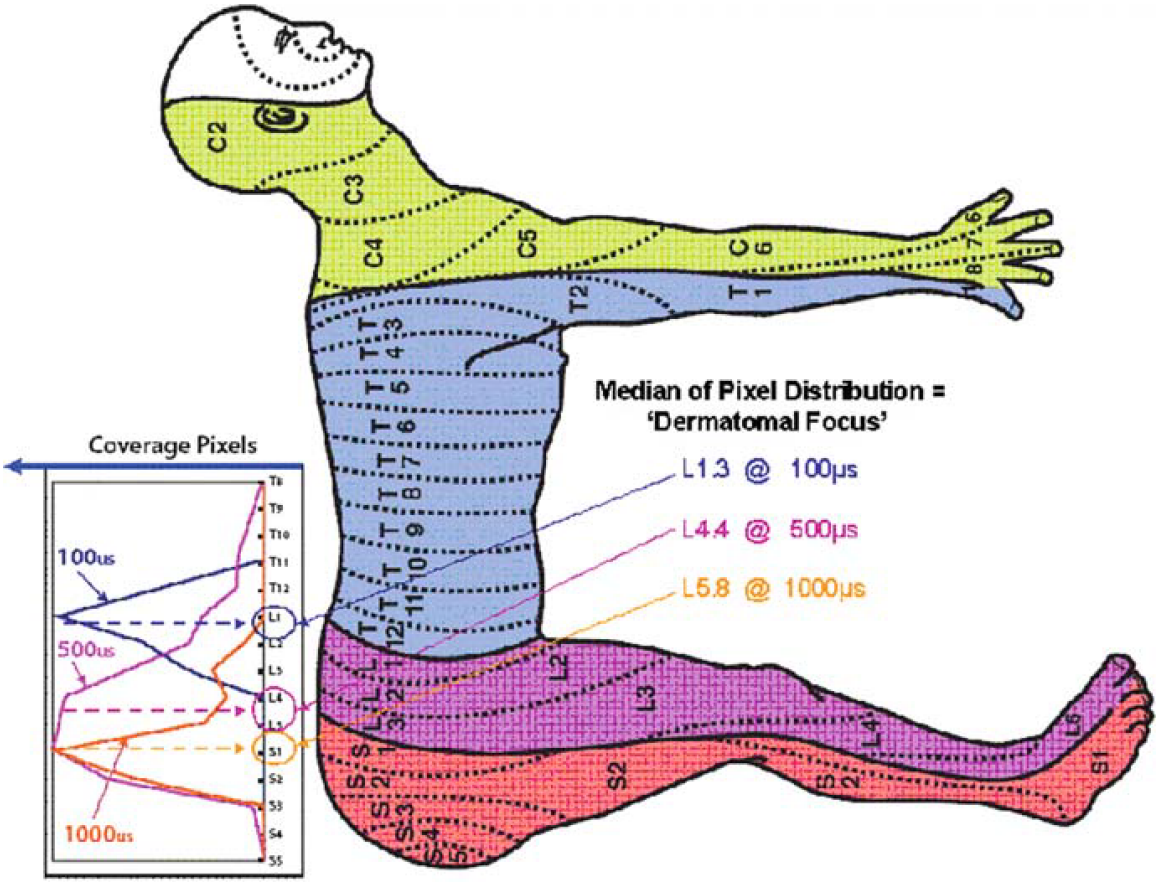

Figure 1.6: The focus of paresthesia determines the location of optimal modulation.

SCS at sensory threshold results in the perception of a paresthesia, which can span multiple dermatomes of the body. Electrode placement and stimulation parameters determine the location of paresthesia focus. This diagram depicts the effect of changing stimulation pulse duration, with SCS electrode placement over the caudal thoracic spinal cord. Longer pulse durations result in caudal shifts of the paresthesia focus. Figure from: Moffitt 2009[64].

Table 1.2: *SCS parameters and sample ranges, adapted from Zhang et al. 2014*

Parameter	Values
Frequency (Hz)	50-150 (a), 15-750 (b), 80± 29 (c), 2-200 (d), 49±16 (e), 39-77 (h), 10000 (h,i), 40-50, (7,9), 40-60 (j)
Amplitude	2-5 V (b), 2.8-5.4V (a), 3±1.5V (c), 3.7±2V (e), 3.6-8.5mA (h), 1.6-3.8 mA (h), 0.05-5 mA (g), 2.36 ± 0.24 mA (i), 2.88±0.15 mA (i), 2.6-11.5 mA (j)
Pulse Duration (μsec)	150-500 (a), 80-500 (b), 270±79 (c), 350±96 (e), 347-591(h), 30 (h,i), 90-500 (g), 80-200 (j)
[2]	(a) Abejon et al 2005[74] (b) Alo et al 2002[75] (c) Butyen 2003[76] (d) North et al 1993[24] (e) Kumar et al 2006[63] (f) Alo and Holsheimer 2002[75] (g) De Ridder 2010[71] (h) Kapural 2015[73] (i) Muhammad 2017[72] (j) Parker 2012[65]

Traditional SCS utilizes tonic stimulation with frequencies $\leq$ 200 Hz (average 63 $\pm$ 54 Hz) [64][24]. Burst waveforms and 10 kHz SCS has been demonstrated to reduce pain at comparable or superior-levels to traditional SCS, without the paresthesia [71][72][73]. Long-term stability of their effects is still being explored, but these new techniques show promise for maximizing efficacy and minimizing undesired side effects. Parameters are manually tuned during surgical placement of the SCS system and effective parameters can vary greatly between patients. **Table 1.2** summarizes SCS parameters previously implemented in clinical settings.

1.3.2 Pain etiologies and efficacy

Over 30,000 stimulators are implanted yearly for patients diagnosed with refractory chronic leg and back pain from various etiologies including complex regional pain syndrome **(CRPS)**, failed back surgery syndrome **(FBSS)**, and fibromyalgia[63][2]. Of those etiologies, the FBSS population is a large proportion of the SCS patient population studied in clinical

trials [62][77]. FBSS results when a chronic back or leg pain condition fails to resolve after a patient receives corrective back surgery [77]. Effective treatment is deemed as a 50% or greater reduction in pain scores. On average 62% of FBSS patients obtain effective relief. Comparable efficacy rates were observed for phantom limb pain (62%) and peripheral neuropathy (67%); while greater efficacy rates occurred in ischemic limb pain (77%), CRPS (83%), and neuralgia (82%) patient populations [62]. Outcomes for clinical trials in the SCI population have varied greatly. Some studies have indicated no evidence of pain relief in patients with clinically complete lesions [78], while other have observed higher success rate in patients with incomplete injuries [79]. When results of all (5) clinical trials in the SCI population are grouped, 57% of patients receive effective pain relief with SCS, revealing its potential as a therapeutic for chronic neuropathic pain following incomplete SCI [62].

Assessing outcomes across etiologies, from 20 years of studies, determined that on average, only 58% of patients receive effective pain relief using traditional tonic SCS ([2], see **Figure 1.7**). The average success rate failed to correlate with study year [2], indicating a lack of improvement in efficacy despite progress with surgical experience and technological innovation.

The variable success of SCS in clinical trials is likely the result of improper selection criteria and neural targeting due to a lack of fundamental understanding of how the technology works. The next section summarizes suggested mechanisms of action, identified by preclinical investigations of SCS.

1.4 Spinal Cord Stimulation Mechanisms of Action: Preclinical Demonstrations

The Gate Control Theory of Pain postulates that Aβ fiber input to the spinal cord inhibits pain encoding through the action of inhibitory interneurons within the dorsal horn [80].

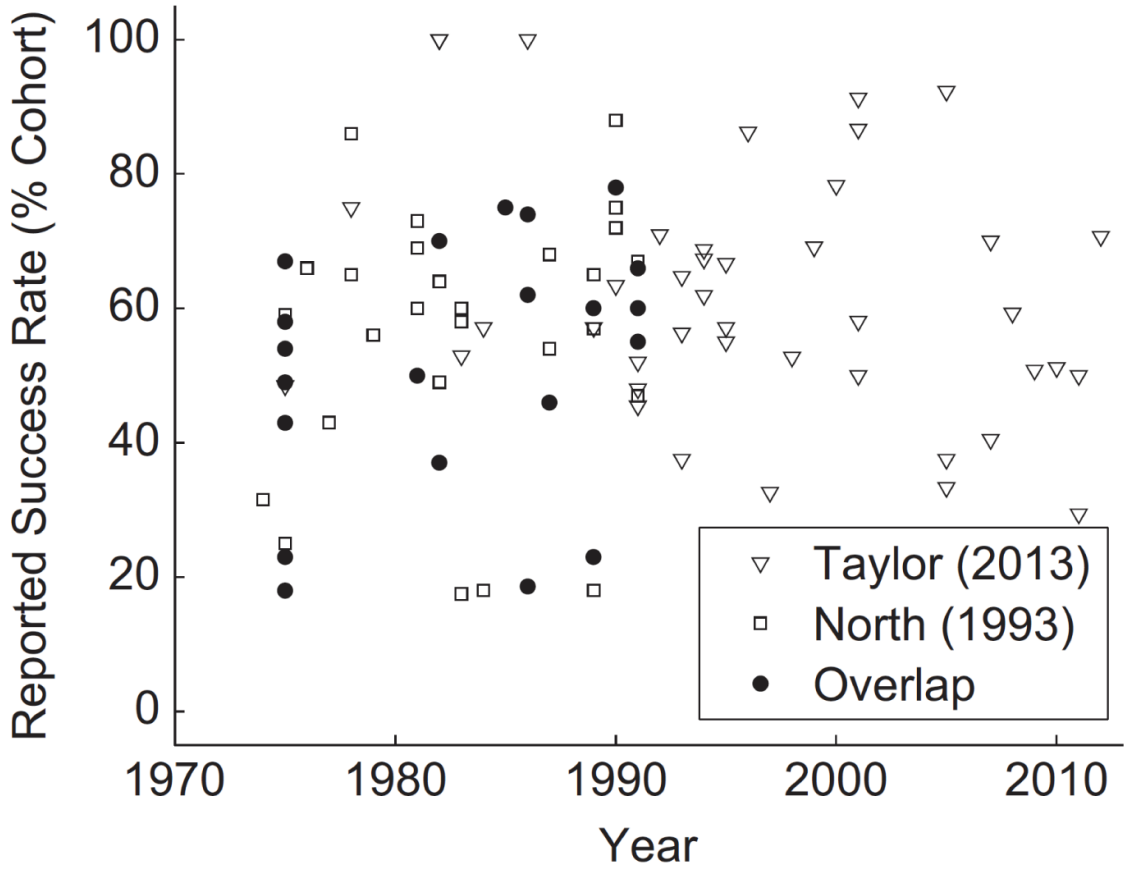

Figure 1.7: SCS efficacy remained stagnant for 20 years.

This scatter plot depicts the reported mean success rates from clinical SCS studies occurring 1973-2013, with the average being 58%. Figure from: Zhang 2014[2], adapted from North 1993, Taylor 2013[24][77]

This theory proposed in 1965 by Melzack and Wall inspired the development of SCS. Since its conception, pain modulation through excitation of Aβ fibers in the dorsal column and subsequent inhibition of nociceptive transmission has been the core mechanism accepted by those developing and utilizing traditional SCS paradigms ([64], see **Figure 1.8**); despite, its inability to explain many clinical observations [1][3]. This includes the ability of SCS to selectively inhibit neuropathic pain and not acute, nociceptive pain [81][82][83][83].

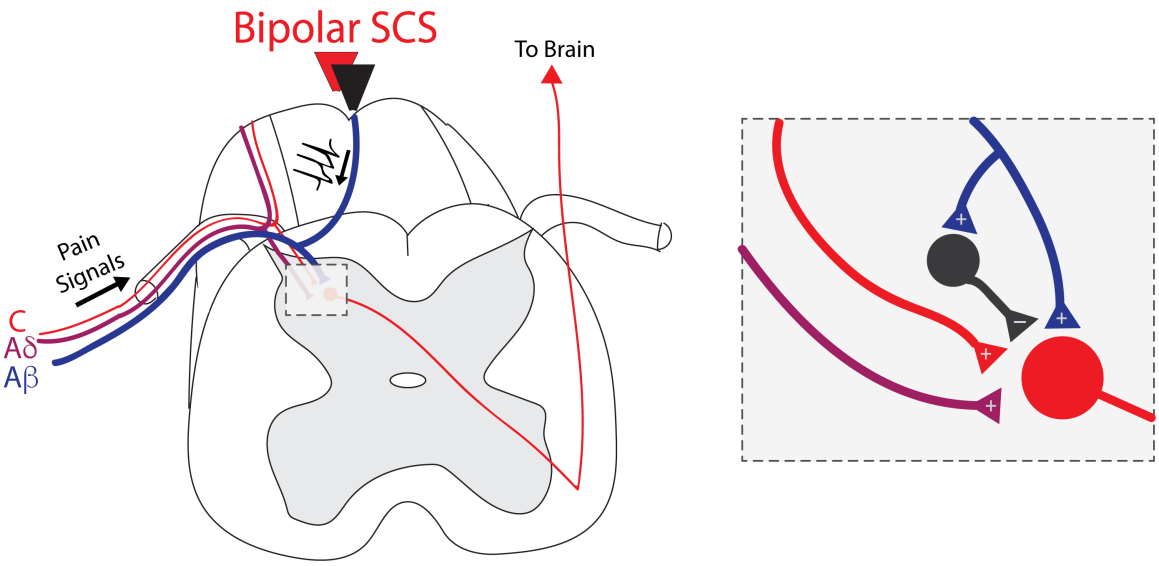

Figure 1.8: Schematic of the presumed SCS mechanism of action

In accordance to gate control theory, it is believed that SCS activates Aβ collaterals in the DC. The antidromic propagations leads to activation of inhibitory interneurons in the dorsal horn that suppresses the transmission of pain signs to the brain. The orthodromic propagation to dorsal column nuclei is said to underlie the perception of the paresthesia. This theory is unable to explain many clinical aspects, including that Aβ activation can produce allodynia, an aspect of neuropathic pain that SCS modulates. Also unexplained is the selectivity of SCS for inhibition of neuropathic, not nociceptive, pain.

Due to the limitations of working with a clinical population, few clinical studies have explored other potential underlying mechanisms of actions. As a result, many mechanistic investigations have relied heavily on computational modeling and/or rodent models to probe the neurobiological basis for analgesia produced by SCS. The insights obtained from these preclinical studies are described below.

1.4.1 Computational investigations of recruitment

Most computational modeling studies aim to investigate recruitment of axonal populations with clinical ranges of SCS. These approaches typically utilize volume conductor models, cable models of axons, or combine both approaches. Volume conductor/ finite element models recapitulate the dimensions and electrical conductivity of tissue associated with the spinal column including the spinal cord (grey and white matter), cerebrospinal fluid, and vertebral bone [84][85][86][87][88][89][90][91]. These models calculate the distribution of electric field magnitudes and extracellular voltages generated in the spinal cord, with epidural placement of SCS electrodes. Cable models of dorsal column and dorsal root axons partially reproduce the biophysical properties of individual axons or neurons, including their channel dynamics [86][87][88][89][90][91][92][93]. Input provided by the volume conductor model (extracellular voltage) permits assessment of excitation of individual or populations of axons, in response to SCS.

Investigations of traditional SCS suggests that a small population (56 fibers) of large diameter, myelinated DC axons is recruited with clinical ranges of SCS [87]. The fibers activated at therapeutic threshold, with electrodes placed at a caudal thoracic (T10/T11) segment, encompass fibers ascending from multiple dermatomes [87][84][94]; with the possibility of paresthesia concordance and subsequent pain relief resulting from activation of a single fiber from the target dermatome [87]. While one study suggested that DR axons have a lower threshold for activation, due to their curvature and angle at the dorsal root entry zone [89], subsequent studies suggest that supra-threshold (discomfort threshold) SCS is associated with recruited of Aβ fibers from dorsal roots [87][84]. Differing results have been reported from investigations of recruitment with 10 kHz SCS. One study suggests that paresthesia-free SCS is obtained by blocking impulses generated in large diameter, myelinated DC fibers; preventing transmission of the paresthesia signal to the brain [90]. Another study finds that amplitudes necessary to activate and/or block conduction in

myelinated DC fibers are outside the range of amplitudes used clinically [91].

While computational models are useful tools for preliminary assessments of recruitment, the strengths of their claims largely depend on experimental validation. Clinical studies [84][65] have enabled low-resolution assessment of SCS recruitment but has provided limited information regarding the analgesic actions engaged in the dorsal horn. Thus, animal models of pain have been used to probe underlying mechanisms leading to SCS-induced analgesia.

1.4.2 Animal investigations of mechanism

Exploration of SCS mechanisms of action frequently employ rodent models of peripheral nerve injury to investigate activation of native antinociceptive spinal and/or supraspinal circuitry. This typically consists of behavioral assessments during awake-behaving conditions or in vivo electrophysiological assessments during anesthetized conditions. In these investigations, stimulation amplitude is determined by identifying the motor threshold (**MoT**), the amplitude of SCS a reflexive muscle contraction, for each subject. SCS-induced analgesia has been explored using amplitudes associated with 50-90% of MoT and 200 μs pulse durations, with traditional frequencies of SCS [95] [96] [97] [98] [99] [100] [101] [102] [103] [104] [105] [106] [107] [108] [109] [110] [111].

Gate control presumes the activation Aα/β fibers that serve as a switch between open (transmission) and closed (block) for supraspinal propagation of nociceptive signals. Modeling and animal studies suggests that myelinated dorsal column afferents are recruited by SCS. While an early study suggested the population contributing to analgesia was Aδ fibers [112], a later study found that the amplitude used to alleviate mechanical hypersensitivity was lower than the Aα/β fiber threshold [113]. This suggests that subsequent SCS relief occurs via supra- or sub- primary afferent recruitment thresholds, which is in

conflict with the assumptions of gate control. The role of spinal GABA, an inhibitory neurotransmitter, has also been explored. Mononeuropathic animals exhibited tactile allodynia, along with decreased extracellular GABA in the dorsal horn [111]. Animals that obtained alleviation of allodynia with SCS (responders) exhibited an increase in GABA levels, in response to stimulation [111]. Non-responders could obtain similar alleviation when SCS was combined with intrathecal administration of GABA or an $GABA_B$ agonist [109]. While intrathecal administration of a $GABA_A$ antagonist has been demonstrated to have no effect on threshold augmentation generated by SCS [109]; another study observed increased spontaneous and evoked activity in spinal projection neurons, shifting toward the production of enhanced excitatory responses and reduced inhibitory responses to SCS [114]. Combined, this confirms the importance of inhibitory interneurons for SCS-induced analgesia, as predicted by gate control. It also suggests that persistent neuropathic pain and ineffective SCS may be the result of insufficient inhibitory drive in the spinal cord. Gate control also predicts gating would only persist for the duration of A fiber stimulation. But an additional observation suggests that the suppressive effects on spontaneous and evoked activity of projection neurons outlasts the SCS stimulation period (˜10 mins)[110]. Other studies indicate that SCS possibly attenuates neuropathic pain by decreasing activation of glial cells [96] and pathways regulating proinflammatory cytokines [107] in the dorsal spinal cord.

Investigations of supraspinal contributions suggests that both spinal and descending brainstem mechanisms work to suppress dorsal horn nociceptive transmission during SCS [100][101][108] [99][105]. Specifically, descending serotonergic pathways appear to have a prominent role in SCS modulation. Descending serotonergic collaterals travel to the spinal cord via the dorsal lateral funiculus **(DLF)**. Bilateral lesion of the DLF prior to SCS reduced its inhibitory effects by ˜50% [105]. Additionally, SCS Non-responders became responders when stimulation was combined with sub-effective doses of 5-HT [100].

Intrathecal application of various 5-HT receptor agonists or antagonists prior to SCS, revealed that 5-HT_{2A}, 5-HT_3, and 5-HT_4 activation contributes to observed attenuation in mechanical hypersensitivity [101]. Further, it indicated that the previously established link between serotonin and GABAergic activity [100] may be facilitated by 5-HT_3 receptors on inhibitory interneurons [101]. While the neuronal source of the descending serotonergic modulation has not been identified, electrophysiological recording indicated changes in the activity of cells located in the locus coeruleus [97] and the rostroventromedial medulla [98] during SCS.

Mechanisms underlying burst and high frequency (1-10 kHz) SCS has also been explored, but still remains unclear. Consensus across these investigations suggests that while burst and high frequency SCS produces attenuated mechanical hypersensitivity comparable to traditional SCS—possibly resulting from reduced Aα/β fiber input [102], the underlying mechanisms are likely different [102][103][115][116] [117][106][104]. Burst stimulation appears to reduce neuronal firing, but this occurs without the increase in GABAergic activity observed with traditional SCS [106]. High frequency SCS is effective at amplitudes subthreshold to paresthesia induction. Evidence indicates that this stimulation does not activate the gracile nucleus of the brainstem like traditional SCS, suggesting that its primary actions are likely in the dorsal horn [103]. The lack of brain stem activation contributes to the absence of a perceived paresthesia, though it is not due to conduction block of ascending fibers in the dorsal column [116]. While induced reduction in neuronal excitability has been proposed as a potential spinal mechanism of high frequency SCS, studies determined that it does not inhibit wind up induced by repetitive C fiber activation [102] or hyperpolarize dorsal horn neurons [117].

1.5 Summary and Goals

I have presented the body of work that establishes the importance of sensory circuitry hyperexcitability in the development and maintenance of persistent neuropathic pain, after nervous system injury. SCS is a therapeutic used clinically to modulate pain resistant to pharmacological treatment; but its efficacy has been stagnant, despite technological advances and application of new stimulation paradigms. An unclear understanding of the neurobiological basis for SCS-induced analgesia has been identified as a key contributor to the lack of improvement in success rates. Computational models have provided the most detailed assessment of axonal recruitment, but the theoretical results are rarely validated with experimental observations. Experimental studies with rodent models of neuropathic pain typically assess SCS modulation with amplitudes associated with MoT. The relationship between MoT and paresthesia/recruitment in humans in unclear. This presents the possibility that the experimental studies employ stimulation parameters that are not properly scaled for clinically-analogous investigations in animal models. Also, there is a dearth of evidence identifying the role of SCS in modulating spontaneous pain, despite being a key feature of its clinical effects. Most studies behaviorally or electrophysiologically assess modulation of stimulus-evoked hypersensitivity. This is likely the result of insufficient methods for assessing behavioral indicators of spontaneous pain and an inability to establish links between spontaneous hyperexcitability in sensory circuits to such behavioral metrics. Here, I developed and utilized ex vivo adult mouse preparations to investigate markers of persistent pain and perform detailed electrophysiological studies of SCS recruitment and modulation. This dissertation sought to (a) identify the relationship between spontaneous sensory hyperexcitability and physio-behavioral indices of spontaneous pain (Chapter 2), (b) characterize axonal recruitment using clinically-analogous SCS (Chapter 3), and (c) characterize a pharmacological model of spontaneous pain and assess modulation of spontaneous activity with SCS (Chapter 4). In the final chapter I discuss implications of this

work and suggest future research directions for continued advancement of the field.

CHAPTER 2
PERIPHERAL HYPEREXCITABILITY AND PHYSIO-BEHAVIORAL INDICES OF PAIN

2.1 Abstract

Spinal cord injury **(SCI)** commonly leads to the development of neuropathic pain in regions below the site of injury as well as impaired sleep and respiratory function. Animal studies suggest SCI-induced neuropathic pain associates with ongoing spontaneous activity in pain encoding sensory fibers (peripheral hyperexcitability), but whether spontaneous pain links with impaired sleep and other pathophysiology is unknown. Here, we use a mouse T10 contusion SCI, known to develop mechanical hypersensitivity, to investigate whether there are emerging physio-behavioral changes that would be indicative of ongoing spontaneous pain. We leveraged non-contact electric field sensor technologies, validated to accurately record respiration and sleep architecture, to assess whether emergent changes seen after SCI in sleep and respiration are associated with electrophysiological evidence of ongoing spontaneous activity in sensory fibers. To achieve this, I developed an *ex vivo* preparation to record from lumbar L1-L6 dorsal root ganglia **(DRG)** *in situ*. I compared recordings of spontaneous activity six weeks after sham or T10 SCI. After SCI, there was greater spontaneous afferent activity and this correlated well with increased hindpaw mechanical sensitivity, increased respiratory rate variability, and increased sleep fragmentation. Observed correlations between spontaneous afferent activity with evoked mechanical sensitivity and fragmented sleep support an important interplay between sleep and pain after SCI. Together, these results highlight the utility of spontaneous peripheral hyperexcitability, alongside sleep segmentation, and respiratory rate variability as potential indices of stimulus-independent neuropathic pain.

2.2 Introduction

Neuropathic pain is a condition that develops following peripheral or central nervous system injury, resulting from trauma or disease. Heterogeneity in the etiologies and presentations of pain contribute to difficulties finding generalized treatment options. The persistent, stimulus-independent nature of neuropathic spontaneous pain enhances its negative impact on quality of life for its sufferers, highlighting the need to accurately assess and treat this chronic condition. As a result, several models of neuropathic pain have developed to help understand the neurobiological mechanisms and explore new treatment strategies, yet experimental assessment tools are optimized for exploring stimulus-evoked neuropathic pain such as allodynia and hyperalgesia [42][43][44]. This is in part due to challenges in identifying and quantifying metrics of chronic, spontaneous pain.

In an effort to identify and quantify spontaneous pain states, studies have uncovered functional changes in central and peripheral neurons. There is increasing evidence that spontaneous primary afferent activity represents one initiation site and chronic driver of maladaptive sensory processing, leading to neuropathic pain perception. Spontaneous activity in both A and C fibers has also been observed in various neuropathic pain states [50] [49] [51] [52] [54]. Key studies conducted in rodent contusion models of spinal cord injury (**SCI**) revealed potential links between stimulus-evoked hypersensitivity (hyperalgesia/allodynia) and the incidence of spontaneous firing in cell bodies of primary afferents below the level of injury [48] [59] [118] [60]. These studies predominantly assessed spontaneous activity from C fiber dorsal root ganglia (**DRG**) neurons, and relied largely on observations of increased incidence in spontaneous activity following DRG dissociation. A caveat using this approach is that the method of DRG dissociation itself may induce hyperexcitability, including increased spontaneous firing that mirrors the effects seen after chronic compression of DRGs [119]. In summary, there is need for additional studies in

more intact circuitry to identify and causally link spontaneous DRG activity after SCI as a metric of an abnormal sensory state.

In addition to identifying the drivers of spontaneous pain, it is important to understand the symptomatic manifestations and how they relate electrophysiological changes. In rodent models, the presence of pain is often determined granularly through visual observation of animal grooming and social habits. Pain-related sensitivity is commonly quantified through mechanical or thermal stimulation of fore or hindlimbs, though these methods represent behavioral stressors which may significantly alter the outcome [43] [44] [48] [59] [118] [60]. Moreover, such tests measure alterations in reflex response sensitivity and do not necessarily translate into supraspinal encoding of the affective dimension of pain. This is particularly a problem in studies on SCI pain where ascending pain pathways may have been severed. The implementation of a conditioned place preference (**CPP**) paradigm–that uses analgesic administration to positively reinforce location with pain relief, introduces the possibility of assessing ongoing spontaneous pain while also clearly testing for the cognitive affective/motivational dimension of pain [120] [121] [122] [60]. A weakness is reliance on the selectivity of drugs to produce analgesia without confounding side effects. We considered an alternative approach to quantify persistent spontaneous pain in an attempt to address limitations of existing behavioral assays. We explored the use of noninvasive methods to assess other behaviors known to be affected by spontaneous pain, including sleep and respiration. These measures are well-suited to studies on SCI-induced pain because SCI has a significant impact on sleep quality [123] [124] [125] [126] and respiration [127] [128] [129] without impairing the neural pathways controlling these behaviors, and these changes may be related to the presence of pain.

Here, we explore the relationship between spontaneous primary afferent activity (peripheral hyperexcitability) and physio-behavioral indices (sleep and respiration) that may

concomitantly shift during the transition to neuropathic pain, after SCI. In the thoracic contusion SCI model of neuropathic pain, we examine metrics associated with sleep architecture and respiratory function, using non-invasive electric field sensors. We also compare these behavioral outcomes to established mechanical sensitivity testing, along with post-mortem observations of spontaneous activity in whole DRGs, below the level of injury. Results from these studies link peripheral hyperexcitability to greater segmentation of sleep and erratic breathing, identifying these metrics as potential stimulus-independent indicators of chronic spontaneous pain.

Parts of this work have been presented previously in abstract form [130].

2.3 Methods

2.3.1 Animals

All procedures were approved by the Emory University Institutional Animal Care and Use Committee. Adult C57/Bl6 mice (n = 18, female) were pair housed in home cages under standard 12:12 hour light-dark cycles with ad libitum food and water. Animals were acclimated to their pair housing for several weeks prior to the start of baseline testing.

2.3.2 Animal surgeries

SCI was induced via moderate contusion of the T10 spinal cord segment [131]. First, mice (n=13, postnatal day 205) were prepared for aseptic surgery and deeply anesthetized with 2-3% isoflurane. A midline skin incision was made and the muscle and fascia were dissected. A dorsal laminectomy exposed the spinal cord at T8-T10. At this point, muscular incisions in six animals were closed using surgical glue (Vetbond) and skin was closed with wound clips (size and company) to simulate the sham control group (Sham Group n=6). Prior to wound closing of the remaining 7 animals, a moderate contusion SCI was induced at the dorsal surface of the T9/10 spinal cord with the Infinite Horizon impactor (IH-400,

Precision Systems and Instrumentations), at 50 kdynes (SCI Group n=7). All mice received post-operative pain relief (2 mg/kg meloxicam, subcutaneous injection, daily for 48 hours), antibiotics (2.5 mg/kg Baytril, subcutaneous injection, daily for seven days), supplemental hydration (0.5 ml sterile saline, i.p. daily for 48 hours), and bladder expression twice daily until each animal was able to void independently.

2.3.3 Physio-behavioral monitoring

Home cage exteriors were instrumented with electric field (**EF**) sensors (Plessey Semiconductors, PS25251, 1 cm^2, +/-5V, 1 kHz sampling) able to passively translate disruptions of the local electric field caused by movement into a voltage trace[132][133][134]. EF sensors were connected to a custom filter (12 Hz lowpass) and amplifier. Data were collected using Digidata and pClamp software (Axon Digidata 1440a, Molecular Devices, USA), and analyzed in Spike2 (Cambridge Electronic Design, UK) and MATLAB. The EF sensors can measure animal motion with high resolution from outside the home-cage [132][133][134]. Moreover, these EF sensors are able to reliably measure extremely small mouse motions with great sensitivity, allowing them to detect respiratory-related movement, validated against whole body plethysmography, when the animal is at rest [132]. Furthermore, EF sensors were recently validated against electroencephalogram and electromyogram to successfully quantify three stages of arousal: wake, rapid eye movement **(REM)** sleep, and non-REM sleep non-invasively from outside the animal's home cage [134].

Four EF sensors were attached to the exterior of the animals' home cage facing inward (see **Figure 2.1A**). During active recording, the home cage was temporarily divided into two chambers, with one animal and two EF sensors in each, by an electrically shielded insert that allows visual, olfactory, and thermal interactions between the two animals. Each chamber was outfitted with individual food hoppers and water bottles. Petri dishes (60 mm)

were placed in one corner of each chamber as a recommended nesting location. Animals were acclimated to the temporary division for several days prior to baseline recordings. Home cage activity, resting respiration features, and sleep architecture was recorded for 12 hours during the dark cycle three times prior to spinal cord injury (baseline) and twice weekly afterwards for 6 weeks.

2.3.4 Sleep analysis

Sleep was analyzed twice weekly during the 12-hour dark cycle (6 pm-6 am) which is the animal active period. Though mice are nocturnal, they still sleep an average of 20-30% of the dark cycle and this period was chosen to minimize environmental sleep disruptions that would alter normal sleep habits. Described previously [134], 3-state sleep architecture (wake, non-REM sleep, and REM sleep) is calculated through changes in animal movement and respiration.

Sleep was assessed cumulatively (non-REM and REM sleep combined) and as individual non-REM and REM sleep during the 12-hour dark cycle (active period). The outcomes discussed below compare the median sleep event duration, the average number of sleep events, and the average number of brief arousals between treatment groups over the 12 hour dark cycle (ee **Figure 2.1B, 2.1D**). The number of sleep events is normalized to how many hours an animal slept, with more events denoted more fragmented sleep. The related metric of brief arousals quantifies the average number of short wake events (<60 secs) occurring per hour of sleeping and differentiates typical arousals that naturally happen at the conclusion of REM from abnormally brief arousals that disrupt the natural cycle of non-REM and REM sleep. A greater number of sleep events and brief arousals suggests more segmented, disrupted sleep, which may indicate lower quality sleep. Though animals were recorded twice weekly, a representative weekly value was calculated for each animal by first calculating nightly means then averaging the two nights per week together. Only

baseline (pre-SCI or Sham procedure) and week 6 post-injury data are discussed here as the objective is to associate behavior with terminal electrophysiological metrics at week 6.

2.3.5 Respiration analysis

Respiration is detected by the EF sensors as a cyclic voltage trace representing the breathing cycle (see **Figure 2.1B**). Respiration features were measured only when the animal was at rest during non-REM sleep or when the animal was quietly resting prior to sleep. Respiration cannot be reliably measured when the animal is active because the voltage trace deflections caused by the breathing cycle are overshadowed by the larger motor movements. Average resting respiratory rate (**RR**) was determined by averaging the instantaneous frequencies of each breathing cycle using the corresponding peak of the voltage trace during a non-REM sleeping event. Average RR represents the number of breaths the mouse will take in a second. RR variability (**RRV**) is the standard deviation of these instantaneous frequencies within a single non-REM sleeping event and represents how erratically an animal breathes in one second. Low RRV ($<$0.3 Hz) indicates consistent breathing while high RRV ($>$0.3 Hz, defined as more than 2 standard deviations away from healthy animal RRV) indicates erratic breathing. All the RR and RRV calculations were performed using a custom MATLAB script that filters the voltage trace (0.1 Hz HP 4^{th} order Butterworth, 10 Hz LP 4^{th} order Butterworth), then finds the periods when the animals are in the resting state, and calculates the breathing cycle peaks, instantaneous frequencies, RR, and RRV. Just as with sleep measures described above, nightly RR and RRV means were averaged to create a baseline and week 6 representative value for each animal.

2.3.6 Mechanical sensitivity

Mechanical sensitivity was measured using Chaplan's up-down protocol for von Frey filaments [135]. Briefly, animals were acclimated to the von Frey filaments (1.65, 2.44, 2.83, 3.22*starting filament, 3.61, 3.84, 4.17, and 4.31 sizes; correlating to 0.008,0.04, 0.07,

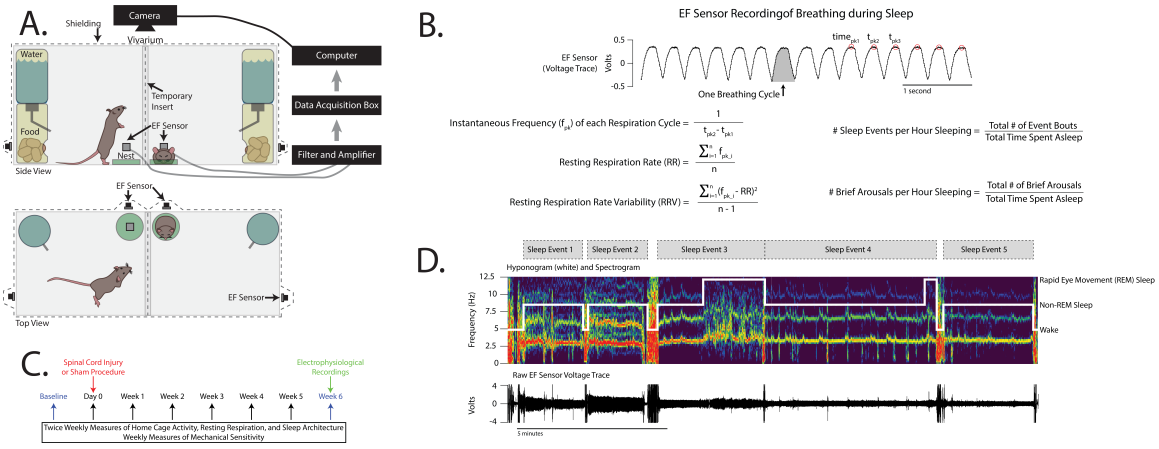

Figure 2.1: Methodology for non-invasive monitoring of animal sleep and respiration.

A) Home cage instrumentation for electric field sensing. A total of 4 individual EF sensor is were used per cage, with 2 dedicated to each animal. **B)** Example recording of breathing with electric field sensor along with equations for the calculation of sleep and respiration metrics. **C)** Measure of behavioral metrics were taken weekly until the terminal electrophysiology experiments. Here we only report on the measures at baseline, and at week 6 in order to compare electrophysiology and behavior. **D)** Example spectrogram (top panel) and overlaid hypnogram (white trace) obtained from electric field sensor recording (bottom panel) for quantification of sleep events.

0.16* starting force, 0.4, 0.6, 1.4, and 2.0 grams), cages, and mesh floor for several days prior to testing. Mechanical sensitivity was assessed in both hind paws three times prior to surgery and once weekly afterwards for 6 weeks. The 50% paw withdrawal threshold (**PWT**) was quantified for both treatment groups. This metric is defined as the stimulus intensity (in grams) required to produce a withdrawal response 50% of the instances when the tip is applied to the plantar surface of the paw (i.e. the animal is equally likely to tolerate or withdraw from that stimulus). This behavioral test is frequently used to infer the emergence of pain presenting as mechanical allodynia and the 50% PWT has been shown to shift in many disease and injury models that include pain. Lower PWTs associate with heightened mechanical sensitivity and may suggest the emergence of allodynia as part of the neuropathic pain state after neural injury. Single-animal values were obtained by averaging the 50% PWT for both hind paws at baseline and week 6 post-injury.

2.3.7 Isolation of multisegmental DRGs

Following 6 weeks of postoperative behavioral testing, animals (postnatal day 247-267) were lightly anesthetized in an isoflurane chamber then given an intraperitoneal injection of ketamine (100mg/kg) and xylazine (10mg/kg). Prior to decapitation, the dorsal skin from the neck to the base of the tail was removed and the region over the spinal column was covered with ice until there was a noticeable slowing of the respiration rate. Next, the spinal column and surrounding tissue were isolated and placed in a dish containing ice-cold, oxygenated (95% O_2 / 5% CO_2) low-Ca^{2+} artificial cerebral spinal fluid (aCSF) composed of (in mM): NaCl 128, KCl 1.9, $MgSO_4$ 13.3, $CaCl_2$ 1.1, KH_2PO_4 1.2, glucose 10, $NaHCO_3$ 26. Both a complete laminectomy and vertebrectomy were preformed to expose the spinal cord and DRGs from segments C8 through S1. Dorsal and ventral roots from each spinal nerve were cut to isolate the DRGs. The isolated tissue was equilibrated to room temperature for 1 hour, then pinned at the dorsal roots in a Sylgaard-lined recording chamber while superfused with an oxygenated aCSF containing (in mM): NaCl 128, KCl 1.9, $MgSO_4$ 1.3, $CaCl_2$ 2.4, KH_2PO_4 1.2, glucose 10, $NaHCO_3$ 26, at ˜40ml/minute. All experiments were undertaken at room temperature.

2.3.8 Extracellular DRG recordings

Prior to recording, connective tissue surrounding the DRGs (dura and pia) were removed to enable sufficient access to cell bodies. Glass suction electrodes (200-250 μm tip diameter) were positioned below the level of injury on lumbar (L1-L6) DRGs and recorded activity (silent or spontaneous) for a minimum of 25 seconds (see **Figure 2.2)**. In all animals, every undamaged lumbar DRG (viable) that remained following isolation was recorded, with the maximum number reaching 11. The number of viable DRGs was predominantly a function of the isolation precision. All recorded data were digitized at 50 kHz (Digidata 1322A 16 Bit DAQ, Molecular Devices, U.S.A.) with pClamp acquisition software (v. 10.7 Molecular Devices). Recorded signals were amplified (5000x) and low-pass filtered at 3

kHz using in-house amplifiers. Post-hoc, data was high-pass filtered at 5Hz, to eliminate baseline drifts in the recordings.

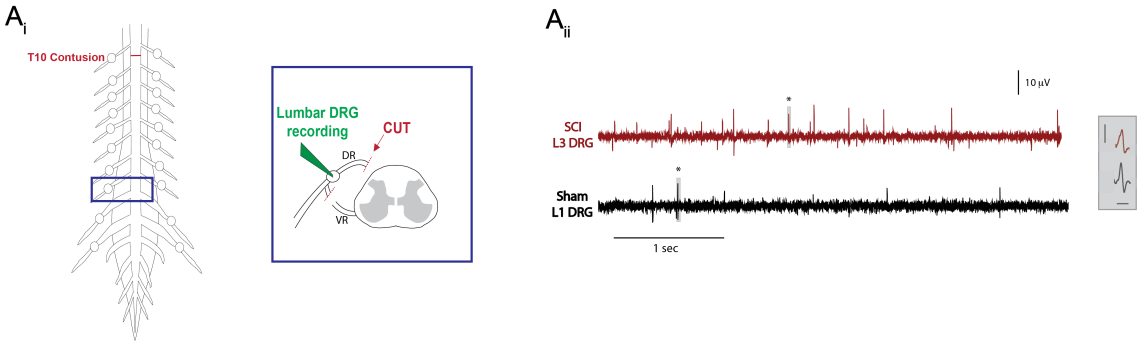

Figure 2.2: Methodology for electrophysiology for isolated DRG preparation

A_i) A schematic of the isolated DRG preparation. Following exposure of the spinal cord and peripheral aspects of primary afferents (DRG, dorsal root, spinal nerve) from C8-S1 segments, the dorsal roots (**DRs**) and ventral roots (**VRs**) were cut at each segment, leaving only a section of the DRs with the attached DRGs and the surrounding ribs and musculature (not shown). **A_{ii})** Example recordings of spontaneous activity in the lumbar L3 DRG from the SCI (red) and L1 DRG from the Sham (black) populations. Displayed is a single sweep from maximally active DRGs from 2 different animals. Single units marked with * are expanded in the inset (scale bars are 2 ms and 10 μV).

2.3.9 Data analysis

Electrophysiological data and behavioral data were analyzed independently, by two different experimenters. Average values reported in results represent the mean ±standard deviation. Post-hoc threshold event detection with Clampfit analysis software (v 10.7 Molecular Devices) enabled identification of spike counts. All software-identified spikes were manually examined to ensure that individual spikes fit the durations expected for single units ($>$1 ms). Counts of spontaneously active **(SA)** and silent DRGs were determined manually. SA DRGs were identified as DRGs producing $>$1 spike within 25 secs. Maximal DRG firing frequency was determined by calculating the average number of spikes occurring within 5 secs bins of the overall recording time. This was determined for a single DRG from each animal, where maximal firing was observed. Incidences of SA DRGs were determined by calculating the percentage of DRGs with observable spontaneous activity, relative to the to-

tal number of DRGs recorded within an animal. Due to the non-uniform sampling of DRGs from each animal, individual incidence values were weighted relative to the total number of possible DRG observations (bilateral DRGs for L1-L6 = 12). This was accomplished by multiplying each value by (# of sampled DRGs / 12), enabling greater weighting of incidences obtained in animals where a larger proportion of the total possible DRGs were observed. In all data presented, the number of animals sampled for analysis is represented by the noted n/12 value.

Statistical differences in behavioral metrics of sleep, respiratory, and sensory function were determined using 2-Way ANOVA, with Sidak's multiple comparison's test (α =0.05) for both treatment groups, at baseline and postoperative week 6. Analysis of differences in DRG firing frequencies and weighted incidences of SA DRGs between treatment groups was performed using the two-tailed Mann-Whitney test. For correlation analysis, we quantified the residual change from baseline to week 6 for PWT, sleep metrics, and RRV. Associations between behavioral metrics (postoperative week 6) and post-mortem electrophysiology were estimated using Pearson correlation analysis. All statistical analysis was performed in Prism (v7).

2.4 Results

2.4.1 Sleep becomes fragmented after SCI

Sleep architecture was assessed at baseline and week 6, for both treatment groups. Though Sham group animals slept more total time at week 6 relative to their baseline ($p < 0.05$), total sleep time did not change in SCI animals, nor were there any significant changes in non-REM and REM sleep time for both SCI and Sham group animals (**Table 2.1**). Baseline values between groups (for all metrics) were not significantly different ($p > 0.6$). For SCI sleep event duration (**Figure 2.3Ai**), number of sleep events (**Figure 2.3Aii**), and number of brief arousals (**Figure 3Aiii**), there was a significant difference from baseline ($p < 0.001$)

Table 2.1: *Summary of sleep architecture results*.
Values represent the mean ±STD.
**p<0.001, ****p<0.0001 for differences between Sham and SCI groups at week 6
# p<0.05, ## p<0.001, **###** p<0.0001 for differences between baseline and week 6 for each group

	Sham (n=6)		**SCI (n=7)**	
	baseline	week 6	baseline	week 6
Sleep Event Duration (s)	284.2 ±42.6	307.0±78.2	285.7±72.9	$126.4\pm24.3^{***}_{\#\#}$
Number of Sleep Events	10.4±2.4	10.6 ±1.0	8.9±1.8	$30.6\pm4.8^{****}_{\#\#\#}$
Number of Brief Arousals	4.5±2.2	4.1±1.2	3.3±1.1	$20.3\pm2.9^{****}_{\#\#\#}$
Total Time Spent Asleep (% of 12 Hour Dark Cycle)	17.9±9.6	$29.6\pm8.0_{\#}$	19.2±6.7	19.9 ±7.5
Total Time Spent in Non-REM Sleep (% of Time Spent Asleep)	87.3±2.7	87.4±3.6	88.8±1.3	86.9±2.6
Total Time Spent in REM Sleep (% of Time Spent Asleep)	12.1±5.9	12.1±5.6	11.2±3.1	12.2 ±2.9

and significant differences when compared to the Sham group at week 6 (p <0.001). The results for sleep architecture assessment are summarized in **Table 2.1**. Analysis of linear associations between these metrics revealed a positive correlation between number of brief arousals and number of sleep events (r = 0.84, p <0.05) in the SCI group, but no correlations between any of the metrics for the Sham group, or across groups.

2.4.2 Respiration becomes more erratic after SCI

The average resting RR at baseline was similar for both groups and unchanged 6 weeks after SCI or Sham surgery (p >0.5, **Figure 2.3Bi**). However; there was a significant increase in RRV for the SCI group at week 6, relative to baseline (p<0.0001). Also, the average RRV for Sham and SCI were significantly different at week 6 (p<0.0001, **Figure 2.3Bii)**. Results are summarized in **Table 2.2**.

Table 2.2: *Summary of respiration results.*
Values represent the mean ±STD.
****p<0.0001 for differences between Sham and SCI groups at week 6.
p<0.0001 for differences between baseline and week 6 for the SCI group

	Sham (n =6)		**SCI (n=7)**	
	baseline	week 6	baseline	week 6
Average RR (Hz)	3.3±0.3	3.3±0.2	3.6±0.6	3.5±0.5
RRV (Hz)	0.2±0.02	0.2±0.03	0.2±0.03	$0.4\pm0.1^{****}_{\#\#\#}$

2.4.3 SCI results in hindpaw hypersensitivity

Mechanical sensitivity was assessed prior to surgery (baseline) and postoperative weeks 1-6 for Sham (n = 6) and SCI (n = 7) groups to confirm that our injury model exhibits the expected time course in the development of mechanical hypersensitivity. Relative to baseline, SCI animals exhibited heightened mechanical sensitivity at all time points except week 1 (p <0.005). Comparison of 50% PWT between treatment groups revealed significantly heighted mechanical sensitivity in SCI animal, when compared to Sham, that persisted after week 2 (p <0.005, **Figure 2.3C**). Average 50% PWTs at week 6 for Sham and SCI were 2.2 ±0.3 g and 0.6 ±0.2 g, respectively.

2.4.4 Spontaneously active DRGs: stimulus-independent indicator of peripheral hyperexcitability

To assess below-level spontaneous primary afferent activity, silent and spontaneously active (**SA**) L1-L6 DRGs were recorded bilaterally from SCI (n =7) and Sham (n = 6) populations 6 weeks after SCI or Sham injury. Compared to Sham (0.6 ±0.3 Hz), SCI animals exhibited greater spontaneous activity (2.5 ±1.2 Hz), as characterized by the maximal DRG firing frequency (p <0.005, **Figure 2.3Di**). The weighted incidence of SA DRGs in the SCI population (29.8 ±16.5%) was significantly greater than Sham (12.5 ±4.6%, p <0.5, **Figure 2.3Dii**). Overall, these results suggest that greater spontaneous activity/peripheral hyperexcitability emerges after SCI.

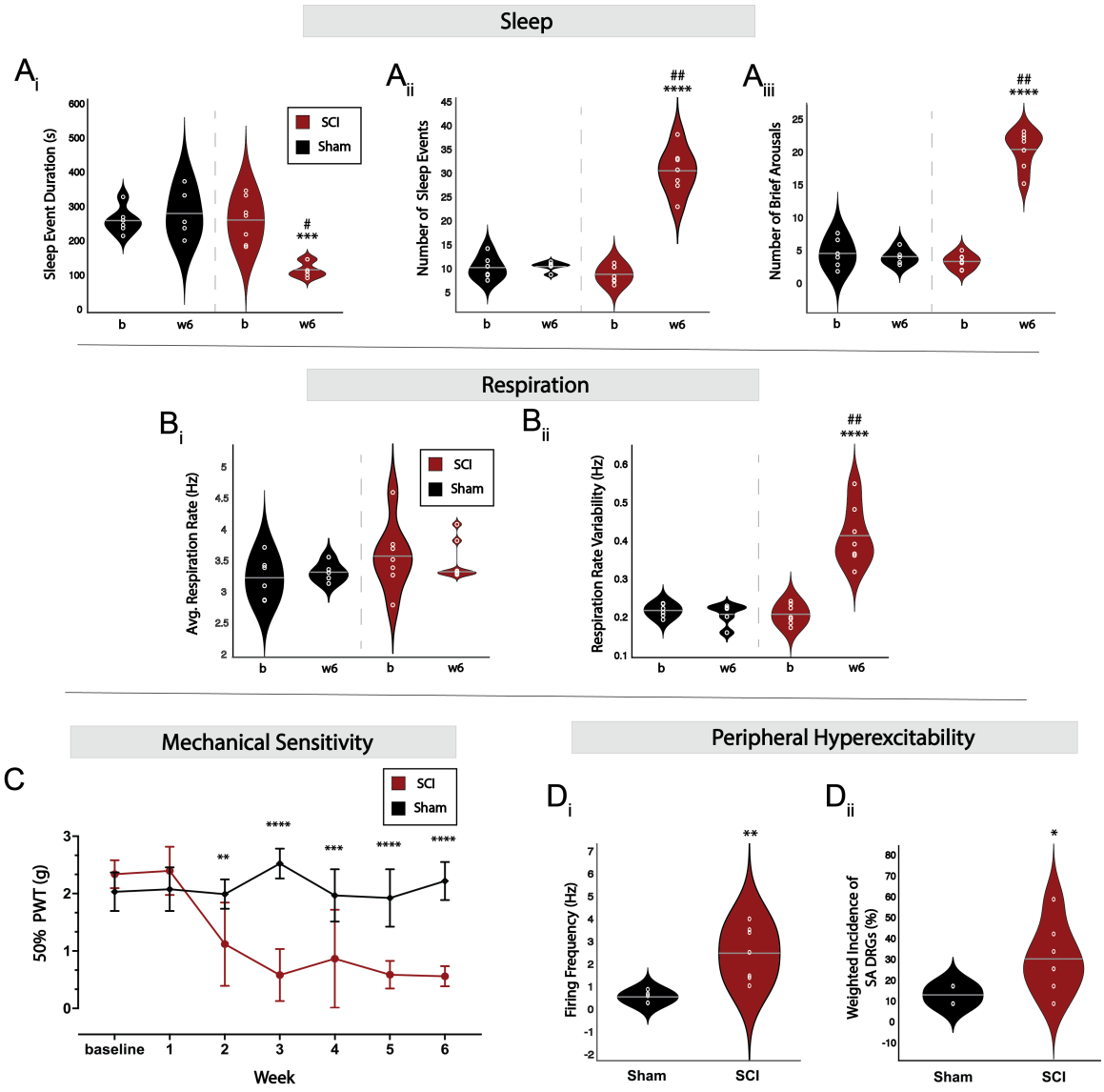

Figure 2.3: Features of sleep, respiratory, and sensory function are altered after SCI.

A) The median sleep event duration (**i**), number of sleep events/hour asleep (**ii**), and number of brief arousals/hour asleep (**iii**) during a 12-hour dark cycle is significantly different when comparing SCI vs Sham at postoperative week 6 (w6); and baseline (b) vs week 6 (w6) in the SCI group **B)** Average respiratory rate appears unaffected by SCI (**i**), while respiratory rate variability differs significantly when comparing SCI vs Sham at postoperative week 6 (w6); and baseline (b) vs week 6 (w6) in the SCI group (**ii**). **C)** Trends in paw withdrawal threshold (PWT) progress as expected over 6 weeks of von Frey behavioral testing. Beginning at postoperative week 2, significant differences are observed in 50% PWT for the SCI group, when compared to Sham. Graph depicts the mean values ±standard deviation. **D)** The maximal observed firing frequency (**i**) and weighted incidence (**ii**) of SA lumbar DRGs in the SCI group are significantly greater than that of the Sham group. For panels A, B and D, the data are presented as violin plots where each data point is the mean value for each animal sampled, the grey line is the mean value for the population, and width providing relative probability density distribution of the sample. SCI (n=7), Sham (n=5). The p-values are denoted throughout, as follows: SCI vs Sham at week 6- *p<0.05, ** p<0.005, *** p<0.0005, **** p<0.0001; baseline vs week 6 in the SCI group- # p<0.001, ##p<0.0001

2.4.5 After SCI, the incidence of spontaneously active DRGs correlate with the change in PWT

Peripheral hyperexcitability can manifest as exaggerated evoked responses or enhanced stimulus-independent, spontaneous activity. To assess the association between different aspects of peripheral hyperexcitability, correlation analysis for metrics of evoked and stimulus-independent (firing frequency and incidence of SA DRGs) sensory activity was performed. Across groups there was no correlation between these evoked or spontaneous ($p>0.05$). However, when looking at each animal's week 6 PWT change from its respective baseline value (residuals), DRG incidence was correlated with the decrease in PWT between baseline and week 6 in the SCI group ($r = -0.82$, $p<0.05$, **Figure 2.4A**). There was no correlation between these metrics, for the sham group.

2.4.6 Indices of spontaneous peripheral hyperexcitability correlate with functional shifts in sleep and respiration

To assess linear associations between the emergent sleep and respiration changes with indicators of peripheral hyperexcitability, we performed correlation analysis with sleep metrics (sleep duration, number of sleep events, and number brief arousals) and RRV. For sleep metrics and RRV, we quantified the residual change from baseline to week 6. There were no correlations across groups or in the Sham group, for any of the residualized metrics. However, in the SCI group, DRG incidence correlated with the residual number of sleep events between baseline and week 6 ($r = 0.78$, $p<0.05$, **Figure 2.4B**) and firing frequency correlated with the residual change in RRV ($r=0.9$, $p<0.01$, **Figure 2.4C**). No metrics of stimulus-independent hyperexcitability correlated with residual changes in sleep duration or number of brief arousals in SCI animals. Nor did the change in PWT correlate with the residualized RRV or sleep metrics in SCI animals.

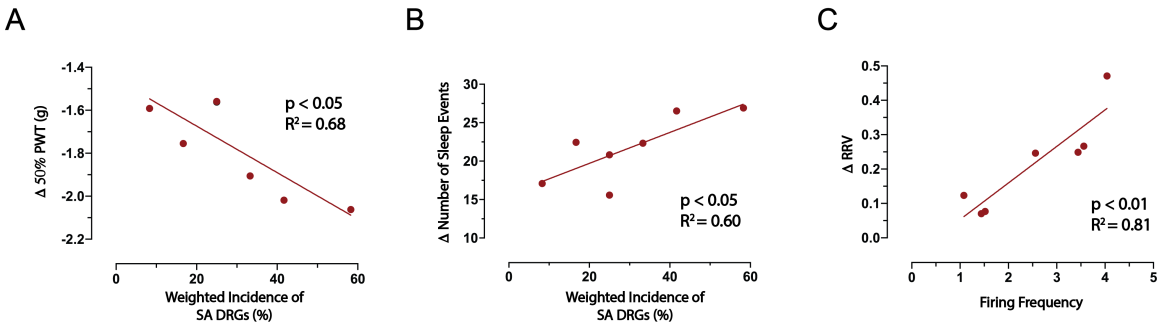

Figure 2.4: Spontaneous hyperexcitability metrics correlate with changes in evoked hyperexcitability, respiration, and sleep after SCI.

A: Incidence of SA DRGs in the SCI group has a negative correlation with the change in 50% PWT threshold (compared to baseline), measured at postoperative week 6. **B:** In the SCI group, the change in the number of sleep events at week 6 (compared to baseline) has a positive correlation with the incidence of below-level SA DRGs. **C:** Maximal firing frequency has a positive correlation with the change in respiration rate variability (compared to baseline) at week 6. Linear associations between metrics were determined by Pearson correlation and regression analysis. Each data point is a representative value for each animal sampled. SCI (n=7)

2.5 Discussion

The relationship between manifestations of pain and concomitant behaviors is highly convoluted and challenging to unravel. In a contusion model of neuropathic pain, we found that dysfunction in respiration, sleep, and mechanosensitivity significantly correlated with spontaneous primary afferent activity (peripheral hyperexcitability). This study is an important step toward understanding the complex changes that occur after SCI. It is the first to link sleep and respiration changes after SCI to peripheral hyperexcitability in mice and supports previous studies linking pain to ongoing spontaneous pain fiber activity [48][136] [137] [60] [118]. Moreover, we developed and applied novel approaches in noninvasive behavioral analysis to uncover previously unknown and understudied components of SCI pathogenesis.

2.5.1 Neural basis of neuropathic pain after SCI

Spontaneous primary afferent activity has been identified as a driver of chronic pain in clinical [34][35] and preclinical [50][49][51] [52][54][48][59] studies. In SCI models of

neuropathic pain, spontaneous activity in DRG neurons has been implicated in the development of behavioral indications of sensory hyperexcitability [48][59][60]. But these studies examined dissociated and cultured DRG neurons, a process which has been demonstrated to induce spontaneous activity [119]. Here we recorded from intact DRGs from multiple segments and confirmed that firing frequency and incidence of spontaneously active DRGs are higher after SCI. Though our recording technique did not permit resolution for classifying the spikes by primary afferent class, evidence suggests that spontaneous activity in A and C fibers are associated with neuropathic pain [50][49][51] [52][54][48][59][55][35] and have been observed in this particular SCI model [60].

Until recently, neural recordings of pain had been performed in isolation from the cognitive behavioral assay putatively measuring pain in rodent models. A landmark study [138] undertook *in vivo* recordings from populations of amygdalar neurons in naturally behaving mice to ascertain and differentiate reflexive from affective motivational components of pain. Their methods characterized a variety of evoked pain stimuli which allowed them to map pain-encoding neurons in the amygdala. Importantly, they were also able to identify that neuropathic pain activated the amygdalar pain matrix via non-pain encoding afferents. Importantly, the entire affective/motivational component of pain but not spinal reflex elements were entirely dependent on activation of this matrix. This work provides a crucial link between behavioral assays of pain and cognitive processing of pain, providing a more stable platform to interpret traditional behavior tests of pain.

In SCI animals, we showed a correlation between the change in PWT and the DRG incidence, where a greater reduction in PWT was observed in animals with a higher incidence of spontaneously active DRGs. DRG firing frequency and incidence were not correlated, suggesting that they may capture disparate aspects of ongoing pain or an alternate none pain encoding sensory signaling pathway (e.g. metabolic status, baroreceptors, hypoxia). The

incidence of spontaneously active DRGs may determine the size/number of dermatomal regions impacted by neuropathic pain—where a larger incidence is associated with a larger region impacted. Firing frequency could instead encode the intensity of pain experienced by a single region. This could explain the link between PWT and DRG incidence. The rodent hindpaw is innervated by axons with cell bodies in L3-L6 DRGs [139]. Broader hyperexcitability of these lumbar primary afferents could contribute to greater hindpaw sensitivity.

2.5.2 Behavioral methods to assess pain

Assessing pain in rodents is extremely challenging. While visual observation of animal grooming and social habits [140][118] can determine whether an animal may experience severe pain, these methods are unable to provide more than a qualitative assumption of pain and these behaviors can be influenced by myriad other symptoms. Several functional assessment assays (rotorod, grip strength, balance beam, Basso, Beattie, Bresnahan (BBB) open field test, vermicelli test, swim test) are able to partially quantify movement and task-related effects of pain [141][142][143][144]. Others (elevated plus maze, open field, light-dark box, grimace scale) are able to estimate putative emotional components of pain, though this is tenuous in mice which have highly adapted prey responses [145][146][147][148]. However, the standard approach to quantify pain-like behavior is through evoked tests (von Frey, Hargreaves, Mechanical Conflict System, Randall-Siletto, tail flick, cold/hot plate, acetone evaporation) that measure an escape response either through movement or vocalization [141][142][146][147][148]. Evoked behavioral tests of pain have been used for a variety of injuries and diseases with components of pain, but they have not performed well when assessing spontaneous pain.

Evoked paradigms of testing identify sensory hypersensitivity, but it is unclear if or how this hypersensitivity relates to increased spinal reflexes rather than the affective/motivational

component of nociceptive processing that requires actions on brain circuitry including the experience of chronic, spontaneous pain (Corder, Ahanonu et al. 2019)[138]. As mentioned above, Corder, et al, have been able to map pain-encoding neurons in the amygdala and connect their activity with several standard evoked behavioral assays used for pain. Importantly, that study confirmed that von Frey filaments applied to the plantar regions of the hind paw to test mechanical hypersensitivity do activate pain-encoding neurons in the amygdala. However, this does not preclude animal responses to evoked mechanical stimuli are also affected by changes in reflex response and sensitization [149][150].

Multiple tests have been developed (conditioned place preference, burrowing tests, weight bearing, gait analysis, thermal preference, automated home cages) to attempt to quantify spontaneous pain [150][151][152][148][147][146][141][153]. A forerunner, the conditioned place preference (**CPP**) assay offers method for measuring the affective/ motivational component of neuropathic pain. Findings suggest CCP successfully identifies animals with neuropathic pain [120][121][122], but this method relies on the efficacy of analgesics, animal mood, and training while having limited electrophysiological evidence supporting the presence of ongoing pain activity [154]. Another test, also included in the Corder, et al, neuropathic testing paradigm, determined that animals experiencing neuropathic pain develop adaptive thermal cold avoidance behavior when given free movement over a temperature gradient ranging from noxious cold (15°C) to preferred temperature (30°C). Though able to identify animals with neuropathic pain, both CPP and thermal gradient tests are unable to capture a spontaneous pain event at the time of occurrence or quantify the severity of spontaneous pain experiences. The limitations of these assays demonstrate a remaining need for behavioral metrics for measuring chronic, spontaneous pain.

Based on other studies conducted by our group, respiration features may provide a

method to identify specific spontaneous pain events. In unpublished data, our group measured respiration rate (RR) and variability (RRV) in awake, restrained mice before and after an injection of formalin, causing a short-term noxious inflammatory pain response, into the hind paw. These data showed increased RR corresponding with formalin. Likewise, other mice (observed in the same EF instrumented home-cages described in this SCI study) received a hind paw injection of complete freund's adjuvant (CFA), causing a long term noxious inflammatory pain response, and developed increased RRV during sleep similar to what we observed after SCI. Moreover, the hind paw mechanical sensitivity of CFA mice correlated with RRV ($p < 0.001$, $R^2 = 73$) suggesting that pain may contribute to RRV during sleep. Because we are able to measure respiratory features continuously, they may be useful in pinpointing spontaneous pain as it occurs.

2.5.3 Sleep changes after SCI

When asked, individuals with SCI are likely to report increased difficulty falling asleep, reduced sleep quality, a need for sleep medication and increased daytime sleepiness [155]. Even though the incidence of sleep dysfunction is greatly increased after SCI sleep dysfunction after SCI remains barely explored, and how this may impact various other comorbid events in SCI remain completely unexplored. That SCI itself already challenges physiological operation of sensory, motor and autonomic systems that impinge on cognition and psychological well-being surely warrants understanding the interrelation between sleep, emergent disorders and their normalization by controlling sleep.

Though SCI patients experience reduced sleep quality [123][124][125][126], there is limited research on the cause-effect relations between sleep compromise and co-morbid conditions after SCI, including chronic pain. While it is well established that sleep disruption and chronic pain are bi-directionally negatively reinforcing [124][156][125], their association in SCI has not been detailed clinically or in preclinical animal models. Though

there are several studies describing respiratory-related sleep dysfunction caused by cervical SCI [124][157][158], only one preclinical study (in rat) has reported non-respiratory-related sleep dysfunction after SCI [159]. The scarcity of preclinical work quantifying sleep changes after SCI is partially due to the invasiveness and difficulty in measuring rodent sleep; current methods to rely on invasive EEG recordings that itself introduces extra surgery, immune response, stress, and altered home cage environments that may complicate behavioral changes and pain after SCI.

The technological advance of the EF sensors has allowed our group to be the first to non-invasively quantify sleep changes in rodents after SCI. We observed that, after SCI, there is an increase in brief arousals contributing to reduced duration of individual sleep events and increased numbers of sleep events as the animals attempt to compensate. Though these measures are interrelated, they each highlight a different aspect of sleep fragmentation: sleep event duration helps infer whether an animal has had the opportunity to cycle through the different stages of non-REM prior to entering REM or waking up. If the sleep event is too short, it is likely the animal has not been able to achieve normal transitions for restorative sleep. The number of sleep events adds a longitudinal component by helping capture whether an animal's normal division of sleeping and waking is altered. The number of brief arousals confirms how frequently sleep disruptions are part of the animal's normal sleeping habits or whether sleep was prematurely interrupted and the animal attempts to enter sleep again quickly [160][161]. SCI animals experienced a combination of these measures strongly indicating disrupted, fragmented sleep.

Though sleep became more fragmented, the distribution of REM and non-REM was not significantly disrupted and the animal slept the same total time of the 12-hour dark cycle even, 6 weeks after SCI. However, though animals did not decrease their total time asleep, their sleep events started out grouped together at two time points during the dark

cycle (peaking at midnight and again at 3 am), but became evenly scattered across the 12 hours 6 weeks after SCI. Given the heightened mechanical sensitivity and increased SA DRGs after SCI, it would be intuitive to hypothesize that REM sleep would be reduced after SCI due to premature arousal caused by the concert of movements that define REM sleep. However, REM sleep is highly variable and occupies such a small proportion of total sleep time (5-15%), any change may have been overshadowed by inherent variability. Additionally, REM sleep occurs immediately prior to natural arousal, thus it is difficult to tell whether REM sleep resolved prior to arousal or caused premature arousal.

2.5.4 Linking pain and sleep dysfunction after SCI.

Many individuals with SCI have persistent ongoing spontaneous neuropathic pain [162] [163] [164] [165] [166] [167]. This pain is among the most disruptive and disabling forms of chronic pain with enormous impairment in daily activities and with a strong affective dimension (e.g. anxiety and depression) [168][169]. Evidence of ongoing spontaneous pain has been demonstrated in rodents [48][136][170][60][170], and should lead to similar alterations in affective state and daily activity. Yet this is difficult to measure [171]. Despite its importance, very few studies have been undertaken that assess spontaneous pain.

It is intuitively obvious that disrupted sleep and pain can coexist in a mutually reinforcing cycle of suffering. As observed clinically, pain can result in poor sleep quality [172][173]. In individuals with SCI, poor subjective sleep quality was associated with higher ratings of pain intensity, anxiety, and depression [156]. Chronic pain can increase arousals during sleep to reduce overall sleep quality [174]. Conversely, sleep impairments impact pain, including the development and maintenance of chronic pain, perhaps more reliably so than the reverse[173]. In preclinical animal models, sleep disruption can cause acute and long-lasting hypersensitivity to painful stimuli [175] and it leads to mechanical sensitivity in both healthy and peripheral nerve-injured rats [176].

Currently there is very limited preclinical animal studies devoted to assessing sleep changes after SCI. Emphasis is on respiratory-related sleep disorders resulting from cervical SCI [127][128][129]. Only one study looked at and observed sleep dysfunction independent of respiration [159]. In our studies we observed a shift to dysfunctional sleep after SCI. This presented as increases in sleep event count and brief arousal count, along with a decrease in median sleep event duration; all of which indicated more segmented sleep. In the SCI population, the change in sleep event count correlated with the incidence of spontaneously active DRGs-where a larger increase in sleep event count (indicative of increased sleep disruption) occurred in animals with a higher DRG incidence. If DRG incidence corresponds to the number of dermatomes impacted by pain, it is reasonable to assume that these animals may experience pain over a larger surface area that coincides with greater difficulty sleeping.

There was also a positive correlation between DRG firing frequency and RRV, suggesting that a higher magnitude of spontaneous primary afferent activity at a single segment may be related to more erratic breathing, after injury. One possibility is that these afferents are not associated with conventional pain pathway but project to brainstem central autonomic circuitry that do not lead to the experience of pain [177].

2.6 Conclusions

Peripheral hyperexcitability has been previously observed in SCI models of neuropathic pain. Here we found correlations between spontaneous lumbar DRG activity (incidence and firing frequency) and metrics of sleep and respiratory dysfunction–complications frequently observed in SCI patients. The findings suggest that in addition to examining primary afferent activity, non-contact recording of sleep and respiratory features may serve as a useful tool for identifying the emergence of persistent spontaneous neuropathic pain in animal models of SCI.

2.7 Research Contributions

Training for animal surgeries and use of the Infinite Horizons (IH) impactor was provided by Kamarcha Martin and the Garraway Lab, headed by Dr. Sandra Garraway. Animal surgeries were performed by Shaquia Idlett-Ali and Mallika Halder. Tissue isolation, electrophysiology experimentation, and analysis was performed by Shaquia Idlett-Ali. Behavioral testing and analysis was conducted by Dr. Heidi Kloefkorn. Shaquia Idlett-Ali authored this chapter with collaboration from Dr. Heidi Kloefkorn and Dr. Shawn Hochman.

CHAPTER 3

CHARACTERIZATION OF AXONAL RECRUITMENT WITH SCS

3.1 Abstract

Spinal cord stimulation **(SCS)** is used clinically to limit chronic pain, but fundamental questions remain on the identity of axonal populations recruited. We developed an ex vivo adult mouse spinal cord preparation to assess recruitment following delivery of clinically analogous stimuli determined by downscaling a finite element model of clinical SCS. Analogous electric field distributions were generated with 300 μm x 300 μm electrodes positioned 200 μm above the dorsal column **(DC)** with stimulation between 50 and 200 μA. We compared axonal recruitment using electrodes of comparable size and stimulus amplitudes when contacting the caudal thoracic DC and at 200 or 600 μm above. Antidromic responses recorded distally from the DC, the adjacent Lissauer tract **(LT)**, and in dorsal roots **(DRs)** were found to be amplitude and site dependent. Responses in the DC included a unique component not seen in DRs, having the lowest SCS recruitment amplitude and fastest conduction velocity. At 200 μm above, mean cathodic SCS recruitment threshold for axons in DRs and LT were 2.6 and 4.4 times higher, respectively, than DC threshold. SCS recruited primary afferents in all (up to 8) caudal segments sampled. Whereas A and C fibers could be recruited at nearby segments, only A fiber recruitment and synaptically mediated dorsal root reflexes were observed in more distant (lumbar) segments. In sum, clinically analogous SCS led to multisegmental recruitment of several somatosensory-encoding axonal populations. Most striking is the possibility that the lowest threshold recruitment of a nonprimary afferent population in the DC are postsynaptic dorsal column tract cells **(PSDCs)** projecting to gracile nuclei.

3.2 Introduction

Peripheral somatosensory afferents enter the spinal cord via dorsal roots and many issue axon collaterals into the most prominent white matter tract known as the dorsal column **(DC)**. The DC contains axons of large diameter A$\alpha\beta$ myelinated primary afferents that encode complex sensory information on touch and proprioception [16]. Though these myelinated primary afferents are the predominant DC constituent, unmyelinated axons and ascending projections from spinobulbar postsynaptic dorsal column **(PSDC)** tract neurons also reside in the DC [12][13][15][14][16]. PDSC tract neurons are known to receive multi-convergent synaptic inputs from various primary afferents [16]. Immediately lateral to the DC is the Lissauer tract **(LT)** which is largely comprised of primary afferent axon collaterals (predominantly C fibers) and implicated in the regulation of spinal receptive field size and gating of pain transmission [11][178].

Epidural spinal cord stimulation **(SCS)** can depress refractory pain signaling via electrodes positioned at the posterior (dorsal) epidural space above the DC. Approximately 50,000 stimulators are implanted yearly for patients diagnosed with various pain syndromes with failed back surgery syndrome having among the highest success rates [62][179]. SCS is thought to recruit DC Aβ fibers and inhibit pain via the Gate Control Theory of Pain. This theory postulates that antidromic Aβ fiber excitation inhibits nociceptive transmission through the action of inhibitory interneurons within the dorsal horn [80][180]. It has been assumed that Aβ fiber recruitment from a single dermatome is the core mechanism of SCS-induced pain control even though SCS may also recruit other neuronal populations (e.g. postsynaptic dorsal column tract cells) and despite its inability to explain many clinical observations [99][3][95][2].

Most experimental inquiries into mechanisms underpinning the actions of SCS utilize

in vivo studies with anesthetized rodents in well-characterized models of neuropathic pain [181][100][114]. Several have used amplitudes scaled relative to motor threshold to assess modulation of nociceptive transmission in pain models [106][96][97][111][107]. However, basic questions on the identity of axons recruited have not been convincingly addressed. Here, we used dimensional electrode scaling and model-based identification of SCS parameters to inform experimental assessments of axon fiber recruitment properties in DC, dorsal roots **(DRs)**, and LT using 'clinically analogous' SCS. LT's proximity to DC, and subsequently the SCS electrode, potentially presents an alternate site of recruitment and modulation.

We examined variability in axonal recruitment to several preclinical SCS parameters including stimulation site, stimulation distance, amplitude, polarity and pulse duration. Results from these studies answer fundamental questions regarding the recruitment of different fiber populations and segmental circuits.

This work has been presented previously in abstract form [182][183], and has been published as a journal article [184] .

3.3 Materials and Methods

3.3.1 Preclinical electrode scaling

To conduct preclinical experiments in the mouse with clinically-analogous SCS, the electrode dimensions were scaled with reference to clinical contact sizes and the mediolateral and dorsoventral dimensions of the adult mouse spinal cord **(Figure 3.1A, 3.1B)**. For both rat and mouse, T10 spinal cross-section profiles were generated by tracing the gray matter and white matter boundaries over one side of the T10 spinal segment, according to the cross-section from the anatomical atlas [185], reflecting the traced profile of the hemisphere over the midline of the segment, and concatenating the original and reflected tracings

to form a symmetric cross-section **(Figure 3.1C)**. The magnitude of the differences in the lengths of the major and minor axes between an unscaled rat T10 spinal segment and scaled mouse T10 spinal segment, was plotted as a function of the mediolateral and dorsoventral scaling factors applied to the mouse spinal segment **(Figure 3.1D)**. Major and minor axis lengths for both the rat and mouse spinal cord were determined respectively from the maximum mediolateral and dorsoventral extents of the white matter tracings. The scaling factor generating the minimum error in cross sectional area between the mouse and rat spinal segment (rat:mouse, 1:1.8) was then related to the human to rat scaling factor of (human:rat, 1:2.5) previously determined; with the overall scaling between human to mouse spinal cord being (human:mouse, 1:4.5) An atlas of the rat and mouse spinal cord [185] provides high resolution images at all spinal levels from rat and mouse as well as a specific scaling factor between human and rat thoracic cord—from which we derived the human-to-rat translation factor and then determined that the rat and mouse thoracic cord are qualitatively anatomically similar. However, no direct scaling data from human to mouse was included in the reference—hence the intermediate step. Based on these scaling factors, verbatim scaled contacts will have lengths of 0.67 mm and widths of 0.30 mm. As dorsal columns are organized by dermatome in the medial-lateral direction [18][19], and as approaches to improve the spatial selectivity of SCS have focused on constraining the medial-lateral dimension of the activation region [69][186], subsequent model simulations were conducted using square contacts with side lengths corresponding to the smaller medial-lateral dimension of the scaled down clinical electrodes (0.3mm x 0.3mm). Constraining electrode dimensions seemed advantageous for experimental studies of recruitment as this allowed for greater specificity in target of SCS, aiding in analysis and understanding of experimental outcomes.

3.3.2 FEM model: mouse spinal cord

A three-dimensional finite element model **(FEM)** of both the *in vivo* mouse spinal cord and the *ex vivo* mouse spinal cord recording setup was created in COMSOL Multiphysics

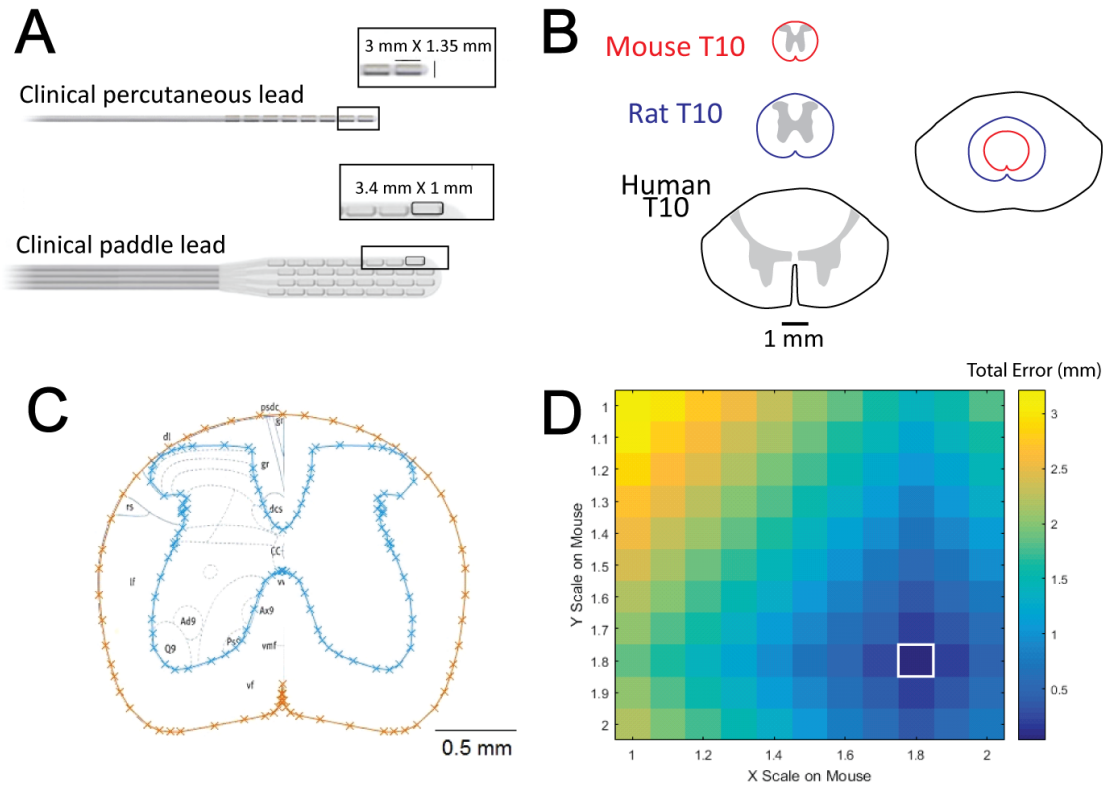

Figure 3.1: Preclinical electrode scaling.

A) Examples of a 1x8 clinical cylindrical percutaneous lead and a 4x8 clinical paddle lead provided by Boston Scientific. The contact dimensions are 3mm x 1.35mm and 3.18mm x 1.4mm, respectively. The appropriate size of SCS electrodes for subsequent computational modeling and preclinical experimentation was determined by scaling the dimensions of these contacts with respect to the cross-sectional area of the mouse spinal cord. **B)** Comparison of relative sizes of human, rat and mouse T10 spinal cord. **C)** Example mouse cross-section generated from an anatomical atlas of the spinal cord. The cyan and orange lines depict the gray and white matter boundaries, respectively. **D)** Rat and mouse error comparisons for major and minor axes: magnitude of the differences in the lengths of the major and minor axes between an unscaled rat T10 spinal cord and scaled mouse T10 spinal cord, plotted as a function of the mediolateral (major) and dorsoventral (minor) scaling factors applied to the mouse spinal cord. Colors denote the magnitudes of the total difference in lengths of the major and minor axes measured in mm. This analysis supports rat:mouse scaling factor of 1.8 (white box). When related to the previously determined human:rat scaling factor, the human:mouse scaling factor is 4.5.

(Version 5.1, COMSOL Inc., Burlington, MA) to compare the electric fields (and thereby currents) generated by the scaled down electrodes in the experimental preparation with those expected to be generated by the same electrode in an *in vivo* mouse and by a commercial epidural lead in a human. For the *in vivo* FEM, the dimensions of the CSF space, dura, epidural fat, and vertebral bony layers were generated by downscaling the x and y dimensions of the corresponding anatomical features from a previously published FEM of the human thoracic spinal cord [94] by factors of 4 and 4.5, respectively, derived from the previously described scaling procedure. Dirichlet boundary conditions ($V = 0$) were used at the lateral and dorsoventral boundaries of the model, and Neumann boundary conditions ($n \bullet J = 0$) were used at the rostrocaudal boundaries of the model. For the *ex vivo* FEM, the model was scaled according to the actual experimental setup and consisted of an insulated rectangular chamber measuring 76 mm in length, 45 mm in width, and 8 mm in depth filled with artificial CSF and a 1 mm diameter ground wire placed 10 mm from the center of the stimulation lead(**Appendix A.1**). In the *ex vivo* model, the faces of the ground wire were set to Dirichlet boundary conditions ($V = 0$), and the other outer boundaries of the model were set to Neumann boundary conditions ($n \bullet J = 0$).

An extruded mouse spinal cord 35 mm in length and a model of the experimental stimulation lead were preserved across both the *in vivo* and *ex vivo* models. The dimensions of the gray and white matter of the mouse spinal cord were obtained by directly tracing the left half of a slice image of the Mouse T10 spinal cord [185] and reflecting the tracing over the midline using MATLAB (Version R2015a, MathWorks, Natick, MA) before being imported into COMSOL. Furthermore, the gray matter was displaced 20 μm ventrally from the original tracing to allow the spacing between the dorsal gray matter and white matter boundary to fulfill the minimum mesh element size requirement of the finest mesh setting in COMSOL (approx. 15.2 μm). Stimulating leads were modeled as conductive thin cubic domains with a side length of 0.3 mm surrounded by a rectangular insulating substrate

Table 3.1: *Tissue conductivities and isotropy used in finite element models of the mouse spinal cord.* Values were based upon and updated from Lee et al. 2011[94].

Tissue	**Isotropy and Conductivities** (σ if isotropic, σ_x, σ_y, σ_z if anisotropic; units S/m)
Gray Matter	Isotropic, $\sigma = 0.23$
White Matter	Anisotropic, $\sigma_x = 0.083$, $\sigma_y = 0.083$, $\sigma_z = 0.60$
CSF	Isotropic $\sigma = 1.70$
Dura	Isotropic $\sigma = 0.6$
Epidural Fat	Isotropic $\sigma = 0.04$
Conductor	Isotropic $\sigma = 5 \bullet 10^{6}$
Insulator	Isotropic $\sigma = 1 \bullet 10^{-7}$
Bone	Isotropic $\sigma = 0.02$

with outer dimensions of 2.4 mm X 0.6 mm X 0.5 mm and suspended from an insulating cylindrical electrode mount 0.4 mm in diameter and centered on the rectangular substrate. The ventral surfaces of each contact on each lead were each set to a uniform current density with Neumann boundary conditions corresponding to the total stimulation amplitude (50, 200 μA) divided by the surface area of each lead [187]. Stimulation currents from each of the two contacts were set to the same amplitude at opposite polarities to depict the electric field generated by bipolar stimulation in the spinal cord proximal to the leads. Domain conductivities representing tissues and materials of interest are shown in **Table 3.1**, and domain permittivities were set equal to the permittivity of free space, consistent with the quasi-static assumption [188]. Results for each model were then obtained by solving for Laplace's Equation ($\nabla \bullet \sigma \nabla \mathrm{V} = 0$) over an adaptively scaled tetrahedral mesh.

Constant-current stimulators provide compliance voltages that automatically adjust to the tissue impedance. Boundary conditions of the model were set with this in mind. As significant clinical variability exists in patient perception thresholds, the theoretical outcomes of the model are representative of electric field strengths expected. The amplitude

of current delivered to the mouse model was scaled using the intended experimental geometry for the voltages and electric fields to conform to the clinical ranges without severe discrepancies. One clear limitation of the mouse model is that it represents a scaling from this normalized, exemplary range.

3.3.3 Spinal cord isolation

All procedures were approved by the Emory University Institutional Animal Care and Use Committee: C57/Bl6 mice (both sexes, n=35, P60 and older) were anesthetized with ketamine (100mg/kg) and xylazine (10mg/kg) mix by intraperitoneal injection, following light anesthetization in an isoflurane chamber. To induce tissue hypothermia, the dorsal skin overlying the vertebral column was removed and mice were placed in an ice bath until there was a noticeable slowing of the respiration rate (2-3 minutes) prior to decapitation and isolation of spinal cord in a dish containing ice cold, oxygenated (95% O_2 / 5% CO_2) low-Ca^{2+} artificial cerebral spinal fluid **(aCSF)** containing (in mM), [NaCl 128, KCl 1.9, $MgSO_4$ 13.3, $CaCl_2$ 1.1, KH_2PO_4 1.2, glucose 10, $NaHCO_3$ 26]. The isolated cord was equilibrated to room temperature for 1 hour, then pinned dorsal side up in a Sylgaard-lined recording chamber while superfused with an oxygenated aCSF containing (in mM), [NaCl 128, KCl 1.9, $MgSO_4$ 1.3, $CaCl_2$ 2.4, KH_2PO_4 1.2, glucose 10, $NaHCO_3$ 26], at ˜40ml/minute. All experiments were undertaken at room temperature.

3.3.4 Histological test of spinal cord viability

In 4 experiments, 8 hours following spinal cord isolation and experimentation, the spinal cord was fixed in 2% paraformaldehyde for two hours, rinsed with phosphate buffer solution (PBS), sectioned with a vibrating blade microtome (Leica VT1000S) in 300 micron thick slices, and stained 30- 60 min in 1:250 Neurotrace (N-21482/Molecular Probes) mixed in PBS with 0.3% triton, then washed twice in PBS without triton. Captured images of stained slices allowed assessment of neuronal anatomical integrity (Nikon Eclipse E800

microscope with DXM1200 camera).

3.3.5 Electrophysiology

The DC is largely comprised of myelinated A$\alpha\beta$ primary afferents fibers that transmit proprioceptive and mechanosensitive information but also includes ascending projections from PSDC tract neurons and unmyelinated axons, while the neighboring LT mostly consists of C fibers with short-range projections and Aδ nociceptors with long-range projections [11] **(Figure 3.2A)**.

Experimental characterization of axonal recruitment was conducted with clinically-analogous SCS using a bipolar electrode constructed of two glass electrodes (300 μm tip diameters, 1.5-2 mm separation) filled with aCSF, and positioned (rostrocaudally) medial over the DC, typically in caudal thoracic segments (T9-T11; **Figure 3.2B**). Circular glass electrodes were used for experimental studies due to the repeatability of the construction process relative to manual cutting of 300 x 300 μm electrodes. A constant-current stimulator [189] was used to deliver a single monophasic pulse of bipolar SCS while contacting (0 μm) or above the spinal cord DC (200 or 600 μm). Stimulation amplitudes were incrementally increased from 1 to 500 μA with 50, 200, 500 μs pulse durations, for assessments of recruitment threshold. The advantage of a constant-current stimulation protocol, based on modeling studies, is that resistivity values normally seen for dura and arachnoid do not significantly affect spinal cord current densities [86]. Thus, our experimental arrangement excludes the presence of dura but still is expected to realistically appraise neural system recruitment at defined electrode configurations and distances from the spinal cord at the stimulus intensities applied.

Glass recording suction electrodes were positioned in the lumbar spinal cord on the DC (200 μm tip diameter), DR (200-250 μm tip diameter), and LT (1-2μm tip diameter, 3-5

MΩ). Targeted recording of LT was accomplished by positioning a glass microelectrode lateral to the dorsal column, in between dorsal root entry zones. Appropriate positioning was confirmed by stimulating the ipsilateral spinal cord 1-3 spinal segments rostral to the recording site and observing that the conduction velocity of evoked response was slower than that recorded in DR and DC of the same segment. Recruitment threshold was defined as the lowest stimulus amplitude producing a greater than 50% response rate in any recording location. Since threshold was typically lowest for DC axonal recruitment (see Results), relative thresholds for recruitment were standardized as the multiple of DC recruitment threshold ($\mathbf{T}_{DC}$) necessary to elicit responses in LT and DR. All recorded data were digitized at 50 kHz (Digidata 1322A 16 Bit DAQ, Molecular Devices, U.S.A.) with pClamp acquisition software (v. 10.7 Molecular Devices). Recorded signals were amplified (5000x) and low-pass filtered at 3 kHz using in-house amplifiers. Unless otherwise stated, reported results are for cathodic stimulation 200 μm above the cord with 200 μs pulse duration. Recruitment order trends for cathodic and anodic stimulation were similar, despite difference in polarity. Cathodic stimulation, in some cases, recruited populations at a similar or lower threshold and SCS experimental studies utilizing monophasic stimulation frequently report observations based on cathodic stimulation [100][111][110][107]. This is likely due to knowledge that cathodic stimulation recruits neural tissue at lower amplitudes than anodic stimulation [190][191][192]. For these reasons, we chose to focus our reporting on cathodic stimulation. In all data presented, the number of animals utilized for analysis is represented by the noted n-value. For each animal, a representative value was determined by averaging the response from multiple sweeps/trials within that animal (a minimum of 5).

3.3.6 Electrode configurations for estimating conduction velocity

Central CV was calculated based on the distance between the site of SCS and the recording electrode. Specifically, central CV of recruited axons was measured between the cathodic

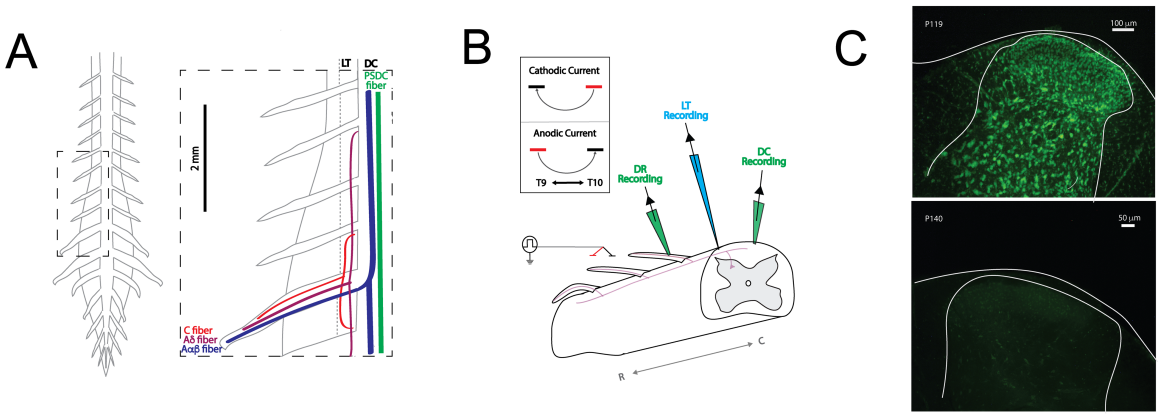

Figure 3.2: Ex vivo adult mouse preparation: experimental setup and viability.

A) Examples of a 1x8 Schematic of gross anatomy of spinal cord from dorsal surface and simplified organization of axon fiber populations subject to recruitment by SCS (inset). Axonal recruitment with SCS was assessed in dorsal roots (DR), dorsal column (DC), and Lissauer tract (LT). While the DC predominately carries non-nociceptive sensory information, the neighboring LT contains projection from nociception transmitting primary afferents. **B**) Schematic of general experimental paradigm. Two electrodes (about 1.5mm apart) are placed on or above the medial DC in a region between T9 and L3. This is used to simulate a bipolar SCS system. Responses to SCS are recorded via glass suction electrodes on the DC and DRs and a microelectrode on LT. *inset*: orientation of bipole (cathode-black, anode-red) and direction of current flow for cathodic and anodic stimulation used for experimental studies. R and C denote rostral and caudal, respectively **C**) Post-experimentation Nissl staining revealed persistent cellular viability 8 hours after cord isolation (top) but dramatic deterioration when superfused for 2 hours in the absence of oxygenation (bottom).

electrode used for stimulation and distal recording electrodes placed either near the midline of the dorsal column or more laterally at the dorsal root entry zone. To estimate peripheral CV, we positioned two suction electrodes on individual DRs at least 3 mm apart (L3, L4, or L5) to calculate differences in time of arrival of the antidromic afferent volley [193]. CVs of different volley components were calculated post-hoc to identify the afferent classifications (i.e. A$\alpha\beta$, Aδ, C) using published findings of primary afferent CV in dorsal roots at room temperature [6][193]. The fastest conducting components observed likely include antidromic responses of proprioceptive (group I&II; here denoted as Aα) and cutaneous afferents (Aβ). For uniformity with previous publications we label the fastest conducting myelinated components as A$\alpha\beta$ fibers responses.

Statistical differences in recruitment threshold, with respect to SCS stimulation distance (0, 200, and 600μm), were analyzed using Ordinary one-way ANOVA with Tukey correction for multiple comparisons. Differences between the relative recruitment thresholds of DC, DR, and LT were analyzed using the Friedman test with Dunn's correction for multiple comparisons. Analysis of conduction velocity differences were performed using a paired t-test. Unless otherwise stated, the results are presented as the mean ±SD with statistical significance being ascribed at $p < 0.05$.

3.4 Results

3.4.1 Anatomical evidence of viability

Nissl positive neuronal staining was observed in tissue fixed 8 hours after experimentation. As a control, a spinal cord isolation was conducted using the same procedures except the cord was superfused without oxygen for two hours, which lead to a near complete absence of Nissl stain **(Figure 3.2C)**. Demonstrated viability and increased access to the spinal neuraxis without anesthetics supported the use of this *ex vivo* model for electrophysiological investigations on SCS.

3.4.2 Preclinical finite element analysis model

Preclinical stimulation was simulated using a bipolar electrode consisting of two square contacts, dimensions which are noted above, with an edge-to-edge spacing of 1.2 mm and positioned epidurally over the dorsal surface at the midline of the spinal cord, for both the *ex vivo* and *in vivo* models described above. The clinical standard for SCS electrode placement involving SCS at conventional frequencies associated with paresthesia-based SCS involves implantation of the electrode at the T7-T8 vertebral segments, with the intent of targeting the dorsal column fibers coursing through the T9-T10 spinal cord level. Using a mouse model of the T9-T10 spinal cord is consistent with this therapeutic approach and with prior literature [194]. The electric field magnitudes generated during *ex vivo* preclinical SCS (50 to 200 μA), with a cerebrospinal **(CSF)** fluid layer of 0, 200, or 600 μm, were compared to those generated in the clinical model with a typical range of SCS amplitudes (3 and 10 mA). Results from analysis were used to guide experimental investigations in the *ex vivo* adult mouse spinal cord. Qualitatively, preclinical SCS positioned 200μm (50-200 μA) above the spinal cord in the *ex vivo* model generated electric field distributions comparable to those generated by clinical SCS **(Figure 3.3)**. Preclinical SCS 0 μm above the spinal cord with the same amplitudes (50-200 μA) suggests broader recruitment of populations in the DC and dorsal horn, than would be observed in the clinical SCS; indicating that lower stimulation amplitudes than those modeled would be advised for analogous recruitment. While, stimulation 600 μm above suggests that higher amplitudes of stimulation would be necessary to capture the range of electric field distributions observed in the clinical case. Comparisons between *ex vivo* and *in vivo* preclinical cases suggests that while 200 μm is suitable for the *ex vivo* preclinical SCS, 600 μm *in vivo* most closely mimics the relative CSF thickness in human and the bone, fat, and dura contributes to the generation of comparable electric field distributions with stimulation this distance above the cord **(Appendix B.1)**.

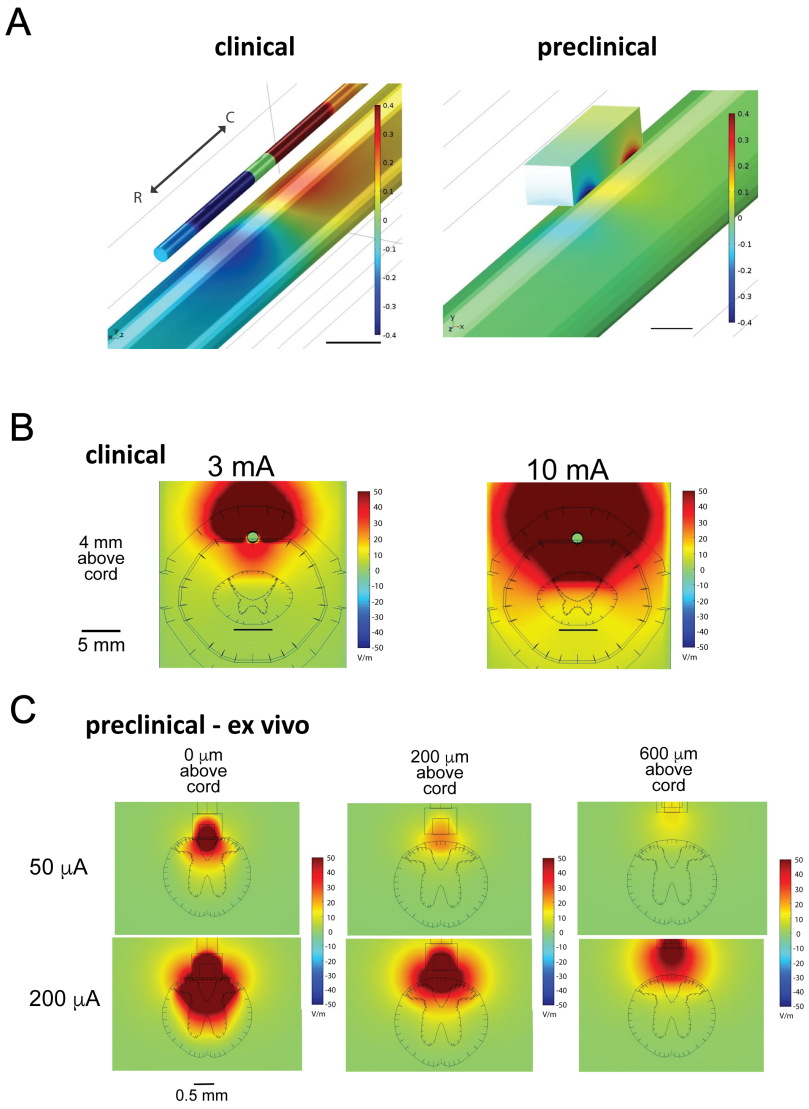

Figure 3.3: Finite element modeling of electric field magnitudes identifies stimulation amplitudes for clinically- analogous SCS in the adult mouse.

A) Rostrocaudal orientation of bipole for clinical (left) and preclinical (right) SCS. The anode (red) is rostral over the spinal cord (T9) and the cathode (blue) is caudal over the spinal cord (T10). Scales capped at ±0.4 V, scale bars correspond to 5mm and 0.5mm **B)** Clinical: Electric field magnitudes in the human spinal cord during stimulation generated using a finite element model of clinical bipolar SCS with a clinical 1x8 percutaneous lead with amplitudes in the typical range. **C)** Preclinical ex vivo: Electric field magnitudes in the spinal cord during SCS generated using a finite element model of the *ex vivo* mouse spinal cord (absence of dura, epidural fat, and bone) in a rectangular bath of cerebrospinal fluid, equivalent to experimental conditions. The properties, mesh settings, and boundary conditions of the finite element model are consistent with that of the clinical model except that all dimensions have been scaled down by a factor of 4.5. Stimulation was simulated using a bipolar electrode consisting of two square contacts of side length 0.3 mm with an edge-to-edge spacing of 1.2 mm and positioned epidurally 0, 200, or 600 μm over the dorsal surface of the midline of the spinal cord. The fields generated at 200 μm above the spinal cord are most comparable to those generated in the clinical conditions.

3.4.3 SCS recruits afferents that invade multiple dorsal roots and conduct at velocities consistent with all primary afferents

Multisegmental recruitment was directly assessed with bipolar SCS (50 and 200 μA, 200 μs) positioned 0 μm (n=5) or 200 μm (n=3) above the DC. Afferent recruitment was seen in all caudal DRs sampled, the most caudal being 8 spinal segments away **(Figure 3.4)**. In the example shown, T9/T10 SCS recruitment was abolished following DC lesion above T11 demonstrating that stimulation recruited axons at the stimulation site with subsequent antidromic propagation to DRs. CVs were divided into three categories approximating reported peripheral CVs of A$\alpha\beta$ (>4.2 m/s), Aδ (0.56-4.2 m/s) and C fibers (<0.56 m/s) at room temperature [6].

To accurately identify afferent classes based on peripheral CV, we used the two-point recording method in DRs **(Figure 3.4B; Table 3.2)**. We observed a rostrocaudal distance-dependence of electrode position on afferent recruitment. By reducing stimulus amplitude (50μA), we also observed that low amplitude SCS only recruited A fibers in DRs from nearby spinal segments (0-3 segments away; n=8) and that higher amplitude SCS (200μA) was required to recruit A fibers in more distant dorsal roots (n=7; **Figure 3.4B; Table 3.2**). Higher amplitude and longer pulse duration SCS also recruits slower conducting Aδ and C fibers in DRs of nearby segments **(Figure 3.4B; Table 3.2)**. Though recruitment of C fibers was not observed in DRs distal to SCS, we cannot exclude the possibility that multisegmentally-projecting unmyelinated C fibers [195] were undetectable due to dispersion of the volley.

3.4.4 SCS evokes synaptically-mediated recruitment of primary afferents

Dorsal root potentials **(DRPs)** and dorsal root reflexes **(DRRs)**—resulting from primary afferent depolarization **(PAD)**—were observed with SCS. These longer latency, synaptically-mediated events had variable onset latency and amplitude (observed in 13 of 23 animals).

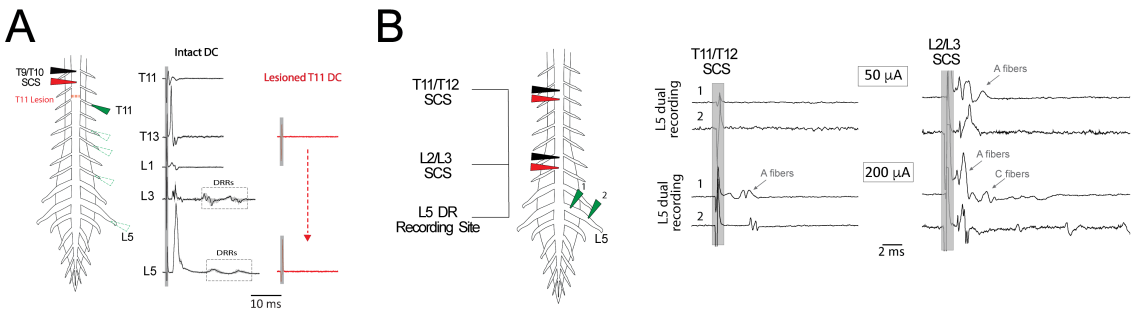

Figure 3.4: SCS recruits primary afferents that invade multiple segmental dorsal roots and conduct at velocities consistent with all classes of sensory fibers.

A) SCS directly activates afferent axons that project to multiple caudal spinal segments. A single pulse of SCS (200μA, 200μs) was applied 200 μm above T9/T10 and antidromic responses in select caudal DRs (T11-L5) were recorded before (black) and after (red) DC lesioning above T11 with iridectomy scissors. Lesion of the DC blocked all stimulus-evoked responses in DRs. Each trace is the average response of 10 sweeps. **B)** Distant dependent recruitment of afferent fiber populations can be identified by differences in peripheral CV. Here, bipolar SCS was applied 200 μm above T11/T12 or L2/L3 at amplitudes of 50 and 200 µA (500μs). T11/T12 SCS led to the recruitment of A fibers in the L5 DR, but only at the higher stimulus amplitude (at arrow). In comparison, SCS at a closer segment (L2/L3) recruited A fibers at the lower intensity with higher magnitude stimulation leading to recruitment of slower conducting C fibers (at arrows). Each trace is the average of 6 sweeps. The peripheral conduction velocities estimated using this configuration are summarized in **Table 3.2.** The gray box identifies the location of stimulation artifact.

Table 3.2: *Distant dependent recruitment of different classes of primary afferents with SCS.* The peripheral conduction velocity of dorsal root afferents was determined using the two-point method on lumbar roots, with SCS positioned 200μm above the dorsal column. This table displays the conduction velocity (mean±SD) of the fastest components in each class of afferents when SCS was applied closer to **(A)** or further from **(B)** the DR recording site (for schematic, see **Figure. 3.4C**). Afferent classification was determined as described previously [6]. In cases where recruitment was observed in less than half of experiments, a null value is listed (-) to best depict the general recruitment result.

A. SCS 7-9 Segments Rostral (n=7)						
Amplitude (μA)		50		200		
Duration (μs)		200	500	50	200	500
Mean Conduction Velocity (m/s)	A$\alpha\beta$	-	-	-	9.6±3.7	12.9±4.8
	Aδ	-	-	-	3.3±0.3	3.4±0.9
	C	-	-	-	-	-
B. SCS 0-3 Segments Rostral (n=8)						
Amplitude (μA)		50		200		
Duration (μs)		200	500	50	200	500
Mean Conduction Velocity (m/s)	A$\alpha\beta$	12.7±8.0	11.7±4.5	12.2±8.3	15.3±8.0	15.7±7.7
	Aδ	-	-	-	2.3±1.2	2.4±0.9
	C	-	-	-	-	0.4±0.03

Recordings at the dorsal root entry zone **(DREZ)** permitted observation of both events, with suprathreshold DRRs' arrival coinciding with the presence of the DRP **(Figure 3.5A,Bi)**. Recordings away from the DREZ led to observations of only DRRs. The jitter and sensitivity of this activity to bicuculline (10 μM, n=4) confirmed it as synaptically-mediated **(Figure 3.5B)**.

Two distinct populations of DRRs were commonly observed in lumbar DRs, the earliest event being 9.0 ±1.6 ms after the onset of the direct antidromic response, with the second DRR event occurring 9.2 ±1.2 ms later. Thresholds for direct antidromic axonal recruitment and synaptically-mediated (indirect) DRRs were comparable with mean threshold for DRR recruitment being numerically only 3.8 ±2.2 μA higher than the antidromic event (n=5; p $>$0.05, paired t-test; **Figure 3.6**). This suggests that the indirect recruitment is activated by excitation of low threshold primary afferents. The population(s) of axons receiving primary afferent depolarization was not identified, but the presence of two different populations of DRRs suggests that one population may be initiating PAD, while two separate populations could be receiving PAD **(Figure 3.5C)**; though it is also possible that the second DRR event reflects recurrent activity initiated by the first DRR event or doublet firing within the same recruited axons.

3.4.5 Characterization of dorsal column recruitment with SCS

Dorsal column recruitment was also characterized in the adult mouse spinal cord as depicted in **Figure 3.7A** (left). Recruitment of axons in DR, DC and LT was compared when SCS was contacting (0 μm), 200 μm, or 600 µm above the spinal cord (n=12). Direct recruitment of axons in LT was identified based on a lack of variability in onset latency and amplitude (**Figure 3.7A**, bottom right). Recruitment order and relative thresholds of recruitment was then determined by increasing the magnitude of constant-current SCS (200μs pulse width; **Figure 3.7A**). Interestingly, when SCS electrodes were contacting or

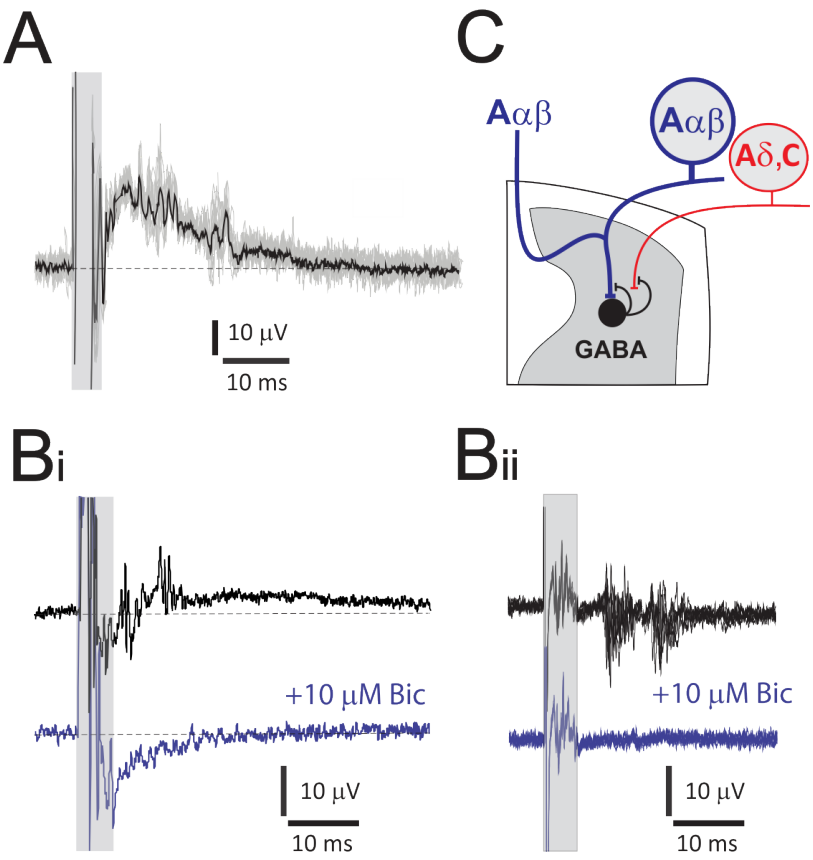

Figure 3.5: SCS recruited GABAergic presynaptic inhibitory pathways observed as bicuculline- sensitive DRPs and DRRs.

A) SCS-generated DRP with suprathreshold DRRs recorded at the L5 dorsal root entry zone. By convention negativity is presented upwards to convey the DRP as primary afferent depolarization. The grey box indicates the location of the stimulus artifact and truncated direct antidromic axonal volley preceding the slow DRP. The average response is presented overlaid (black) with 10 individual events underneath to demonstrate variability in timing of individual DRRs (grey). **B)** SCS evokes DRP and DRRs that are blocked following application of the $GABA_A$ receptor antagonist bicuculline (10 μM). **Bi)** Presented are averages of 10 sweeps from the T13 dorsal root entry zone. Both DRP and DRRs are blocked after the addition of bicuculline (blue). **Bii)** Bicuculline-sensitive DRRs are seen in the absence of an underlying DRP. Shown are 6 events overpaid from a L2 DR recording obtained further from the root entry zone. In both panels, grey box indicates the location of the stimulation artifact and direct primary afferent recruitment. **C)** Schematic depicting possible circuitry responsible for GABAergic actions on afferent axons leading to a form of presynaptic inhibition called primary afferent depolarization (PAD), here experimentally observed as DRPs and DRRs. SCS antidromically recruits A$\alpha\beta$ afferent axons responsible for recruiting the spinal circuit leading to PAD. A$\alpha\beta$ afferents synaptically recruit last-order GABAergic interneurons via interposed interneurons or directly (depicted with dotted line). GABAergic axo-axonic synapses on primary afferents activate bicuculline-sensitive $GABA_A$ receptors that mediates the Cl- efflux to produce PAD. As these experiments cannot identity of afferent axons generating PAD possible actions on all afferent classes as shown

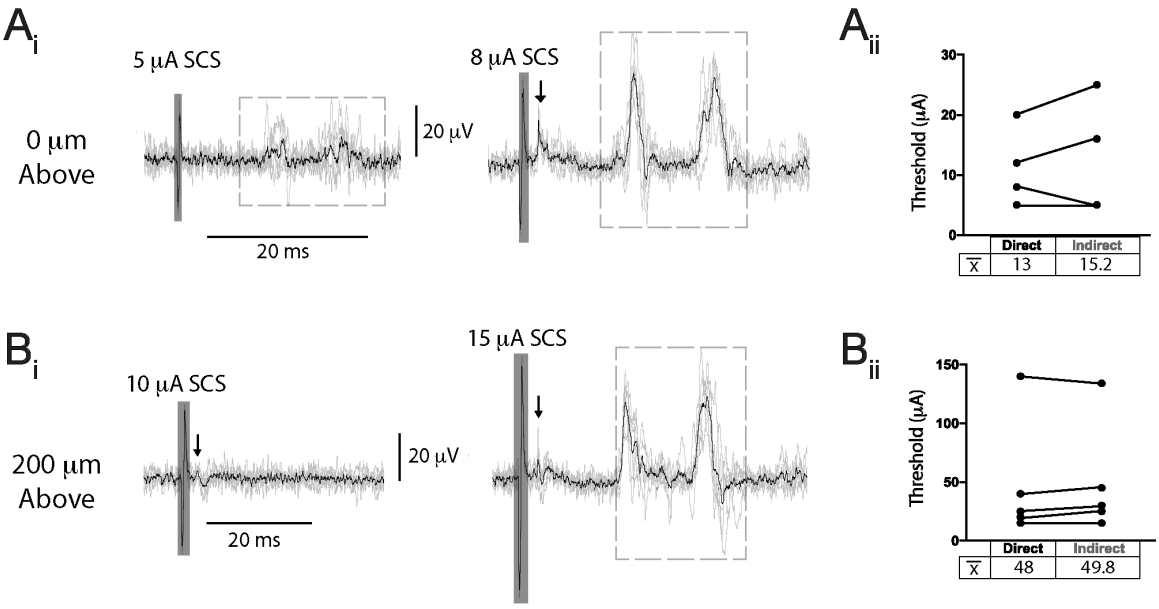

Figure 3.6: SCS evokes direct and indirect primary afferent recruitment at comparable thresholds.

SCS was applied contacting (0 μm) (**A**) or 200 μm above (**B**) T9/T10 while recording a lumbar DR. Stimulus amplitude was incrementally increased (1-200 μA, 200 μs) and the recruitment threshold for direct primary afferent recruitment and synaptically-mediated primary afferent activity (indirect) was identified post-hoc. Mean threshold for indirect recruitment was not significantly higher than that observed for direct recruitment when SCS was applied contacting (0 μm, n=4; 15.2 ±10.1 vs. 13.0 ±6.9 μA, respectively) or 200 μm above (n=5, 49.8 ±48.3 vs. 48.0 ±52.3 μA, respectively) (**A$_{ii}$**, **B$_{ii}$**, paired t-test). Black arrows indicate direct recruitment, dashed grey boxes denote indirect recruitment, while dark grey boxes depict the stimulation artifact. Black lines are the average of 6 traces.

above the DC, axonal recruitment was first seen in the DC regardless of stimulation polarity (n=12). The mean threshold current for recruitment with SCS contacting the DC was lower for cathodic (6.3±4.3 μA) than anodic (9.1±3.7 μA) stimuli (p<0.05, n=12). When stimulation was positioned 200 or 600 μm above the spinal cord, recruitment thresholds were similar at 30.5±26.6 (cathodic) vs. 26.3±13.3(anodic) (p=0.213, n=12), or 231.9±127.5 (cathodic) vs. 278.5±106.0 (anodic) (p=0.125, n=10), respectively. Compared to thresholds observed with SCS contacting the spinal cord DC, threshold values were ˜3-5 times higher at 200 μm above (p <0.05) and 31-37 times higher at 600 μm above the DC (p <0.001; **Figure 3.7B**). Thresholds for SCS positioned 600 μm above were 8-11 times that seen with placement 200 μm above (p <0.001).

3.4.6 Relative thresholds for dorsal roots and Lissauer's tract recruitment

We also compared the relative recruitment of antidromic events in DR and LT relative to the threshold seen in dorsal column ($\mathbf{T}_{DC}$) when SCS was contacting or positioned above the DC (n=12; **Figure 3.7A,C**). When contacting the DC, events in DR and LT were recruited at 3.8±2.4 (p<0.05) and 5.0±4.5 (p<0.001) times T_{DC}, respectively. At 200 μm above, events in DR and LT were recruited at 2.6±1.0 (p<0.05) and 4.4±3.1 (p<0.0001) times T_{DC}, respectively. In comparison, there were no differences in relative recruitment threshold between DR and LT when touching (p >0.9) or when 200 μm above (p= 0.26). At 600 μm above, only DC recruitment was seen in most experiments (n=7/10), even at maximal current amplitudes (>200 μA). However, when DR and LT recruitment was seen, both thresholds were similar to T_{DC}, being 1.5±0.4 (n=5) and 1.5±0.1 (n=2) times T_{DC}. No axonal recruitment was elicited in 3 of 10 experiments with placement 600 μm above.

3.4.7 Comparison of the lowest-threshold axons in dorsal column and dorsal roots

The one-point method was used to compare the central CVs of the first recruited components in DC and DR (at entry zone) at the same segmental level **(Figure 3.8A)**. On

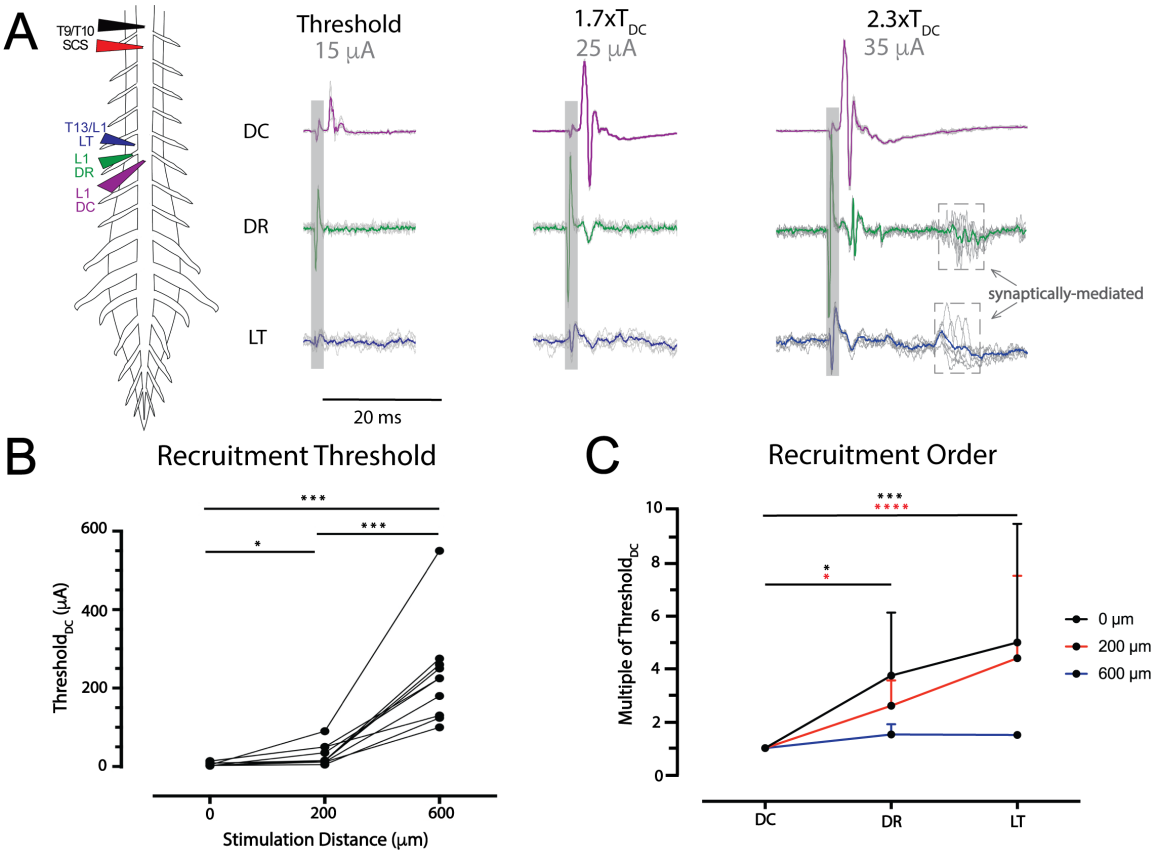

Figure 3.7: SCS recruitment thresholds are lower for dorsal column axons.

A) Example configuration for investigations of recruitment threshold and order. To identify the recruitment threshold of dorsal axon tracts, bipolar SCS (T9/T10, 1-600µA, 200µs) was applied contacting or above the spinal cord, with simultaneous recordings of DR, LT, and DC at the same segmental level. In the example above DC (purple) is recruited first at threshold (T_{DC}), with DR (green) recruitment observed at 1.7x T_{DC} and LT (blue) recruitment observed at 2.3x T_{DC}. The light gray box identifies the location of the stimulation artifact, while the arrows point to dashed boxes denoting the presence of indirect recruitment/reflexes. The colored trace is an average of 6 sweeps. **B)** $Threshold_{DC}$ (T_{DC}) was determined with stimulation 0, 200, or 600µm above the T9/T10 (n=12). T_{DC} significantly increased at 200 µm above and 600 µm above (* $p < 0.05$, *** $p < 0.001$, matched one-way ANOVA, Tukey's multiple comparison). **C)** DC recruitment was observed at the lowest threshold and significantly lower than threshold for DR and LT for SCS at 0 (n=12) or 200µm (n=12) above the spinal cord. With SCS 600 µm above, recruitment beyond DC was observed in only n=2 out of 10 cases. The plot depicts the mean and SD for the test conditions. (* $p<0.05$, *** $p<0.001$, **** $p<0.0001$, Friedman test with Dunn's multiple comparisons).

average, the CV of the first detectable recruited DC component is 43-69% faster that the first observed DR component. This observation was independent of stimulation duration and distance ($p < 0.01$). Results of this analysis are summarized in **Table 3.3**.

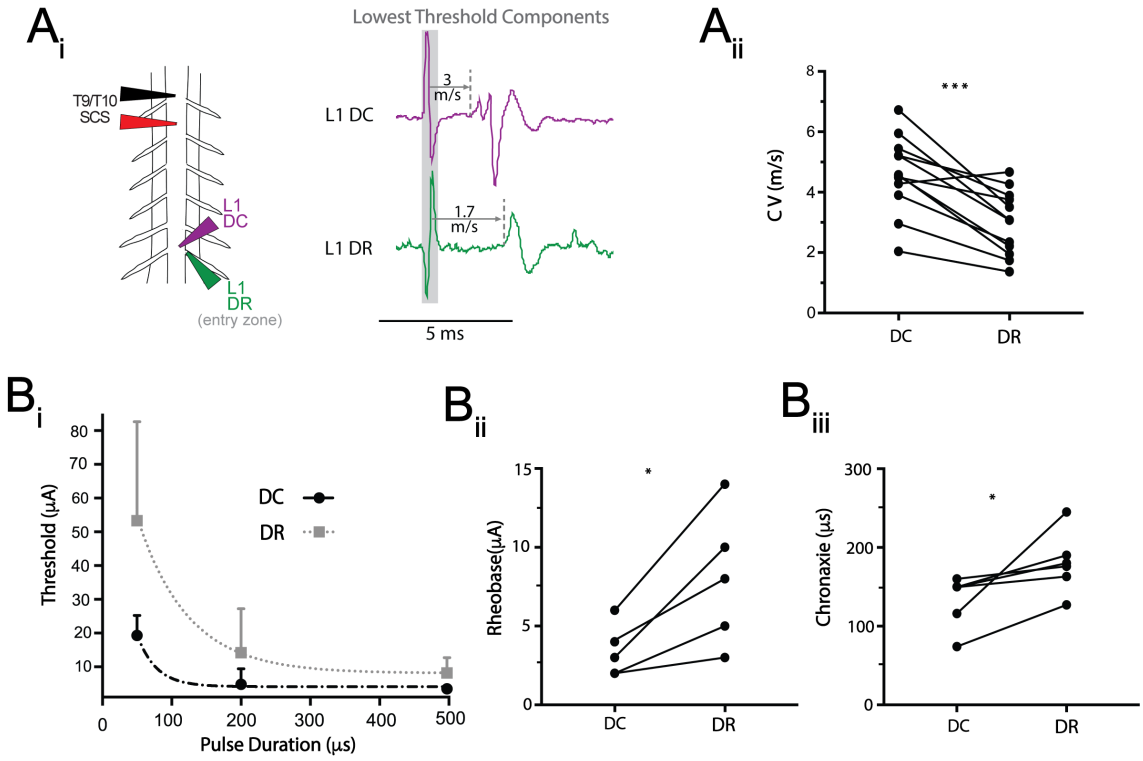

Figure 3.8: The lowest threshold recruited fibers in DC and DR differ in conduction velocity and relative recruitment properties.

A) The conduction velocity (CV) of the first recruited component in DC is greater than that of the DR (n=12), as confirmed by the paired t-test ($\mathbf{A_{ii}}$ ***, $p = 0.0001$, SCS position 0 μm above). **Table 3** contains the results from different stimulation conditions. **B)** The strength-duration relationship for the first recruited populations in DC and DR differed (n=5) with rheobase ($\mathbf{B_{ii}}$) and chronaxie ($\mathbf{B_{iii}}$) being lower in DC than in DR (Wilcoxon matched-pairs signed rank test,* $p<0.05$ SCS positioned 0 μm above). (**Bi**) Strength-durations curves for DC and DR are plotted by fitting a one-phase decay exponential model (RMSE 4.6 and 16.4, respectively) to the mean and SD of the threshold values for 50, 200, and 500 μs pulses.

The strength-duration relationship of the lowest-threshold detectable axons in the DC and DR was assessed with SCS contacting the DC **(Figure 3.8B)**. Rheobase and chronaxie were determined by fitting a one-phase decay exponential to the cathodic threshold values in DC and DR with SCS pulse durations of 50, 200, and 500 μs (n=5). Both rheobase and chronaxie values were significantly lower for DC axons. Mean values for rheobase were

Table 3.3: *Central conduction velocity for SCS-evoked responses in dorsal column and dorsal root.*
Conduction velocities were measured with simultaneous recordings in the dorsal column and the dorsal root entry zone, at sites caudal (L1 or L2) to the SCS electrode (T9/T10). Shown is the mean±SD conduction velocity of the lowest threshold fibers in the dorsal column and dorsal root at room temperature. Statistical analysis was performed using the one-tailed paired t-test for samples where both dorsal column and dorsal root recruitment was observed.

Stimulation Distance (μm)	**Pulse Duration (μs)**	**Mean Conduction Velocity (m-s^{-1})**		**N**
		DC	DR	
0	50	4.9±1.7	2.9±1.3****	12
	200	4.6±1.3	3.0±1.1***	12
200	200	4.3±0.9	3.0±0.8****	12
600	200	5.0±1.2	3.1±0.9**	5

3.5±1.5 μA for DC and 8.0±3.8 μA for DR ($p<0.05$). Chronaxie values were 133.3±32.8 μs and 180.2 ±38.6 μs for DC and DR, respectively ($p<0.05$).

To assess possible differences in recruitment with medial and lateral electrode placement along much of the rostrocaudal axis, we recorded from 9 DRs sampled between T3-S2 (n=4) while stimulating with our SCS electrode at T9-T10 and simultaneously recording from DC at L3 **(Figure 3.9A)**. Across DR recordings, recruitment thresholds (relative to DC threshold) were lower with lateral compared to medial placement (except at T3), with the largest shift occurring in thoracic roots closest to the site of stimulation **(Figure 3.9B)**. With all samples grouped across animals (medial/lateral, 36 samples each), there was a significant difference between DR relative recruitment threshold for medial and lateral placement, ($p<0.05$, Friedman test with Dunn's multiple comparisons). Nonetheless, DC threshold was always lower than DR recruitment threshold regardless of SCS mediolateral placement ($p<0.0001$, **Figure 3.9C**).

To further demonstrate that the DC contains an axonal population distinct from those in

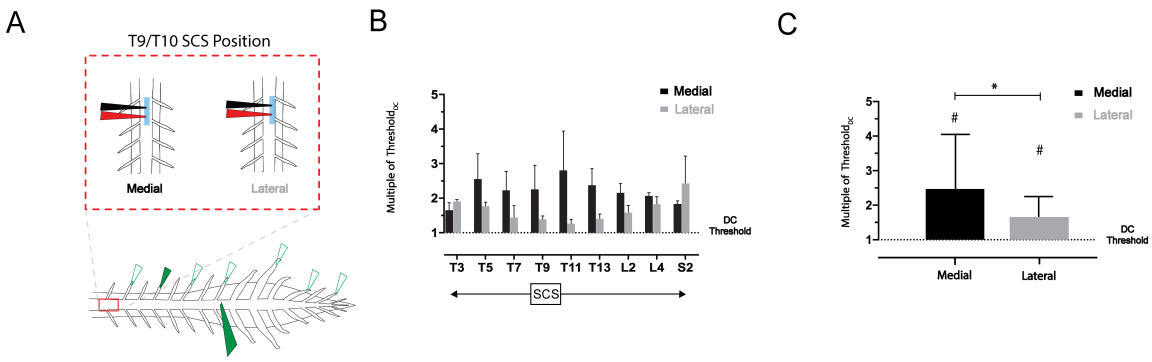

Figure 3.9: The low DC threshold observed is independent of mediolateral position of SCS. **A)** Schematic of experimental paradigm: 9 DRs across T3-S2 spinal segments were recorded with a simultaneous recording of the L3 DC. Recruitment thresholds of both populations were assessed with medial and lateral SCS placement (T9/T10). **B)** Thresholds of DRs rostral and caudal to the site SCS were greater, relative to the DC threshold (dotted line at y=1). (n=4). **C)** Grouped samples from n=4 (9 roots sampled each, 36 total samples for both medial and lateral placement) shows that while lateral placement leads to a reduction in the relative DR threshold (*, $p<0.05$), both medial and lateral placement have higher thresholds than DC (dotted line at y=1), for recruitment, (# $p<0.0001$, Friedman test with Dunn's multiple comparisons). Bar charts display mean and SD.

the DR, we undertook dual-site SCS collision experiments to selectively block conduction in the lowest threshold axons not projecting to DRs (n=4). DC-contacting monopolar SCS electrodes were placed two thoracic segments apart (T10 and T12) for dual-site stimulation **(Figure 3.10)**. Caudally conducting axonal volleys were recorded and compared in the DC and DR at the same lumbar segment. Stimuli were adjusted so that T10 SCS only recruited an antidromic volley in the DC while higher intensity T12 SCS recruited volleys in both DC and DR. When T10 SCS preceded T12 SCS by a 2 ms interval, preferential conduction block in the DC volley was seen in all experiments (to 22±8% vs. of control amplitude), leaving the DR volley largely unaffected (volleys 93±7% of control amplitude; $p<0.05$). **Figure 3.10B** shows examples recorded at L3 and L5 spinal segments. Thus, conduction block of the lowest threshold DC axons does not impair antidromic recruitment of dorsal root afferents.

Overall, these experiments show that T9/10 thoracic SCS recruited a distinct population of axons in lumbar DC with lower threshold and faster CV than antidromically-identified

primary afferent responses recorded in homologous segmental lumbar DR axons. As SCS-recruited DC axons also had lower threshold than antidromically-activated primary afferents that originated from DRs spanning the 19 spinal segments sampled (T3-S2), it is highly unlikely these axons are of primary afferent in origin.

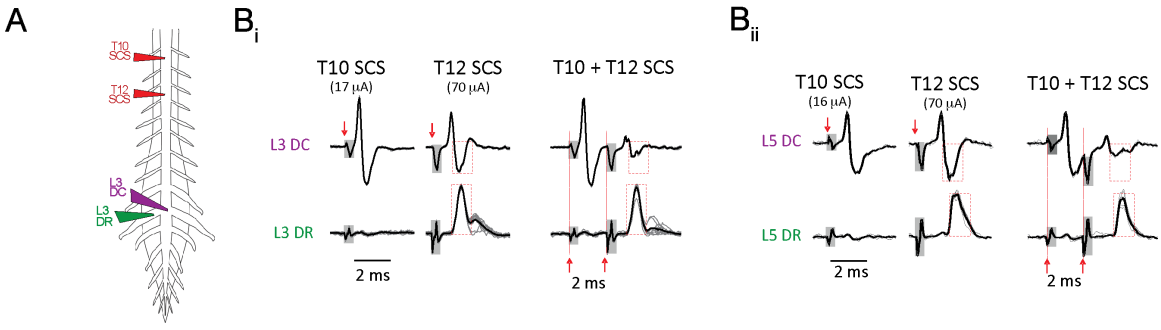

Figure 3.10: Collision testing further supports lowest threshold axons in DC as distinct from DR axons.

Conduction block of the lower threshold DC axons at the same segment as recruited DR does not block antidromic recruitment of DR afferents. **A)** Electrode configuration for comparison of recruited axonal volleys recorded in the DC and DR of the same lumbar segment following monopolar SCS at T10 and T12 thoracic segments. **B)** Shown are comparison axonal volleys recruited in the DC (upper row) or DR (lower row) of the same lumbar segment when T10 and T12 SCS stimuli were delivered individually or sequentially (T10 then T12) with a 2 ms interstimulus interval. Stimulus onsets are marked by red arrows and stimulus artefacts are identified as grey boxes. **Bi)** T10 SCS stimulation at lower intensity preferentially evoked an antidromic volley only in the L3DC (left), while T12 SCS at higher intensity evoked recorded volleys in the L3DR and L3DC (middle). The amplitude of the T12 SCS evoked volleys in DC and DR are shown bounded by a red dashed box for comparison with amplitudes observed after collision testing when T10 SCS preceded T12 SCS (right). There was preferential conduction block of axons in their refractory state in the DC volley (top row) while the DR volley (bottom row) was largely unaffected (compare red boxed regions). **Bii)** Preferential conduction block of the DC volley was also seen at the L5 spinal segment.

3.5 Discussion

We developed an isolated *ex vivo* adult mouse spinal cord preparation as an accessible platform to characterize the axonal populations recruited following delivery of SCS using electrodes scaled to generate clinically-comparable electric fields. To our knowledge, these are the first studies employing quantitative methods to scale multiple SCS parameters for experimental studies on recruitment in smaller mammalian models.

With SCS electrodes placed above the caudal thoracic cord (T9/T10), primary experimental observations include the following: 3.5.1) Compared to afferent recruitment near the SCS electrode (0-3 segments away), higher stimulus amplitudes were required for antidromic recruitment of A$\alpha\beta$ afferents at more caudal dorsal roots (7-9 away). These higher amplitudes also lead to antidromic recruitment of slower conducting fibers near the stimulation site **(Table 3.2)**. 3.5.2) In lumbar cord dorsal roots, direct antidromic activation of A$\alpha\beta$ afferents also corresponded with recruitment of bicuculline-sensitive (GABAergic) presynaptically inhibitory actions on terminals of unidentified primary afferents (recorded as DRPs and DRRs). 3.5.3) The lowest-threshold fastest-conducting axons recruited at lumbar segments were preferentially recruited in the dorsal column (DC) and at thresholds significantly lower than seen for afferents in dorsal roots (DRs) or the Lissauer tract (LT). These axons retained the lowest recruitment threshold with SCS placed more laterally and compared to primary afferent recruitment that originated from distant DRs (spanning T3-S2 spinal segments). Based on known anatomy and process of exclusion, they are possibly PSDC ascending tract cells. The implications of these observations are elaborated below.

3.5.1 Factors affecting multisegmental recruitment of primary afferents: evidence beyond convention

The capacity for SCS electrodes to antidromically recruit afferents across many spinal segments demonstrates that SCS is capable broad axonal activation beyond the segment/ dermatome of interest. While clinically, stimulation parameters are determined by identifying the regime that leads to a region with the greatest paresthesia perception (e.g. paresthesia dermatome focus) overlapping with the region of pain, the complete paresthesia perception can cover a broader dermatomal area [94][64]. This suggest that the population of axons responsible for the paresthesia can be recruited simultaneously at multiple spinal segments, while one segment may have the greatest recruitment. We also show that the higher stimulus amplitudes and longer pulse durations required for antidromic recruitment

of faster-conducting myelinated fibers at more distant segments can also recruit putative pain-encoding unmyelinated C fibers closer to the stimulation site **(Figure 3.4)**. This observation predicts that SCS aimed at selective recruitment of myelinated fibers would benefit from use of lower magnitude/short pulse durations placed at spinal segments closer to the targeted site for modulation.

The strength-duration relationship predicts that increases in pulse duration and amplitude enhance axonal recruitment. Clinically, increased SCS duration has resulted in observations of the elicited paresthesia spreading to multiple dermatomes [196]. Longer pulse durations resulted in marked increased recruitment of smaller-diameter medial dorsal column axons which is consistent with sacral shifts in paresthesia coverage [94]. Higher stimulation amplitudes have been associated with increased cross-sectional area of DC recruitment [87]. We observed differences in rheobase and chronaxie for DC compared to DR populations. Such measures are not normally estimated with extracellular stimulation because obtained values strongly depend on distance of axons from stimulation site. Nonetheless, SCS leads to threshold and CV differences between DC and DR populations, and differences quantified on the basis of a strength duration curve may be of instructive importance for subsequent consideration of stimulation strategies. For example, shorter-duration higher-intensity pulses could increase separation of DC from DR while longer duration pulses at lower stimulus intensity may more uniformly recruit both populations.

Computational studies also suggest that DR/primary afferent recruitment may be related to discomfort thresholds in patients with SCS [87][84], and this may be due to co-recruitment of Aδ fibers. Our observation that the increased stimulus strength required to recruit A$\alpha\beta$ fibers from distant caudal segments also recruits smaller diameter (Aδ, C) fibers from nearby segments **(Figure 3.4C)** may underlie unwanted side effects at a different dermatome reported clinically [197].

Recruitment requiring increased stimulus amplitudes from more distant segments is consistent with earlier observations [20][21]. As smaller diameter afferent axons have higher thresholds for activation by extracellular stimuli [198][199] these observations have been interpreted as a distance-dependent reduction in diameter of ascending axons [200][201]. Recruitment differences may also reflect somatotopic differences in axon diameter of functionally-distinct A$\alpha\beta$ fiber populations [19].

Our experimental results with clinically-analogous SCS suggest that a non-primary afferent DC axon population is recruited first (detailed in section 3.5.3, below). SCS-evoked responses in DR (A$\alpha\beta$) and LT (presumably Aδ) are then subsequently recruited at similar several-fold higher intensity **(Figure 3.7)**. While recruitment beyond DC was not always observed with SCS 600 μm above the cord, when broader recruitment was observed, DR and LT were recruited at comparable relative thresholds. Aβ and Aδ recruitment thresholds were also reported to be similar following DC stimulation in rat [112]. While Aδ fibers are not thought to project in the DC [8][17] (however for monkey and cat see [21][202]), that LT is immediately adjacent and contains Aδ fibers that project many segments [11] may support their similar recruitment threshold by SCS.

Observed negligible recruitment thresholds differences in DR (A$\alpha\beta$) and LT (presumably Aδ) is a significant observation since the primary conceptual basis of SCS modulation of pain is via selective recruitment of Aβ fibers that act via inhibitory mechanisms associated with the Gate Control Theory of Pain [180]. We are unaware of experimental literature that demonstrates SCS selectively recruits Aβ afferent fibers.

3.5.2 Aαβ primary afferent recruitment coincides with recruitment of spinal circuits mediating presynaptic inhibition of primary afferents

We related clinically-analogous SCS to segmental distribution of recruited afferents fiber classes. While we observed broad rostrocaudal antidromic recruitment of primary afferents originating from many spinal segments, we focused on assessment of axonal recruitment that would correspond to an equivalent expected distribution in humans with failed back surgery syndrome [64]. In mouse this roughly corresponds to L1-3 segments [203]. We show that T10 SCS at the lower modeled intensity of 50 μA recruited the lowest threshold primary afferents as well as spinal circuits that have been associated with presynaptic depression of primary afferent input (described below). These results are consistent with demonstration of dermatomal overlap and activation of circuitry that could modulate pain signaling. While one might view this as encouraging, whether such afferent recruitment is causally linked to pathways that generate paresthesia and/or modulate pain is unknown (also see Section 3.5.4).

Primary afferent depolarization (PAD) is thought to arise predominantly from GABAergic axo-axonic synapses acting on $GABA_A$ receptors that cause a Cl^- efflux constituting an ionotropic form of afferent presynaptic inhibition [204][205]. **Figure 3.5C** depicts simplified representation of circuitry generating axo-axonic presynaptic inhibition of primary afferents. Here PAD was experimentally recorded as a slow depolarizing dorsal root potential (DRP) and/or dorsal root reflex (DRR). DRRs represent suprathreshold spiking arising from an underlying slower depolarizing DRP [204] and their expression here is likely due to bath temperature [206][207].

An important observation was that threshold for recruitment of the lowest threshold ($A\alpha\beta$) primary afferents was comparable to threshold for recruitment of interneuronal circuits responsible for generating presynaptic inhibition by PAD and DRRs **(Figure 3.5)**.

While SCS recruited A$\alpha\beta$ afferents to recruit the circuitry mediating PAD, the identity of the primary afferent axons receiving presynaptically-inhibited via PAD cannot be determined from these experiments. They likely include negative feedback onto functionally homologous A$\alpha\beta$ primary afferents [204] but could also include actions on C fibers, and hence suppress central actions of nociceptors [208].

3.5.3 Are axons of PSDC neurons the lowest threshold axons recruited with SCS?

We observed that the lowest threshold axons recruited at lumbar segments with SCS had differentiable recruitment properties (CV, rheobase, chronaxie) compared to DR afferent axons. That these axons had lower threshold and were distinct from primary afferent axons recorded along the rostrocaudal axis explored (T3-S2) argues against them being collateral branches of primary afferents originating from more rostral or caudal segments [17][19][209]. Dual-site SCS collision experiments demonstrated ability to selective block these DC axons independent DR afferent axon recruitment, further supporting their axonal identity as distinct from primary afferents.

Postsynaptic dorsal column tract cells (PSDCs) are ascending tract neurons that project via the DC to brainstem gracile nuclei [16] and may be the non-primary afferent axonal population recruited by SCS. A$\alpha\beta$ primary afferent axons enter the DC, project both rostrally and caudally, and regularly issue axon collaterals out to gray matter as they project [17][19]. In contrast, PSDCs are not thought to issues collaterals after entering the DC (see **Figure 3.11**) [13]. In the absence of branching, PSDCs may retain the higher values of CV reported here and previously [210][211][212][213].

3.5.4 Are orthodromic actions of PSDC neurons responsible for SCS paresthesias?

The possibility that PSDCs are the non-primary afferent DC axon population recruited at intensities lower than A$\alpha\beta$ primary afferents (**Figure 3.7**; see below) may indicate their im-

portance in SCS induced modulation of pain that could be independent of peripheral side effects. Assuming activation of A$\alpha\beta$ afferents is responsible for evoking motor reflexes that define motor threshold in clinical SCS approaches [95], and given that that SCS is effective at amplitude values below motor threshold, recruited axons may include PSDCs. As PDSCs receive multimodal afferent input [210][214][212][213][215] and project to dorsal column gracile nuclei [13], their orthodromic activation by SCS could be directly responsible for initiating paresthesias. Lumbar PSDCs represent ˜30% of the cells that project to the gracile nucleus, while only ˜25% of lumbar enlargement long system primary afferents reach the gracile nucleus [17][13]. Importantly, as PSDC neurons are largely absent in the thoracic cord [13], PSDC axons recruited at T10 would originate from caudal segments consistent with locations of observed paresthesia reported clinically [216][24]. In contrast, the observed broad rostrocaudal recruitment of sensory axons with T10 SCS **(Figure 3.9)** is consistent with anatomical projections of A$\alpha\beta$ fibers in the DC known to originate from many segments above and below the SCS site [17][19]. It would be harder to causally link broad afferent recruitment to the selective generation of paresthesias caudal to the SCS site.

An interesting possibility is that paresthesias and depression of pain perception are both due to PSDC actions. As PSDC tract neurons only issue local axon collaterals near their cell bodies in the dorsal horn [211], antidromic recruitment of PSDCs located in lumbar segments could synaptically interact with other spinal neurons that then modulate lumbar spinal sensory transmission [215]. It is also possible that PSDCs activate supraspinal antinociceptive mechanisms, including that of the descending serotonergic system [99][105][101]. Overall, preferential PSDC recruitment may represent a critical but currently unexplored neural circuitry underlying conventional SCS-induced paresthesia and analgesia.

3.5.5 Factors associated with experiments conducted in the isolated adult mouse spinal cord

We developed an *ex vivo* adult mouse spinal cord preparation that permitted detailed electrophysiological investigations without anesthetic-interference. To enhance viability, studies were conducted at room temperature. The concomitant slowing of conduction velocity aided separation of A$\alpha\beta$, Aδ and C fiber volley components when recording along relatively short distances, but did not provide the actual values of conduction velocities that would be seen *in vivo*. Guidelines for classifying primary afferents in DRs at room temperature were obtained from a study that characterized CV in peripheral nerve and DRs at 22 and 37°C [6]. Nissl staining suggested that dorsal horn neurons are preserved and electrophysiological recordings demonstrated neuronal participation in synaptically-mediated DRRs. However, it is likely that circuit excitability may be depressed via unknown mechanisms including cord transection induced spinal shock [217]. Recordings of afferent evoked population synaptic responses as field potentials in the dorsal horn suggested limited recruitment of polysynaptic pathways unless excitability was increased pharmacologically (preliminary observations). As distinct descending brainstem systems are known to be involved in SCS pain modulation [99], its removal represents a further limitation of the isolated spinal cord model system. However, modern genetic approaches enable studies on neuromodulatory actions from brainstem in the isolated spinal cord via optogenetic activation of their descending axons [218].

Traditional preclinical SCS studies are primarily undertaken in the rat *in vivo*. They vary in their electrode design (ball, paddle, monopolar, bipolar, etc.) and often assign SCS intensity as a percentage of motor threshold (e.g. 70-90%) [106][97][98][111][107]. Our experimental paradigm leveraged computational modeling to inform detailed recruitment studies to realistically appraise neural system recruitment with clinically-analogous stimuli at defined electrode configurations and distances from the spinal cord - features not present

in previous preclinical studies of SCS. To achieve this, we strategically developed a model system that allowed us to explore this with optimal access to the dorsal column, dorsal roots and SCS distance above the cord. Obtained results inform subsequent SCS studies in mouse using scaled electrodes and effective stimulus frequencies to determine whether the delivered currents have modulatory actions on known afferents/pathways including in mouse in vivo pain models.

Importantly, though our experimental arrangement excludes the presence of dura, at the constant current stimulus intensities applied, resistivity values normally seen for dura do not significantly affect spinal cord current densities [86]. Changes from the modeled electrodes (square) to those utilized for experiments (circular) account for an overall surface area difference of 0.02 mm^2. While it is possible that this difference could affect recruitment when SCS is contacting the cord surface, there is little evidence to suggest that a difference of this scale would significantly impact relative recruitment thresholds and recruitment order of axonal populations when stimulating through CSF. The main point of the electrode scaling technique was to quantitively estimate relevant dimensions for studies with the mouse spinal cord. Previously, rodent studies frequently employed contacts with dimensions that are larger than what would be recommended for a mouse [109][111][95], including those comparable to electrodes used clinically [97][98][100][107].

3.6 Conclusions

We paired clinically-analogous SCS with an experimentally-accessible adult mouse spinal cord preparation to provide detailed studies on the variability in axonal recruitment to several preclinical SCS parameters including stimulation site, stimulation distance, amplitude, polarity and pulse duration. Results demonstrate a hierarchical sensitivity of recruitment of various axonal populations and introduce the possibility that the primary actions of SCS may be independent of primary afferent recruitment. **Figure 3.11** summarizes the proposed

anatomical relation between relative axonal recruitment.

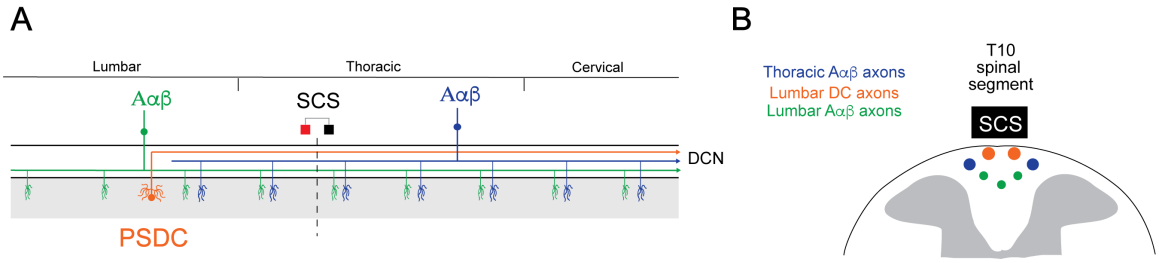

Figure 3.11: Factors associated with differences in SCS recruitment of A$\alpha\beta$ afferents and non-primary afferent fiber populations.

A) Shown are anatomical considerations in relation to axonal recruitment results. SCS recruited A$\alpha\beta$ axons originating from both rostral and caudal spinal segments. An additional non-primary afferent population was recruited at lower threshold in the lumbar DC. Based on known anatomy, these are likely PSDC tract cells. PSDC axonal recruitment would be expected to have direct orthodromic actions in brainstem gracile nuclei that associate with sensory integrative actions within the lumbar cord. PSDC antidromic axonal recruitment may have segmental synaptic actions on lumbar circuits via local intraspinal axon collaterals. A$\alpha\beta$ afferent axons would have widespread rostrocaudal spinal synaptic actions including via GABAergic presynaptic inhibition of primary afferent signaling, and also project directly to the brainstem gracile nuclei. **B)** Cross section of dorsal spinal cord at level of SCS (T10) depicts how differences in axon depth and diameter may explain relative recruitment threshold and conduction velocity (CV) in these axonal population. Lumbar DC axons (putative PSDCs) have the lowest threshold and fastest CV. Lumbar A$\alpha\beta$ have slower CV that may be explained by a smaller axon diameter while their higher threshold may be due to greater depth and/or smaller diameter. Thoracic A$\alpha\beta$ had lower threshold values relative to DC axons. This is partly explained by lateral location but may also be due to greater location depth. Thoracic A$\alpha\beta$ CV was not estimated.

3.7 Research Contributions

This chapter was adapted from an article published in the Journal of Neurophysiology [184]. Scaling procedures and finite element modeling were performed by Dr. Tianhe Zhang and Dr. Natalie Brill (Boston Scientific). Tissue isolation, electrophysiology experimentation, and analysis was performed by Shaquia Idlett-Ali and Mallika Halder. Shaquia Idlett-Ali authored this chapter with collaboration from Dr. Shawn Hochman.

CHAPTER 4
SCS MODULATION IN AN EX VIVO MODEL OF SPONTANEOUS HYPEREXCITABILITY

4.1 Abstract

Spinal cord stimulation is used clinically for relief of chronic neuropathic pain. The gate control theory presents a theoretical framework of the therapy's mechanism of action, but the true mechanisms remain unclear. Typically, preclinical studies investigate mechanisms leading to modulation of stimulus-evoked pain, despite the critical ability for spinal cord stimulation to modulate chronic, stimulus-independent pain. Here, we utilize a spinal cord-dorsal root ganglia preparation to generate a model of spontaneous hyperexcitability in sensory circuits using 4-aminopyridine **(4-AP)**. We first demonstrate that 4-AP induced activity of axons in lumbar dorsal roots and in Lissauer's tract with subjacent neurons in the superficial dorsal horn **(LT/DH)**. Then we test the gate control theory by investigating modulation of spontaneous nociceptive activity with T9-T11 spinal cord stimulation **(SCS)** at dorsal column and dorsal root recruitment thresholds. In the 4-AP model of sensory hyperexcitability, spontaneous activity manifested three distinguishable events; (i) episodic rhythmic dorsal root potentials with superimposed burst firing, (ii) episodic field potentials with superimposed spikes in LT/DH, and (iii) additional spontaneous spiking events in dorsal roots and LT/DH. We also observed that dorsal column threshold SCS at 50 Hz modulated spontaneous spiking activity in LT/DH during SCS but could not modulate the episodic field potentials or produce prolonged modulation following cessation of stimulation. These results demonstrate the utility of a 4-AP model of spontaneous hyperexcitability and the limited and perhaps antagonistic contribution of gate control, via Aβ recruitment, to SCS modulation of spontaneous nociceptive activity.

4.2 Introduction

Spinal cord stimulation (**SCS**) is a clinical therapeutic for ongoing, stimulus-independent neuropathic pain. Conventional SCS is undertaken at frequencies between 20-150Hz. SCS is presumed to act by selective recruitment of larger diameter non-pain encoding Aβ axon collaterals in the dorsal column that suppress pain afferent signaling by the gate control theory of pain. Though this mechanism of pain control is an attractive model, there remains limited experimental evidence detailing the neurobiological underpinning of SCS-induced pain modulation. To investigate mechanisms of action, preclinical investigations frequently explore modulation of stimulus-evoked hypersensitivity in nerve injury models [95][96][97][98][99][100][101][102][103][104] [105] [106] [107] [108] [109] [110] [219]. To our knowledge, no experimental studies investigate its role in modulation of stimulus-independent persistent pain—a key clinical feature of SCS pain relief. Spontaneous activity generated centrally and peripherally has been identified as potential source of neuropathic pain. Increasing evidence suggests the involvement of continuous primary afferent activity in the development of chronic pain [50][49][51][52][54][55][35] [48] [59], with dysregulation of voltage-gated K^+ channels in dorsal root ganglion neurons emerging as an initiator of the abnormal sensory activity [59]. Spontaneous activity also presents as a potential selective target of SCS, as acute evoked pain can still be perceived with SCS [81][82][220][83].

Here we report on the development of an *ex vivo* multisegmental spinal cord-dorsal root ganglia (**SC-DRG**) preparation as a system for testing whether SCS modulates spontaneous hyperexcitability in spinal sensory circuits. We focus on pharmacologic induction of spontaneous hyperexcitability using 4-aminopyridine (**4-AP**) to block voltage-gated K^+ channels [221][222][223][224] as 4-AP has been shown to alter spinal circuitry in a manner consistent with the emergence of rhythmic spontaneous neuropathic pain [223]. We first

characterize the actions of 4-AP on central and peripheral targets, observing their distinct manifestations of spontaneous hyperexcitability. We then examine the potential for SCS to modulate spontaneous nociceptive activity, using threshold-based stimulation to test the gate control theory and elucidate the mechanism leading to depression of pain.

4.3 Methods

4.3.1 Multisegmental spinal cord-dorsal root ganglia preparation

All procedures were approved by the Emory University Institutional Animal Care and Use Committee: C57/Bl6 adult mice (both sexes, n=16, P60 and older) were anesthetized with ketamine (100mg/kg) and xylazine (10mg/kg) mix by intraperitoneal injection, following light anesthetization in an isoflurane chamber. To induce tissue hypothermia, ice was packed on top of the vertebral column, following removal of the overlying dorsal skin. Animals were euthanized via decapitation and the vertebral column below the C5 vertebra (with surrounding ribs and muscle) was excised and pinned in a Sylgaard-lined dish containing ice cold, oxygenated (95% O_2 / 5% CO_2) high-Mg^{2+}/low-Ca^{2+} artificial cerebral spinal fluid (**aCSF**) containing (in mM), [NaCl 128, KCl 1.9, $MgSO_4$ 13.3, $CaCl_2$ 1.1, KH_2PO_4 1.2, glucose 10, $NaHCO_3$ 26]. In later sections I abbreviate the name of this aCSF as "low Ca^{2+} aCSF". Both a complete laminectomy and vertebrectomy were preformed to expose the spinal cord (**SC**), dorsal roots (**DR**), and dorsal root ganglia (**DRG**) from segments C8 through S1. The *ex vivo* preparation **(Figure 4.1A)** was equilibrated to room temperature for 1 hour, then pinned dorsal side up in a Sylgaard-lined recording chamber while superfused with an oxygenated aCSF containing (in mM), [NaCl 128, KCl 1.9, $MgSO_4$ 1.3, $CaCl_2$ 2.4, KH_2PO_4 1.2, glucose 10, $NaHCO_3$ 26], at ˜40ml/minute. All experiments were undertaken at room temperature.

4.3.2 Electrophysiology

Glass suction recording electrodes were positioned in the lumbar spinal cord on DRs (200-250 μm tip diameter) for characterization studies and in Lissauer's tract (**LT**) (1-2μm tip diameter, 3-5 MΩ) for modulation studies. A glass recording suction electrode was also positioned in the lumber spinal cord on the dorsal column **(DC)** (200 μm tip diameter) to determine threshold for DC axonal recruitment (T_{DR}; see section 4.3.5). Characterization consisted of identifying the dose-response features of the 4-AP model and investigating the role of synaptic transmission in the generated spontaneous activity. Modulation studies investigated the potential for SCS to reduce spontaneous activity in LT and the superficial dorsal horn **(DH)**. We exclusively focused on LT/DH as their activity is consistent with recruitment of nociceptive circuits [223] Targeted recording of LT was accomplished by positioning a glass microelectrode lateral to the dorsal column (DC), in between dorsal root entry zones. Appropriate positioning was confirmed by stimulating a DR one segment caudal to the recording site and observing preferential recruitment with 200 or 500 μs pulse durations, indicative of high threshold afferents **(Figure 4.1B, 4.1C)**. Both spiking and extracellular field potentials (**EFPs**)–reflecting population synaptic responses–could be observed with the microelectrode, confirming the ability to observe spontaneous nociceptive activity in LT/DH. All recorded data were digitized at 50 kHz (Digidata 1322A 16 Bit DAQ, Molecular Devices, U.S.A.) with pClamp acquisition software (v. 10.7 Molecular Devices). Recorded signals were amplified (5000x) and low-pass filtered at 3 kHz using in-house amplifiers.

4.3.3 Model of sensory hyperexcitability

A broad-spectrum voltage-gated K^+ channel blocker, 4-AP, was utilized to generate a model of sensory circuit hyperexcitability in the *ex vivo* SC-DRG preparation. 4-AP has been demonstrated to increase the excitability of neurons in preclinical and clinical studies [222][225][223] and recruits spinal nociception-encoding circuitry consistent with the

emergence of spontaneous neuropathic pain [223]. To characterize the dose-response relationship of the model, 4-AP was bath applied at increasing concentrations (5-40μM) during recording of a lumbar DR. To demonstrate that dorsal horn circuitry was involved in generating the emergence of dorsal root potentials **(DRPs)**, reduction in the responses to 4-AP (30 μM) were compared in the presence of bicuculline (**BIC**, 10-20μM), to block $GABA_A$ receptors presumed responsible for generating primary afferent depolarization **(PAD)** underlying the DRPs, or after bath replacement with a low-Ca^{2+} aCSF to limit synaptic transmission. Burst frequency and amplitude was quantified, when appropriate.

To determine whether 4-AP increased spontaneous activity in primary afferents directly, DRGs and distal DRs were isolated in a minibath using a plastic barrier with petroleum jelly sealant. If single-unit spiking was observed, tetrodotoxin (**TTX**) was increased serially to concentrations of 20, 50, and 500 nM (10 minutes each) in order to deduce the classes of primary afferents [221][6] activated by 4-AP as Aβ, Aδ, and C fibers, respectively [221] [6].

For studies on modulation of nociceptive activity by SCS, 20μM 4-AP was bath applied during simultaneous recordings of lumbar of LT/DH and a DR. The following features of the LT/DH activity was quantified before, during and after SCS: frequency of all synaptic events (EFPs) (Δbaseline $>$0.1mV), frequency of large synaptic events (Δbaseline $>$0.15mV), and frequency of single-unit spikes (Δbaseline $>$0.35mV).

4.3.4 Fos labeling

To obtain histological evidence of 4-AP induced activation of nociceptive circuitry in the dorsal horn, we stained spinal cord slices for *c-fos* protooncogene activation of the protein Fos —an indirect metabolic marker for neuronal activity [226]. In accordance with a previous study [227], we electrically stimulated a lumbar DR at a high intensity (200 μA, 500

μs) at 10 Hz for 10 mins, followed by a 2-hour incubation period. Electrical stimulation served as a positive control for subsequent studies. For the 4-AP experiment, we applied 4-AP for 10 mins, followed by a wash out and 2-hour incubation period. These experiments were conducted at 27 °C, as Fos-immunoreactivity **(Fos-ir)** was previously demonstrated to be temperature-dependent [227].

Following experimentation, the cord was then removed from the recording chamber and fixed in 4% paraformaldehyde for 2 hours. After fixation the cord was placed in 20% sucrose in phosphate buffered saline **(PBS)** until sectioning. The following processing methods were adapted from Alexander et. al. 2015 [228]. Transverse sections 20 μm thick were cut through the lumbar cord on a freezing microtome and mounted on slides. Sections were washed in 0.01 M PBS with 0.1% Triton X-100 (PBS-T), blocked for 1 h in 5% normal goat serum in PBS-T, and incubated at room temperature overnight in rabbit anti-Fos antibody (1:250; Santa Cruz Biotechnology) in PBS-T with 2% goat serum. Sections were washed in 3×PBS-T and incubated with donkey anti-rabbit conjugated to Cyanine Cy3 (1:250; Jackson Immunoresearch) for 2 h at room temperature. Sections were then washed in PBS three times and coverslipped.

Fos-ir in the spinal cord was quantified by visual counting of cells in the dorsal horn showing nuclear staining. Positive staining cells were counted separately in dorsal horns ipsilateral and contralateral to the stimulated root. Counts were pooled to calculate an average and standard deviation of the number of dorsal horn cells expressing Fos protein.

4.3.5 Spinal cord stimulation

To explore modulation of spontaneous activity with electrical stimulation, mouse-scaled electrode dimensions were utilized to generate clinically-analogous SCS with a constant-current stimulator (previously described in Chapter 3) [184]. A single pulse of SCS (200

μs) was applied contacting (0 μm) the thoracic DC (T9-T11) while stimulation amplitudes were increased incrementally from 5 to 50 μA, to determine the recruitment thresholds for DC ($\mathbf{T_{DC}}$) and DR ($\mathbf{T_{DR}}$) of a selected lumbar segment. Here T_{DC} and T_{DR} was defined as the lowest observed stimulus amplitude producing a 100% response rate for each population. Following the initiation of spontaneous sensory circuit activity, SCS of 10, 50, or 100 Hz with amplitudes of T_{DC} or T_{DR} was applied while recording activity in LT/DH. Repetitive SCS was delivered intermittently (16s on, 4 sec off) for a period of 10 minutes. This was preceded and followed by a 20-minute period to establish a baseline. The stimulation parameters were applied in a variable order for each experiment.

4.3.6 Data analysis

Spontaneous activity was quantitatively assessed by calculating the fast Fourier transform **(FFT)** of 20-sec segments from LT/DH and DR recordings. The presence of one or more sharp peaks was indicative of rhythmicity. FFT analysis was conducted using built-in MATLAB (2019b) functions.

In all data presented, the number of animals utilized for analysis is represented by the noted n-value. For each animal, a representative value was determined by averaging the response from 6 sweeps/trials within that animal. Statistical significance of normalized data was determined via ANOVA with Holm-Sidak multiple comparison test or a t-test, depending on the data.

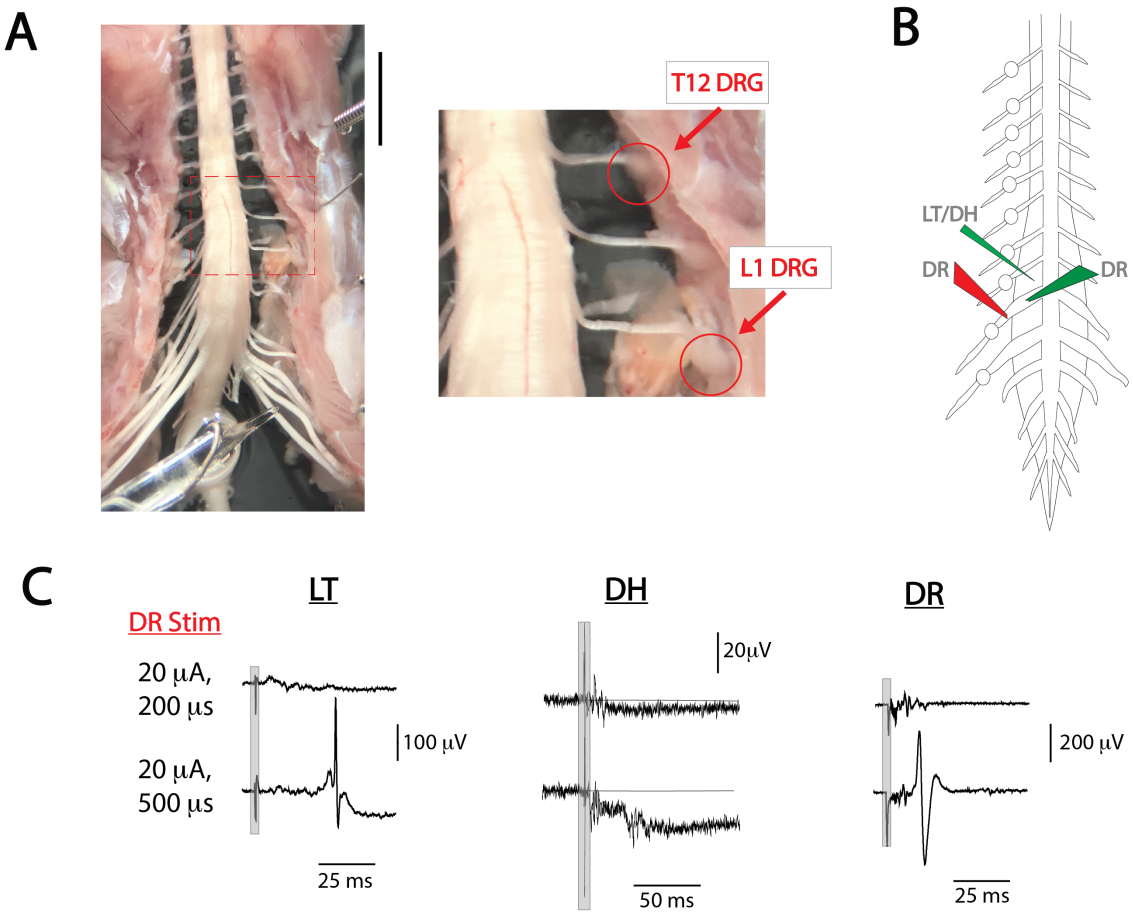

Figure 4.1: SC-DRG preparation for studies of sensory circuit hyperexcitability.

A) Image of SC-DRG preparation pinned to a Sylgaard-lined dish following excision. Scale bar = 5 mm. In the expanded view, the circles denote the location of DRGs with attached DRs, and severed VRs. **B)** Schematic of experimental arrangement for LT/DH identification. DRG (circles) attachment was maintained on one side to permit space for proper electrode placement. The distal end of a lumbar DR was stimulated at long pulse durations during simultaneous recordings of the DR entry zone and the LT region rostral to it. **C)** Examples of recordings observed during high threshold stimulation in LT (left), the DH (middle), and the DR (right). 500 μs pulses recruited C-fiber responses in the LT and DR and excitatory field potentials in the superficial DH. The gray box denotes the stimulation artifact

4.4 Results

4.4.1 Spontaneous, synaptically-mediated dorsal root activity is generated by 4-AP

Multisegmental spontaneous activity was generated following bath application of 4-AP, which was broadly observed in DR, LT/DH, and DC populations (not shown). As our goal was to first charachterize the 4-AP model of spontaneous circuit hyperexcitability, we first focused our investigations on the recruitment of lumbar DR activity, as these recordings are reliably expressed and was alway coupled with the presence of LT/DH activity. 4-AP induced DRPs with overlying repetitive bursts (dorsal root reflexes [**DRRs**]) **(Figure 4.2A)**. DRP amplitude and frequency increased in a 4-AP concentration dependent manner (n=3, **Figure 4.2B**). The average amplitude and frequency of DRPs was 13.2±2.1 μV and 1.1±0.4 Hz with 5 μM 4-AP. Raising the concentration from 5 μM increased the amplitude of DRPs by average magnitudes of 1.9 (10μM, $p<0.01$), 2.8 (20μM, $p<0.001$), and 3.4 (30 and 40 μM, $p<0.001$). DRP frequency also increased by average magnitudes of 1.9 (10μM), 2.5 (20μM), 2.7 (30μM) and 3.2 (40μM) but was only significantly different at 40 μM ($p<0.05$, **Figure 4.2C**). To investigate the role of central circuits in the observed spontaneous DR activity, burst frequency with 30 μM 4-AP was quantified and compared when aCSF was switched to a low-Ca^{2+} aCSF to limit synaptic transmission or following the addition of 10 μM BIC to block $GABA_A$ receptors **(Figure 4.2D)**. The average burst frequency was 2.7±0.4 Hz with 30 μM 4-AP (n=4). This reduced by 53% ($p<0.05$), 64% ($p<0.05$), and 78% ($p<0.01$), for low-Ca^{2+} aCSF, 10 μM BIC, and 20 μM BIC, respectively **(Figure 4.2E, F)**. In 2 of 3 experiments, the higher dose BIC (20 μM) completely blocked 4-AP induced bursts. Thus, the emergent bursting involves a network of synaptically-connected neurons whose DRP and bursting events involved activation of $GABA_A$ receptors.

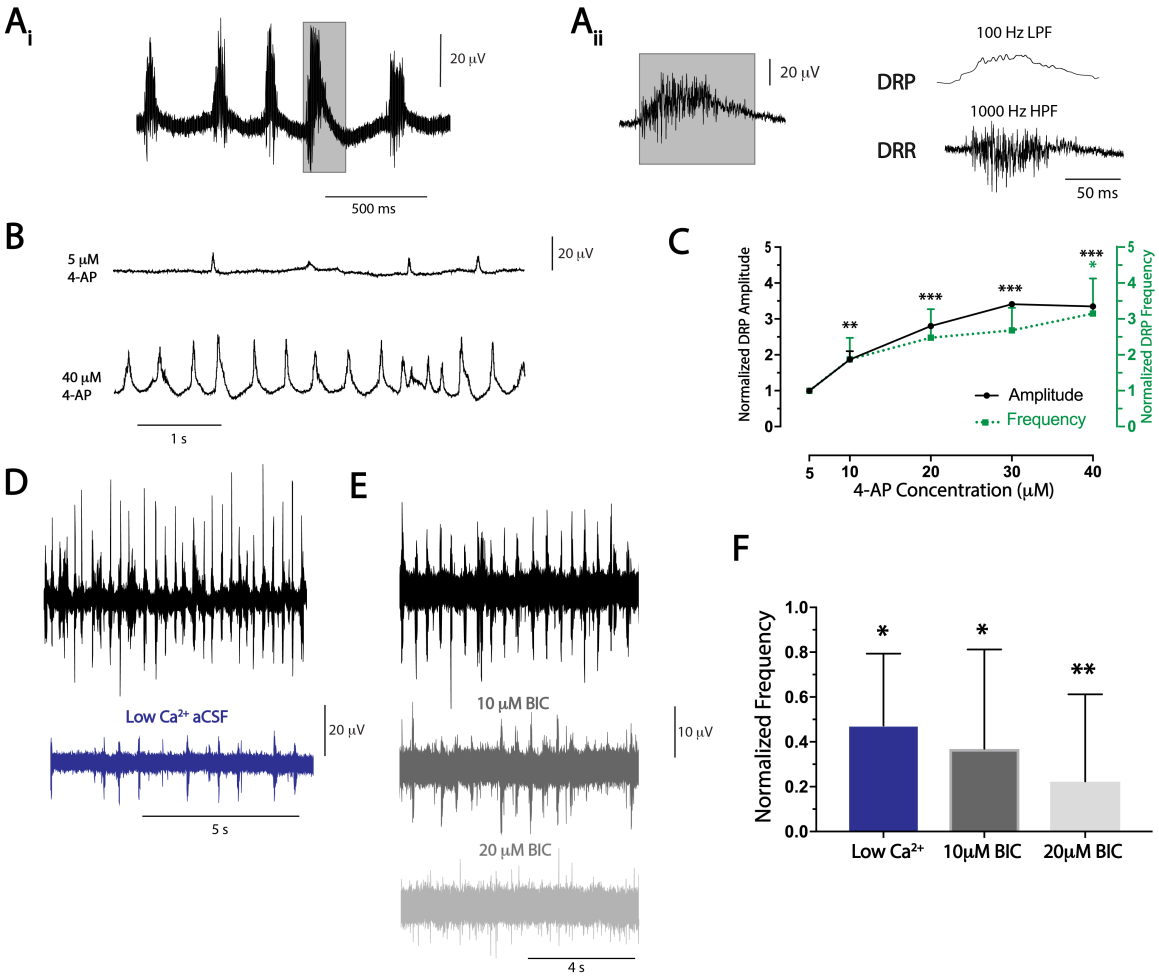

Figure 4.2: 4-AP induces spontaneous bursts and DRPs in DRs.

A) Example recording from a lumbar DR following bath application of 30 μM 4-AP. An example burst is highlighted by the grey box **(i)** and the same burst is expanded before and after 100 Hz LP (right, top) or 1000 Hz HP (right, bottom) filtering **(ii)** to observe the underlying DRP and DRR. **B)** Example recording of spontaneous DRPs at 5 μM (top) and 40 μM bath application of 4-AP. Each is a single trace after 100 Hz LP filtering. **C)** DRP amplitude and frequency increase with higher concentrations of 4-AP. Each data point is the average across the population, normalized to the magnitudes obtained at 5 μM 4-AP (n=3). Ordinary one-way ANOVA with Holm-Sidak multiple comparisons test was performed to identify significant differences from 5 μM 4-AP [*, $p<0.05$; **, $p<0.01$; ***, $p<0.001$] **D, E)** Burst frequency (generated with 30 μM 4-AP) is altered by decreasing extracellular Ca^{2+} and reducing $GABA_A$ signaling with bicuculline (BIC). The top black traces are recordings prior to switching to low Ca^{2+} aCSF (blue) or bath application of 10 and 20 μM BIC (grey). The displayed recordings are all single traces. **F)** low-Ca^{2+} aCSF (n=4) or BIC (n=3) reduces burst frequency, initiated by 4-AP (30 μM). All data was normalized to baseline values and t-tests were performed to identify significant differences from baseline [*, $p<0.05$; **, $p<0.01$].

4.4.2 Peripheral actions of 4-AP generate spontaneous spiking in primary afferents

In addition to the the circuit-based DRPs and bursting in DRs, spontaneous firing emerged that appeared independent of the synaptically-mediated activity **(Figure 4.3A)**. To determine whether these events originated in peripheral afferents we used an isolated minibath containing 4-AP (˜30-50μM) and constructed around 3 to 4 lumbar DRs with attached DRGs (**Figure 4.3B**). Recording of DRs with 4-AP exposure revealed the emergence of spontaneous spiking activity, without the presence of repetitive bursts and DRPs (n=3). As similar spontaneous spiking activity was seen when 4-AP (30 μM) was applied in the whole bath preparation in the presence of a higher concentration of BIC (20 μM) (n=3, **Figure 4.3C**), we concluded they are peripheral in origin. To assess the classes of primary afferents peripherally activated with 4-AP, we similarly isolated afferent activity (whole bath application of 4-AP+BIC) and applied tetrodotoxin **(TTX)** at incremental doses known to progressively block Aβ, Aδ, and C fibers [221][6]. Observations from these experiments suggest that in addition to the spinal oscillations, 4-AP also initiates spontaneous firing in some A and many C primary afferents (n=3, **Figure 4.3D**).

4.4.3 Spontaneous nociceptive activity is generated by 4-AP

As Lissauer's tract and the subjacent substantial gelatinosa (LT/DH) prominently encode nociceptive activity, extracellular recordings of LT activity strongly suggest that 4-AP (20 μM) produces spontaneous nociceptive activity. In LT this activity manifests as putative Aδ (large) and C fiber (small) single-unit spikes **(Figure 4.4A)**. When the microelectrode is positioned below the surface of LT (**LT/DH**), nociceptive activity can manifest as spikes and/or extracellular field potentials (**EFPs**) that reflect the population synaptic events from the underlying superficial dorsal horn **(Figure 4.4A)**. The average frequency of induced nociceptive population events (fields with or without superimposed spikes) is 1.1±0.5 Hz (n=7), while the frequency of nociceptive spikes independent of EFPs is 0.5±0.1 Hz (n=5). Simultaneous recordings of lumbar LT/DH and the segmental DR revealed that the EFPs

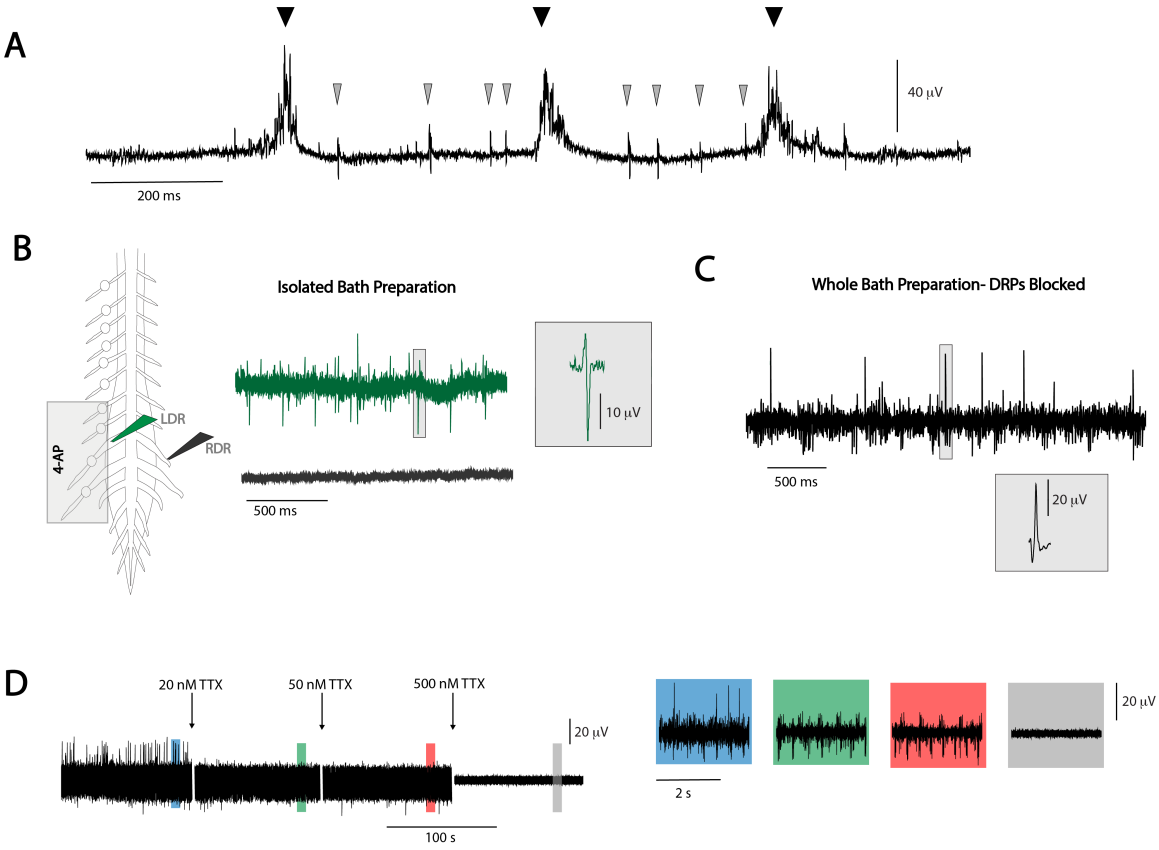

Figure 4.3: Peripheral actions of 4-AP produce spontaneous primary afferent spiking.

A) An example recording from a lumbar DR after 4-AP application (30 μM). Both DRPs (black triangles) and spontaneous spikes (grey triangles) can be observed. **B)** An isolated minibath arrangement was constructed to limit the exposure of 4-AP to peripheral aspects of the *ex vivo* preparation (DRG & DRs). The green trace (top) was from a lumbar DR with 4-AP exposure and the black trace (bottom) was from the contralateral DR. Spontaneous spiking was observed in the root with 4-AP exposure. *inset*: magnified spike highlighted in the green trace (top) by the grey box. **C)** When DRPs are blocked with a higher concentration of BIC (20 μM), single-unit firing is observed in the L2 DR with bath application of 30 μM 4-AP, instead of bursts. *inset*: magnified spike highlighted by the grey box. **D)** Selective block of spontaneously active afferents using concentration-based TTX application suggests that 4-AP produces hyperexcitability in A and C fibers. The colored boxes (right) display expanded regions of the recordings before (blue) and after 20 (green), 50 (red) and 500 nM (grey) TTX.

frequently coincide with large DRPs observed in the DR, but on average are generated at less than half the frequency of the DRPs (2.5±0.7 Hz, n=5). The events generated in LT/DH and DR are rhythmic **(Figure 4.4B)**, but lower frequencies (<2Hz) had greater contributions to the LT/DH activity, than what was observed in the DR **(Figure 4.4C)**. Large bursts in DRs can have two components (fast and slow), and the slow component appears to be related to large EFPs in the DH **(Figure 4.4D)**. This suggests that spontaneous events induced in the superficial DH produce antidromic bursts in slower conducting primary afferents (Aδ and C), likely through primary afferent depolarization (PAD).

Activation of nociceptive circuits in the DH was confirmed with neuronal labeling for the activity dependent reporter Fos. We compared Fos labeling in the pain-encoding superficial dorsal horn under control conditions to that seen after electrical recruitment at C fiber intensity (200 μA, 500 μs at 10 Hz for 10 mins) or after bath application of 4-AP (20 μM) for 10 minutes **(Figure 4.5)**. Both electrical stimulation and 4-AP led to significantly increase Fos labeling in the pain-encoding superficial dorsal horn. As expected for the electrical stimulation experiment, Fos labeling was greater on the stimulated side, while increases in Fos labeling with 4-AP were similar bilaterally.

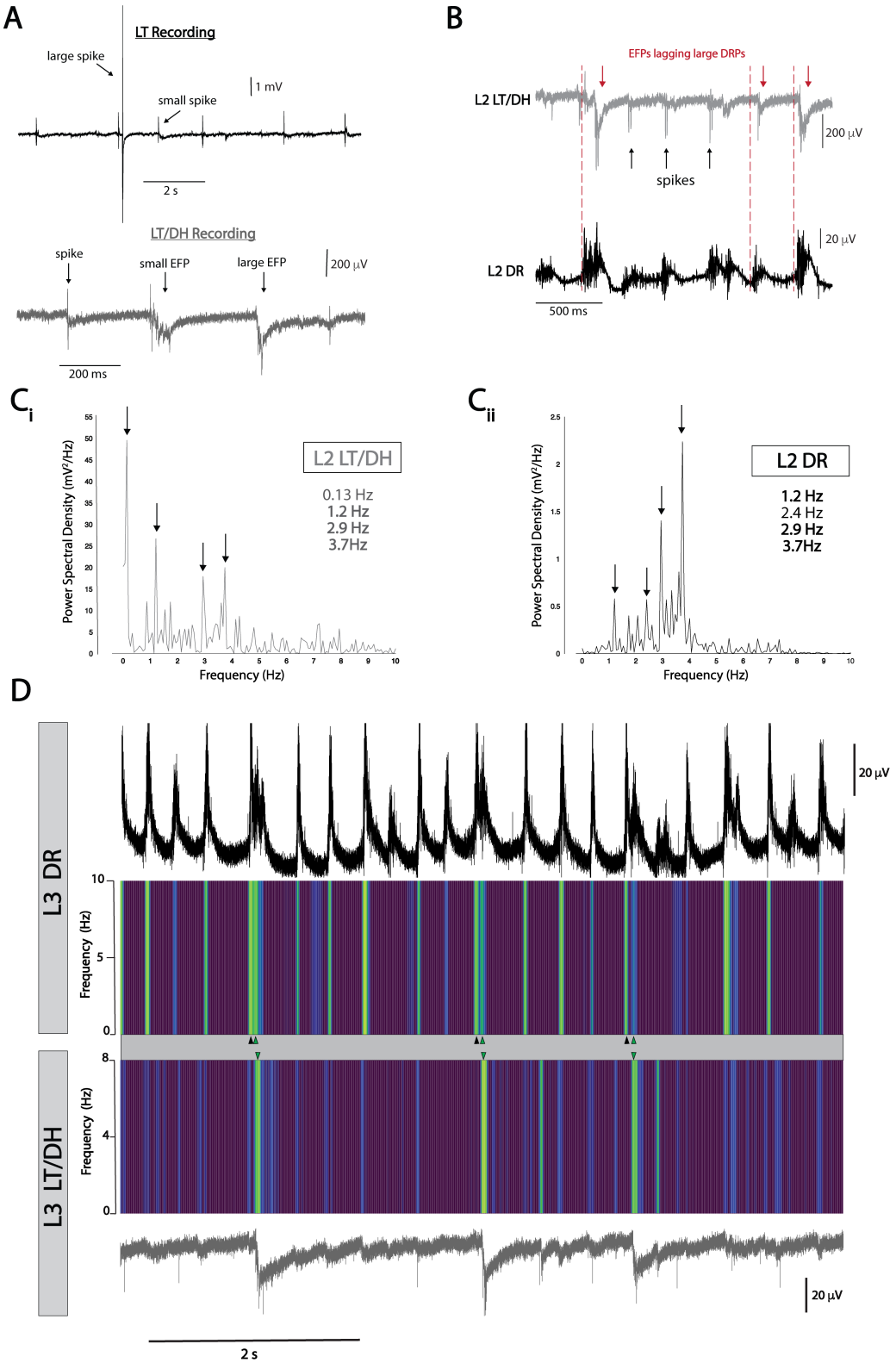

Figure 4.4: 4-AP produces rhythmic activity in LT/DH that can coincide with DR activity.

A) Spontaneous nociceptive activity can be observed as repetitive spikes in LT (top) and/or field potentials (EFP) from the underlying dorsal horn (bottom). **B)** Example of simultaneous recordings of LT/DH and DR after bath application of 4-AP (20 μM). In this recording, the EFPs are observed after large DRPs are generated in the segmental root. Spikes can also be observed that appear to coincide with smaller amplitude DRPs/DRR. **C)** FFTs of the recordings from B reveal that both LT/DH **(i)** and DR **(ii)** produce rhythmic activity, the largest frequency component is different for each. For LT/DH the largest frequency contribution to the signal is at 0.13Hz, with other sharp peaks at 1.2, 2.9, and 3.7 Hz. For DR, peaks at 1.2, 2.9, and 3.7 Hz are also observed but the largest frequency component is at 3.7Hz. **D)** The slower component of large DR bursts coincides with EFPs in the superficial DH. Displayed are raw recordings from the L3 DR (black) and L3 LT/DH (grey), along with their associated spectrograms over the same time course. The bright green bands in the spectrogram denote the timing of large events in both populations. The black triangles identify the location of the fast burst in the DR, the green triangles denote the slow component. The slow component in the DR coincides with a large EFP in the superficial DH.

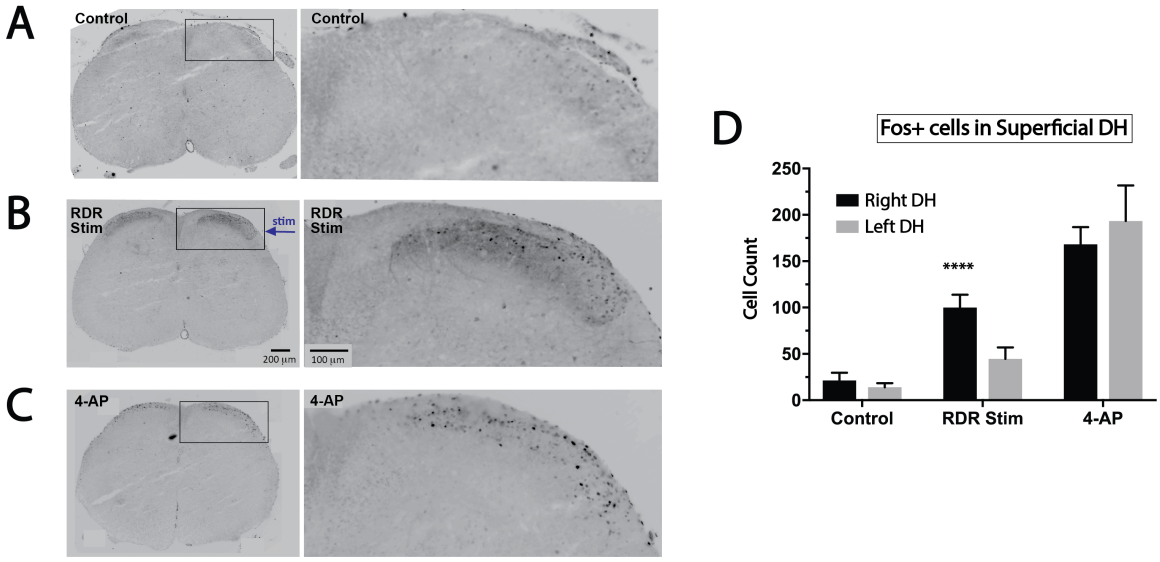

Figure 4.5: Fos labeling confirms the selective activation of superficial DH neurons consistent with activation of nociceptive circuits.

A) Few Fos+ cells were observed in the control condition (electrode placed with no stimultion). **B)** Electrical stimulation the right L2 DR at high intensity (200 μA, 500 μs) at 10 Hz for 10 mins served as a positive control for Fos labeling. 10 Hz stimulation of the RL2 DR at C-fiber threshold resulted in Fos+ cells in the superficial DH of L2. **C)** Bath application of 4-AP (20 μM) also resulted in Fos+ cells in the lumbar superficial DH. **D)** For the stimulation case, greater Fos+ cells were observed in the DH ipsilateral to DR stimulation (n=1, average across10 sections); 2-way ANOVA with Holm-Sidak multiple comparisons test was performed to identify significant differences between counts on the left and right sides of the DH of a single lumbar segment, [****, $p<0.0001$]. Preliminary evidence suggests that 4-AP (n=1, average across 7 sections) produces greater nociceptive activation in the DH, than electrical stimulation. Very little nociceptive activation was observed in control animals (n=2, average across 13 total sections), where an electrode was placed on the right DR with no stimulation. Statistical analysis was not performed across groups, due to the small sample size.

4.4.4 Stimulus-independent nociceptive activity can be modulated by SCS

To investigate if SCS can modulate spontaneous nociceptive activity, we first identified the stimulation intensity for consistent threshold recruitment for the DC and DR of a selected lumbar segment **(Figure 4.6A)**. We then, applied 10, 50 or 100 Hz stimulation at T_{DC} or T_{DR}. The 2 min window following stimulation was analyzed to identify if SCS reduced the frequency of nociceptive spikes or synaptic events (EFPs). Examination of spiking activity during SCS (inter-SCS interval) revealed that 50 Hz stimulation at T_{DC} reduced nociceptive spiking by 54%, on average (n=4, $p<0.05$, **Figure 4.6B, 4.6C**). Interestingly, this effect was not seen at the higher stimulation intensity required for Aβ fiber recruitment at T_{DR}. There were no parameters of SCS that produced prolonged modulation of spikes in LT/DH and none of the examined parameters modulated EFPs during or after SCS (not shown).

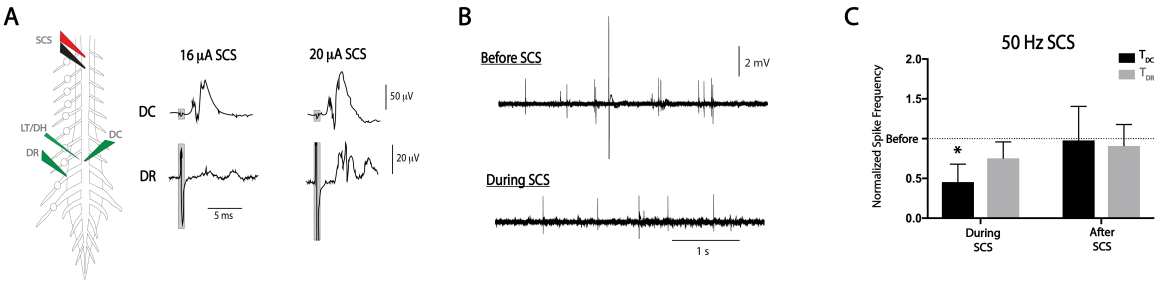

Figure 4.6: 4-AP induces spontaneous nociceptive activity that can be modulated by SCS.

A) Schematic of modulation experiments (left). Example SCS thresholds for DC (T_{DC}) and DR (T_{DR}) were identified for subsequent experiments investigating modulation of LT/DH activity (right). Each trace is the average of 6 sweeps. The gray box denotes the stimulation artifact. **B)** Example recordings of spiking activity in LT before (top) and during (bottom) SCS at T_{DC} threshold. Each trace consists of 6 overlying sweeps. **C)** SCS modulation of nociceptive spiking occurs during 50 Hz stimulation at T_{DC} but does not persist after stimulation. The data is normalized to the spike frequency prior to stimulation (before). 2-way ANOVA with Holm-Sidak multiple comparisons test was performed to identify significant differences from baseline (before) [*, $p<0.05$]

4.5 Discussion

Expanding upon our previous work, we demonstrated successful implementation of an adult *ex vivo* mouse spinal cord (SC) preparation with intact dorsal root ganglia (DRG) as a model system to study modulation of spontaneous hyperexcitability in nociceptive circuits . Permitting access to the DRGs, DRs, and SC at segments ranging from C8 to S1, this system circumvents the accessibility issues that arise from *in vivo* preparations while allowing greater interrogation of a more intact sensory system than typical *in vitro* and *in vivo* preparations. Using this preparation and bath application of 4-AP, we generated a model of stimulus-independent sensory hyperexcitability involving activation of neuropathic pain pathways. Emergent activity was expressed as: (i) episodic population DRPs with superimposed burst firing in DRs, (ii) spiking in a pain tract (LT) with coincident population synpatic events (EFPs) in the subjacent superficial dorsal horn (DH), and (iii) independent spontaneous spiking events seen both in DRs and LT **(Figure 4.7A)**. Interestingly, the larger episodic population events observed in LT/DH were coincident with longer-lasting DRP population activity seen in DR recordings. The timing of the longer-latency events in the DRP and the onset of LT/DH activity suggest they originate from a common circuit involving higher threshold afferents. These events occurred at a lower frequency. We did not explore the synaptic circuit composition of episodic events recorded in LT/DH.

The frequency and amplitude of emergent episodic DRP/bursting activity in DRs was 4-AP dose-dependent. DR bursting was dependent on synaptically-connected neural circuitry as it was depressed when synaptic transmission was reduced using a low Ca^{2+}-containing aCSF. Episodic DRP/bursting was also dependent on activation of $GABA_A$ receptors as burst frequency was depressed after application of a low dose of the receptor antagonist BIC, and could be completely abolished at higher BIC dose. After the spontaneous DRPs were suppressed, the remaining spontaneous firing in individual axons mirrored the axonal

firing observed with selective application of 4-AP applied to locally isolated lumbar DRGs and DRs. The population of single axonal units recorded was shown to consist of both A and C fibers.

Spiking activity seen in DRs could arise from primary afferents themselves that then lead to the DRP or from central circuits leading to dorsal root reflexes (DRRs) coincident with DRPs. The DR spiking commonly appears after the onset of the primary afferent depolarization (PAD) responsible for the DRP, suggesting that they arise from central presynaptic inhibitory circuitry as DRRs. Overall, these observations demonstrate that rhythmic bursting in DR is due to activity originating in the dorsal horn and propagated antidromically in dorsal roots. Coincident bursts of spiking and population synaptic potential responses recorded in LT and subjacent superficial dorsal horn associate DR activity with recruitment of nociceptive circuits.

4.5.1 Neuronal activation and amplification with 4-AP

4-AP is a broad-spectrum voltage-gated K^+ channel blocker [229], with the fast A-type potassium current (I_A) being more sensitive than the delayed rectified current (I_{DR}) in DRGs [230]. When formulated as a therapeutic (fampridine), 4-AP has demonstrated clinical utility for improving motor symptoms following spinal cord injury (SCI) and multiple sclerosis (MS) through suggested mechanisms thought to include restoration of conduction in demyelinated axons, increased neuromuscular transmission, and facilitated recruitment of spinal locomotor circuitry [225][231]. Unfortunately, 4-AP can also produce abdominal pain, and paresthesia in treated patients ([232][233]. These sensory abnormalities are suggested to result from actions on cutaneous nerves and DRs [232][233].

In preclinical studies, 4-AP generates rhythmic epileptiform activity in hippocampal slices [234][222] and spinal cord [231][235][223]. In the spinal cord, this is seen as

synchronous bursts of activity in dorsal and ventral roots that originate from spinal circuits [231][235][223] [236]. Bursting activity tested in dorsal roots and superficial dorsal horn was sensitive to inhibition of synaptic transmission [231] [223]. In spinal cord slice recordings from juvenile rats, 4-AP has previously been shown to generate suprathreshold episodic bursting in superficial dorsal horn neurons including pain-encoding lamina I spinoparabrachial projection neurons. It also unmasks polysynaptic C-fiber pathways [223]. The same study observed preferential reduction in activity by anticonvulsants rather than classical analgesics, further suggesting that 4-AP induces a neuropathic pain-like phenotype. Building on this, the present work demonstrated similar episodic bursting with 4-AP in our newly-developed adult mouse isolated spinal cord preparation. This allowed the study of more intact neural circuitry and enabled us to explore the modulatory potential of SCS on a stimulus-independent hyperexcitability model expressing neuropathic pain-like activity. 4-AP recruitment of nociceptive primary afferents was verified with preferential block by high dose TTX. Additionally, 4-AP recruitment of nociception-encoding spinal circuitry was confirmed by direct recordings of episodic activity from a pain-processing tract (LT) that corresponded with subjacent population synaptic activity in the pain-encoding superficial dorsal horn (EFPs), a region also selectively expressing large increases in the activity-dependent marker Fos. Future studies should determine whether this rhythmic activity is also preferentially sensitive to anticonvulsants over conventional analgesics as reported in the Ruscheweyh and Sandkuhler (2003) study [223].

Consistent with earlier findings, we also observed that the frequency of induced DRPs/ bursting is depressed following partial block of synaptic transmission in low Ca^{2+}- containing aCSF and also significantly depressed or completely blocked following block of $GABA_A$ receptors with BIC. Though most previous studies were conducted in neonate and juvenile spinal cord slices, we have been able to reproduce some of these findings in our adult, more intact preparation. While both neuronal and glial connexin proteins and gap

junctions are also implicated in generating the emergent network oscillatory activity [235], we have not yet tested the actions of gap junction blockers in our intact adult spinal cord preparation.

Spontaneous primary afferent activity (A and C fibers) has been identified as a potential driver of neuropathic pain [50] [49] [51] [52] [54] [55] [35]. We sought to determine whether 4-AP can lead to emergent spontaneous primary afferent activity, as the peripheral actions of 4-AP are less defined. 4-AP application to peripheral nerve and DRs in vitro was shown to produce regenerative firing and after-potentials in response to single evoked stimuli but stimulus-independent ectopic firing was not seen [232][233]. 4-AP was similarly not observed to generate ectopic firing when applied directly to the nerve, but ectopic firing was seen in all classes of cutaneous afferents when applied to nerve endings in a skin-nerve preparation [237].

To determine whether 4-AP can produce spontaneous afferent activity, we applied 4-AP on DRG and DRs in isolation using a minibath partition **(Figure 4.3B)**. We observed spontaneous activity emerge in dorsal root axons and used the differential sensitivity to progressively increasing doses of TTX to demonstrate that emergent activity originated from A and C primary afferents. Unlike centrally-applied 4-AP, no episodic population activity emerged. Compared to earlier studies our observed spontaneous firing is easily explained by the presence of afferent cell bodies located in the DRGs of our preparation. 4-AP blocks multiple A-type voltage-gated K^+ channels expressed in DRG [228]. Importantly, reduced DRG expression of A-type channels is seen in multiple chronic pain models [224]. While this was typically associated with an evoked hypersensitivity, arterial injection of 4-AP in an in vivo model of peripheral neuroma could induce ectopic firing in silent axons and increase the firing rate of axons that were previously spontaneously active [238]. Paired with our observation that 4-AP also induces spontaneous episodic activity in nociception-

encoding spinal circuits (LT and superficial dorsal horn), we are in a strong position to use our model system to study the effects of SCS on nociceptive hyperexcitability at both central and peripheral sites of origin.

4.5.2 Modulation of stimulus-independent nociceptive activity

Previously (Chapter 3, [184]), we demonstrated that SCS recruits DC axons, at stimulation amplitudes below the recruitment threshold for Aβ primary afferents of DRs. We hypothesized that postsynaptic dorsal column **(PSDC)** tract cells could be the DC constituent with the lowest recruitment threshold. Here, we investigated the potential for clinically-analogous SCS to modulate spontaneous nociceptive activity in the SC-DRG preparation and found that SCS preferentially modulated spikes during 50 Hz stimulation at T_{DC}.

While none of the tested parameters of SCS modulated the frequency of episodic synaptic discharges (EFPs), 50 Hz SCS at T_{DC} reduced the firing frequency of spontaneous spiking in axons in LT but only during the period of stimulation (quantified at the inter-SCS period). Modulation did not persist after the cessation of 50 Hz stimulation and did not occur for any other parameters of SCS. To our knowledge, this is the first experimental study to investigate SCS modulation of stimulus-independent nociceptive activity. As LT contains axons of subjacent interneurons along with collaterals of Aδ and C primary afferents ,and DH population responses were not affected, we assert that the depressed activity seen is via modulation of primary afferent spiking.

We observed selective modulation of lumbar LT/DH spikes during recruitment of low threshold DC axons but not at slightly higher stimulus intensities that would recruit DC primary afferent collaterals. The assumed mechanism of action for SCS involves recruitment of low threshold primary afferents (Aβ) that activate inhibitory interneurons in the

dorsal horn and prevents nociceptive transmission from lamina V WDR projection neurons. Our findings indicate that PSDCs cells may contribute to SCS modulation of nociceptive activity.

Though PSDC orthodromically project to DC nuclei, they also have local axon collaterals in the spinal segment from which they originate [211]. It is possible that PSDC recruitment activates inhibitory interneurons via their axon collaterals, and that these inhibitory interneurons depressed on ongoing nociceptive activity to subthreshold levels resulting in unchanged frequency of synaptic events but reduced frequency of spiking **(Figure 4.6C, 4.7B)**. While this is what one would predict if SCS only functioned via the gate control theory, modulation can persist for 30 minutes after SCS cessation clinically [82]. In vivo studies have also observed persistent modulation 30 minutes post-SCS [102][239]. Together, this suggests that the prolonged modulation observed may be due to supraspinal systems such as antinociceptive contributions from descending serotonergic circuitry [105][101][99]. Importantly, as modulation was not observed during SCS at an intensity that would recruit the low threshold primary afferents our finding indicate that the presumed form of gate control does not contribute to SCS modulation, and that antidromic activation of DC axons alone cannot account for the modulation of chronic neuropathic pain.

Interestingly, spiking activity was not reduced with SCS at an intensity that also recruited Aβ fibers. It has recently been shown that a population of amygdalar neurons encode a unique assembly of neurons that are necessary for producing the affective/emotional dimension of pain [138]. Using a peripheral nerve injury model of neuropathic pain with allodynia, they observed that recruitment of presumed Aβ fibers were now able to activate the pain encoding cells in the amygdala. Thus, rather than close the pain gate, Aβ fibers may have unmasked projections that instead amplify pain. Regarding our work, significantly reduced spontaneous activity— originally generated by SCS recruitment of DC

axons below Aβ threshold (putatively PSDC cells; see 3.5.3)— is lost when Aβ fibers are also recruited. This may be due to competing activation of nociception-reducing and nociception-promoting pain circuit activation.

As the 4-AP induced rhythmic DH EFPs and DRPs may reflect a centralized paroxysmal form of neuropathic pain, our observations suggest that SCS would be ineffective with the stimulation strategies attempted. Regardless, this initial study of SCS employed a mechanistic approach with well-defined stimulus intensity and duration protocols to provide the first foray into SCS control of spontaneous sensory hyperexcitability. As such this foundational investigation may serve as a launchpad for more detailed exploration of the SCS parameter space for control of spontaneous nociceptive activity. Future studies may assess whether different frequencies, stimulation patterns, longer duration stimulations or higher stimulus thresholds would be more effective. For example, in a single trial with higher intensity SCS stimulation at 50 Hz (anodic polarity, 200 μs pulse width at 200 μA for 5 seconds every 20 seconds) led to lasting depression of episodic activity in LT/DH in the intervening periods (not shown; n=1).

Traditional SCS employs frequencies $\leq$200 Hz with successful modulation obtained at 63Hz, on average [24][64]. Many preclinical studies use 50 Hz SCS to investigate modulation of stimulus-evoked hypersensitivity [102][103][110] [95] [97][107] [100] [104] [239]. While projection neurons from the dorsal horn can have variable responses to different SCS frequencies, one characteristic response consists of a non-monotonic frequency-response relationship, where peak modulation is observed at 50 Hz [114]. Our model recapitulates the frequency dependent nature of SCS modulation, as 10 and 100 Hz did not reduce synaptic or spiking events in LT/DH. A caveat of our studies is that recordings were obtained at room temperature and we cannot exclude the possibility that frequency dependence of modulation may be sensitive to differences in temperature given a temperature could clearly

alter the spatiotemporal features of stimulus delivery.

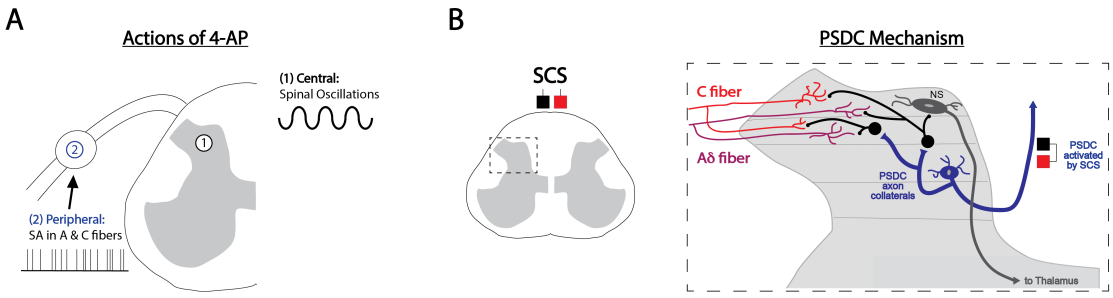

Figure 4.7: 4-AP produces spontaneous activity that may be modulated by PSDC cells.

A) 4-AP produces distinct manifestations of spontaneous activity, depending on the site of action. **B)** SCS may modulate spontaneous activity by recruiting PSDC cells (blue) that pre- or postsynaptically depress nociceptive circuits via inhibitory interneurons (black).

4.6 Conclusions

Here, we used an isolated SC-DRG preparation to determine if–in accordance with the gate control theory–activation of Aβ collaterals in the thoracic DC was sufficient for modulating spontaneous neuropathic pain-like activity in the lumbar spinal cord. We found that only DC threshold (recruiting putative PSDC tract cells) SCS modulated nociceptive spiking, during 50 Hz stimulation. Aβ (DR) threshold stimulation could not produce modulation for any of the frequencies tested. We also found that none of the stimulation parameters were able to reduce spontaneous synaptic nociceptive activity or produce prolonged modulation. The findings suggest that antidromic actions resulting from DC axonal recruitment cannot solely account for spontaneous pain modulation observed clinically.

4.7 Research Contributions

Tissue isolation, electrophysiology experimentation, and analysis was performed by Shaquia Idlett-Ali. Fos experiments and histological processing and analysis were conducted by Mallika Halder and Michael Sawchuk. Shaquia Idlett-Ali authored this chapter with collaboration from Dr. Shawn Hochman.

CHAPTER 5
CONCLUSIONS AND FUTURE WORK

5.1 Conclusions

The objective of this dissertation was to generate knowledge that leads to a better understanding of both neuropathic pain and pain relief provided by electrical spinal cord stimulation (SCS).

In Chapter 2, I explored stimulus-independent physio-behavioral indices of ongoing, neuropathic pain. For this work, noncontact electric field sensors were utilized with a thoracic contusion mouse model of spinal cord injury (SCI), known to generate mechanical hypersensitivity. Examination of respiration rate variability (RRV) and sleep metrics (sleep event number, sleep event duration, and brief arousal number) revealed significant differences from baseline, 6 weeks after SCI. I also found that spontaneous activity in the cell bodies of primary afferents were greater in dorsal root ganglia (DRG) of the SCI group, when compared to sham. The incidence of spontaneously active DRG in the SCI group correlated with hindpaw mechanical sensitivity (50 % PWT), where a greater incidence was observed in animals with lower PWTs. Incidence of DRG spontaneous activity was also correlated with increases in the number of sleep events/ hour, indicative of greater sleep segmentation for animals with a larger incidence of spontaneously active DRG. Observed correlations between spontaneous sensory activity with evoked mechanical sensitivity and sleep dysfunction support an important interplay between sleep and pain after SCI. DRG spontaneous firing frequency, instead of incidence, was positively correlated with RRV. Interestingly, spontaneously active DRG incidence and firing frequency where not correlated, suggesting that they may encode difference aspects of neuropathic pain. Overall, mea-

sures of spontaneous afferent activity correlated with sleep segmentation, RRV, and paw mechanosensitivity. As spontaneous afferent activity after SCI has previously been shown to be causally linked with perception of stimulus-independent neuropathic pain [60], it is plausible that afferent activity is also responsible for observed changes in respiration, sleep and mechanosensitivity.

In Chapter 3, I developed an isolated adult mouse spinal cord for investigations of axonal recruitment with SCS. To generate clinically-analogous stimulation in the mouse model, I leverage finite element modeling to identify appropriate scaling of electrode dimensions and stimulation parameters to mirror the electric fields generated with clinical SCS. Analogous electric field distributions were generated with 300 μm x 300 μm electrodes positioned 200 μm above the dorsal column with stimulation between 50 and 200 μA. With simultaneous recordings in the lumbar dorsal column (DC), dorsal root (DR) and Lissauer's Tract (LT), I assessed antidromic axonal recruitment with SCS and found that axons in the DC had the lowest recruitment threshold with faster conduction velocity than the lowest threshold DR component. On average, DR and LT components were recruited at 2.6 and 4.4 times the DC threshold, respectively. Importantly, these findings suggest that the lowest threshold DC population recruited by SCS are not collaterals of Aβ primary afferents, but instead arise from a non-afferent fiber population likely to be postsynaptic dorsal column tract (PSDC) cells. Clinically, SCS generates paresthesias and pain relief; and the previously assumed mechanism of action identifies Aβ primary afferents as the source of both sensory phenomena. As PSDCs project to DC nuclei and have local axon collaterals in the dorsal horn, my observations suggest that PSDC recruitment potentially contributes to paresthesias and/or depression of pain perception.

In Chapter 4, I extend the isolated spinal cord preparation to include attached lumbar DRGs to conduct the first known experimental appraisal of SCS modulation of stimulus-

independent (spontaneous) nociceptive activity. To model spontaneous nociceptive activity, I employed bath application of the broad voltage-gated potassium channel blocker, 4-aminopyridine (4-AP). Evidence that the 4-AP model led to recruitment of superficial dorsal horn spinal nociceptive circuits was confirmed using activity dependent *Fos*-labeling. 4-AP induced spontaneous activity that included rhythmic dorsal root potentials with superimposed burst firing in dorsal roots. Rhythmic extracellular field potentials (EFPs) with superimposed spikes in LT and subjacent dorsal horn were also observed and often corresponded to events seen in dorsal roots. Pharmacological experiments additionally demonstrated that single-unit firing arose from A and C primary afferents of the lumbar DR, and were generated independently of central circuits. I then explored whether SCS at DC and DR threshold could modulate spontaneous activity when tested at 10, 50, and 100 Hz. Only DC threshold SCS at 50 Hz was found to modulate spiking activity in LT/DH, and this occurred only during stimulation. There was no evidence of modulation of spontaneous synaptic events (EFPs) during or after SCS. Though in clinical studies SCS has been demonstrated to generate prolonged modulation 30 minutes after cessation of stimulation, this was not observed in my studies. Overall findings suggest that the recruitment of dorsal column axons may not be sufficient for modulation of stimulus-independent neuropathic pain. Further, SCS recruitment of Aβ fibers had no effect on spontaneous activity, contrary to the assumed mechanism of Aβ fiber recruitment in gate control of pain. **Figure 5.1** summarizing the major findings of this work.

Overall, this dissertation provides greater insight into the development of neuropathic pain and the underlying mechanisms leading to pain relief with SCS. The findings support further investigation of SCS stimulation parameters to modulate spontaneous nociceptive activity.

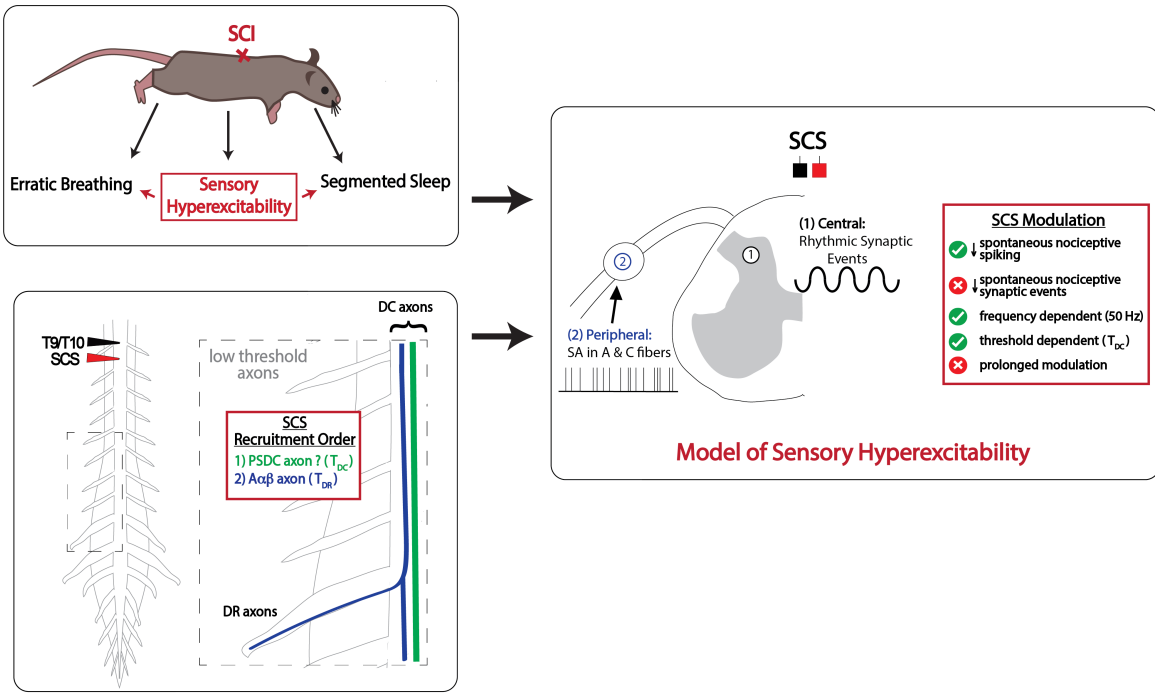

Figure 5.1: Summary of dissertation findings

I first found that peripheral sensory hyperexcitability is correlated with metrics of erratic breathing (RRV) and segmented sleep (sleep event count), in an SCI model of neuropathic pain. Next, I observed that a non-primary afferent population in the DC is recruited with SCS before Aβ primary afferents in the DR. That population possibly consists of PSDC tract cells. Lastly, in a model of spontaneous sensory hyperexcitability–that included spontaneous nociceptive activity, I found that only DC threshold (T_{DC}) SCS modulated spontaneous nociceptive spiking during 50 Hz stimulation. Depression of spontaneous nociceptive synaptic activity and prolonged modulation was not observed with any parameters. These findings suggest that SCS modulation can not solely function via the gate control theory to produce relief of persistent spontaneous pain.

5.2 Suggestions for Future Work

5.2.1 Mechanism of action: direction of new studies

In this dissertation *ex vivo* adult mouse preparations were used to study recruitment and modulation with SCS. A benefit of transitioning studies to mouse models includes the availability of genetic tools for cell-type specific targeting and modulation. In the ideal scenario there would be an existing transgenic mouse line that would permit selective recruitment of PSDCs via membrane expression of Channelrhodopsin (ChR). Such a tool could be used in collision experiments to confirm that PSDCs are the lowest threshold DC population recruited with SCS—evident by observation of optogenetic PSDC recruitment blocking the low threshold DC volley observed with SCS. Selective optogenetic recruitment of PSDCs would also help determine if maximal recruitment of these cells lead to modulation of nociceptive activity in the model of sensory hyperexcitability.

Further exploration of SCS mechanisms would be enhanced by *in vivo* single-cell recordings in the transgenic line that enables selective fluorescent labeling and recruitment of spinal projection neurons [240]. Nociceptive signals originating in the periphery or the spinal cord cannot be perceived if they are not transmitted to brain via spinal projection neurons. As such, neuronal activity of projection neurons could serve as an indicator of possible pain perception. Simultaneous recordings of spontaneous activity in dorsal roots and projection neurons could further support the role of spontaneous primary afferent activity in neuropathic pain states if NMDA antagonists reduce the spontaneous firing rate observed for projection neurons. *In vivo* models would also enable investigations of descending serotonergic contributions to SCS analgesia. If lesioning of the dorsal lateral funiculus (DLF) [105] or the local application of serotonin receptor (5-HT2A, 5-HT3, and 5-HT4) antagonists [101] inhibit SCS modulation of projection neuron activity, it would further define the importance of brainstem antinociceptive circuits and suggest that SCS

should be optimized to recruit them.

5.2.2 Paresthesias and pushing past the plateau

The most important finding from this work is that the lowest threshold population of axons in the DC produces partial modulation of spontaneous nociceptive activity in the spinal cord, and that this population is unlikely to be collaterals of Aβ primary afferents. Dogma assumes that in addition to the analgesia-producing antidromic actions, orthodromic actions of Aβ recruitment lead to paresthesias. Instead, PSDC recruitment with SCS seems plausible given the corroboration of these preclinical findings with clinical observations.

In clinical studies, sensory threshold (producing paresthesias) was variable between patients and body orientation-dependent [65][84]. But it typically coincided with the emergence of a DC volley, as observed by epidural compound action potential (ECAP) recordings [65]. Discomfort threshold occurred at about **2 times** the sensory/DC threshold and was associated with the emergence of a higher threshold [65], presumed slower conducting (smaller diameter) population of axons in the DC [84]. This higher threshold population led to a feeling of "tightness", not pain, alongside difficulty completing a motor task [65]. As this thesis showed that the lowest threshold axons are not afferent in origin, reported discomfort threshold may instead be associated with recruitment of low threshold primary afferents—possibly group Ia and/or Aβ axons. In my studies, DR primary afferents were recruited at **2.6 times** DC threshold and were slower conducting. Together it is reasonable to suggest that paresthesias result from orthodromic actions of PSDC recruitment, not Aβ primary afferents. As our results also demonstrate that more medial SCS electrode placement provides greater separation of recruitment threshold between DC non-afferent axons and Aβ primary afferents, medial electrode placements in clinical applications should permit a greater range of SCS amplitudes subthreshold to Aβ /discomfort recruitment.

In clinical settings, paresthesias serve as a rapid biomarker for therapeutic SCS. The concordance of the paresthesia with the region of pain has been deemed necessary for attaining analgesia, resulting in paresthesia-based optimization of parameters for traditional SCS. The variable success rates observed and the plateau in mean efficacy with traditional SCS demonstrates the inconsistent nature of this biomarker for predicting successful outcomes and the need for new parameter optimization approaches. EEG (electroencephalography) and fNIRS (Functional Near-Infrared Spectroscopy) systems are non-invasive, portable technologies that have been used to identify novel markers of pain activity in the brain. Most studies employed one or both of these technologies to explore indicators of acute pain activity in healthy subjects [241][242]. Some explore evoked outcomes in patients exhibiting neuropathic pain (fibromyalgia) [243][244] but no known studies have investigated markers for ongoing, spontaneous neuropathic pain. If a novel neuropathic pain "signature" could be identified by the hemodynamic and/or electrical activity of the brain in resting states, it could provide an additional near real-time metric for SCS parameter optimization in clinical settings. This alternative approach could provide a path toward improved success rates, since parameters would also be optimized to alter this "pain signature", instead of approaches reliant solely on the production of paresthesia overlap. If history is any indicator, the current approaches to improve efficacy through changes in the SCS technology itself (electrode design, frequency paradigms, etc.) are redundant and insufficient for overcoming the efficacy plateau.

Appendices

APPENDIX A

PRECLINICAL *EX VIVO* FEA MODEL

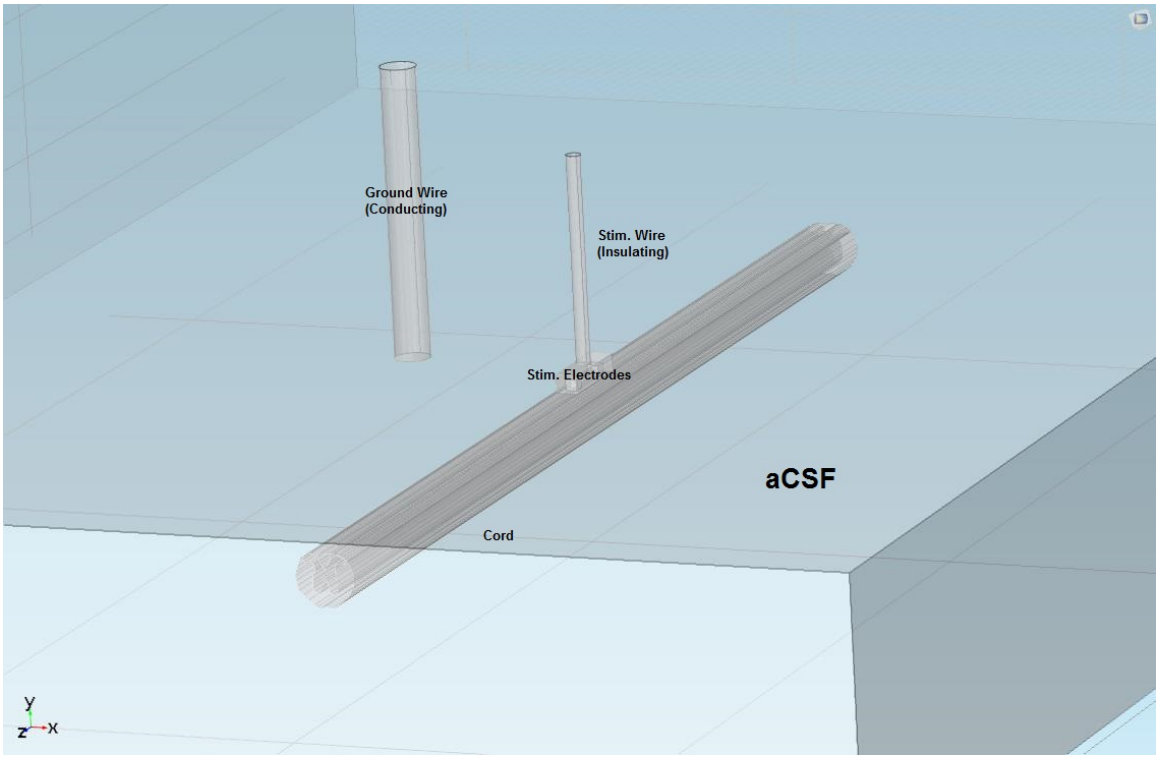

Figure A.1: Preclinical *ex vivo* FEA model set up

APPENDIX B

PRECLINICAL *IN VIVO* FEA MODEL

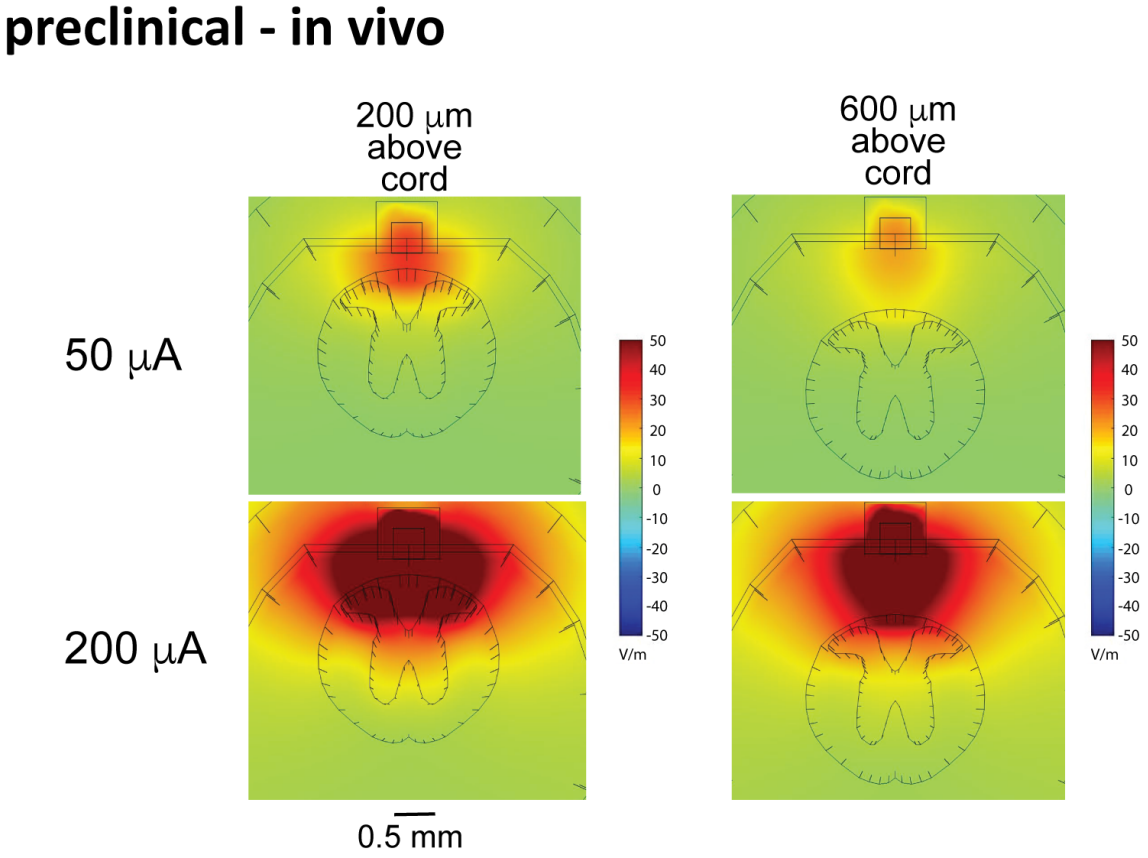

Figure B.1: Preclinical *in vivo* FEA model results

Electric fields in the spinal cord during SCS generated using a finite element model of the in vivo mouse spinal cord. Comparable electric fields were observed with stimulation 200 μm above the cord, at a low amplitude (50 μA) and 600 μm above the cord at a high amplitude (200 μA). Electric field magnitudes (V/m, scales capped at $\pm$50 V/m) are plotted over a cross-section of the spinal cord directly underneath the midpoint of the stimulation bipole.

REFERENCES

[1] B. A. Meyerson and B. Linderoth, "Mode of Action of Spinal Cord Stimulation in Neuropathic Pain," *Journal of Pain and Symptom Management*, vol. 31, no. 4 SUPPL. Pp. 6–12, 2006.

[2] T. C. Zhang, J. J. Janik, and W. M. Grill, "Mechanisms and models of spinal cord stimulation for the treatment of neuropathic pain," *Brain Research*, vol. 1569:19-31, pp. 19–31, 2014.

[3] M. P. Jensen and R. M. Brownstone, "Mechanisms of spinal cord stimulation for the treatment of pain : Still in the dark after 50 years," *European Journal of Pain*, pp. 1–8, 2018.

[4] H. Smits, M. van Kleef, J. Holsheimer, and E. A. J. Joosten, "Review Article: Experimental Spinal Cord Stimulation and Neuropathic Pain: Mechanism of Action, Technical Aspects, and Effectiveness," *Pain Practice*, vol. 13, no. 2, pp. 154–168, 2013.

[5] D. L. Felten, M. K. O'Banion, and M. S. Maida, "9-Peripheral nervous system," in *Netter's Atlas of Neuroscience*, D. L. Felten, M. K. O'Banion, and M. S. Maida, Eds., Third Edit, 2016, pp. 153–231.

[6] V. Pinto, V. a. Derkach, and B. V. Safronov, "Role of TTX-sensitive and TTX-resistant sodium channels in Adelta- and C-fiber conduction and synaptic transmission.," *Journal of neurophysiology*, vol. 99, no. 2, pp. 617–628, 2008.

[7] E. C. Emery, P. Ernfors, E. C. Emery, and P. Ernfors, "Dorsal Root Ganglion Neuron Types and Their Functional Specialization," *The Oxford Handbook of the Neurobiology of Pain*, no. August, pp. 1–30, 2018.

[8] V. E. Abraira and D. D. Ginty, "The sensory neurons of touch," *Neuron*, vol. 79, pp. 618–639, 2013.

[9] L. Li, M. Rutlin, V. E. Abraira, C. Cassidy, L. Kus, S. Gong, M. P. Jankowski, W. Luo, N. Heintz, H. R. Koerber, C. J. Woodbury, and D. D. Ginty, "The functional organization of cutaneous low-threshold mechanosensory neurons," *Cell*, vol. 147, no. 7, pp. 1615–1627, 2011.

[10] V. E. Abraira, E. D. Kuehn, A. M. Chirila, M. W. Springel, A. A. Toliver, A. L. Zimmerman, L. L. Orefice, L. Bai, B. J. Song, K. A. Bashista, T. G. O'Neill, J. Zhuo, C. Tsan, J. Hoynoski, M. Rutlin, L. Kus, V. Niederkofler, M. Watanabe,

S. M. Dymecki, S. B. Nelson, N. Heintz, D. I. Hughes, and D. D. Ginty, "The Cellular and Synaptic Architecture of the Mechanosensory Dorsal Horn," *Cell*, vol. 168, no. 1-2, pp. 295–310, 2017.

[11] M. Lidierth, "Long-range projections of Ad primary afferents in the Lissauer tract of the rat," *Neuroscience Letters*, vol. 425, no. 2, pp. 126–130, 2007.

[12] T. P. Enevoldson and G Gordon, "Postsynaptic dorsal column neurons in the cat: a study with retrograde transport of horseradish peroxidase," *Experimental Brain Research*, vol. 75, pp. 611–620, 1989.

[13] G. J. Giesler, R. L. Nahin, and A. M. Madsen, "Postsynaptic dorsal column pathway of the rat. I. Anatomical studies," *Journal of Neurophysiology*, vol. 51, pp. 260–275, 1984.

[14] J. T. Patterson, P. A. Head, D. L. McNeill, K Chung, and R. E. Coggeshall, "Ascending unmyelinated primary afferent fibers in the dorsal funiculus," *The Journal of comparative neurology*, vol. 290, pp. 384–390, 1989.

[15] J. T. Patterson, R. E. Coggeshall, W. T. Lee, and K Chung, "Long ascending unmyelinated primary afferent axons in the rat dorsal column: immunohistochemical localizations," *Neuroscience Letters*, vol. 108, pp. 6–10, 1990.

[16] W Willis and R. E. Coggeshall, "Sensory pathways in the dorsal funiculus," in *Sensory mechanisms of the spinal cord*, Vol 2., New York: Kluwer Academic/Plenum Publishers, 2004, pp. 597–664.

[17] L Bai, B. P. Lehnert, J Liu, N. L. Neubarth, T. L. Dickendesher, P. H. Nwe, C Cassidy, C. J. Woodbury, and D. D. Ginty, "Genetic identification of an expansive mechanoreceptor sensitive to skin stroking," *Cell*, vol. 163, pp. 1783–1795, 2015.

[18] H. K. P. Feirabend, H Choufoer, S Ploeger, J Holsheimer, and J. D. van Gool, "Morphometry of human superficial dorsal and dorsolateral column fibres: significance to spinal cord stimulation.," *Brain : a journal of neurology*, vol. 125, pp. 1137–1149, 2002.

[19] J. Niu, L. Ding, J. J. Li, H. Kim, J. Liu, H. Li, A. Moberly, T. C. Badea, I. D. Duncan, Y.-J. Son, S. S. Scherer, and W. Luo, "Modality-Based Organization of Ascending Somatosensory Axons in the Direct Dorsal Column Pathway," *Journal of Neuroscience*, vol. 33, no. 45, pp. 17 691–17 709, 2013.

[20] S. L. BeMent and J. B. Ranck, "A quantitative study of electrical stimulation of central myelinated fibers," *Experimental Neurology*, vol. 24, pp. 147–170, 1969.

[21] K. W. Horch, P. R. Burgess, and D. Whitehorn, "Ascending Collaterals of cutaneous neurons in the fasciculus gracilis of the cat," *Brain Research*, vol. 117, pp. 1–17, 1976.

[22] C. Peirs, S.-P. G. Williams, X. Zhao, C. E. Walsh, J. Y. Gedeon, N. E. Cagle, A. C. Goldring, H. Hioki, Z. Liu, P. S. Marell, and R. P. Seal, "Dorsal Horn Circuits for Persistent Mechanical Pain," *Neuron*, vol. 87, no. 4, pp. 797–812, 2015.

[23] R. Schmidt, *Encyclopedia of Pain*, G. F. Gebhart and R. F. Schmidt, Eds. Berlin, Heidelberg: Springer Berlin Heidelberg, 2013, pp. 3558–3561. arXiv: `arXiv:1011.1669v3`.

[24] R. B. North, D. H. Kidd, M Zahurak, C. S. James, and D. M. Long, "Spinal cord stimulation for chronic, intractable pain: experience over two decades.," *Neurosurgery*, vol. 32, no. 3, 384–94; discussion 394–5, 1993.

[25] Å. B. Vallbo, "Microneurography: how it started and how it works," *Journal of Neurophysiology*, vol. 120, no. 3, pp. 1415–1427, 2018.

[26] K. Orstavik and E. Jorum, "Microneurographic findings of relevance to pain in patients with erythromelalgia and patients with diabetic neuropathy," *Neuroscience Letters*, vol. 470, no. 3, pp. 180–184, 2010.

[27] J. L. Ochoa, M. Campero, J. Serra, and H. Bostock, "Hyperexcitable polymodal and insensitive nociceptors in painful human neuropathy," *Muscle and Nerve*, vol. 32, no. 4, pp. 459–472, 2005.

[28] M. A. Cline, J. L. Ochoa, and H. E. Torebjörk, "Chronic hyperalgesia and skin warming caused by sensitized c nociceptors," *Brain*, vol. 112, no. 3, pp. 621–647, 1989.

[29] C. Weidner, R. Schmidt, M. Schmelz, H. E. Torebjörk, and H. O. Handwerker, "Action potential conduction in the terminal arborisation of nociceptive C-fibre afferents," *Journal of Physiology*, vol. 547, no. 3, pp. 931–940, 2003.

[30] H. E. Torebjörk and R. G. Hallin, "Responses in human A and C fibres to repeated electrical intradermal stimulation," *Journal of Neurology Neurosurgery and Psychiatry*, vol. 37, no. 6, pp. 653–664, 1974.

[31] H. E. Torebjörk and R. G. Hallin, "Identification of afferent c units in intact human skin nerves," *Brain Research*, vol. 67, pp. 387–403, 1974.

[32] H. Bostock, M. Campero, J. Serra, and J. L. Ochoa, "Temperature-dependent double spikes in C-nociceptors of neuropathic pain patients," *Brain*, vol. 128, no. 9, pp. 2154–2163, 2005.

[33] R. Schmidt, I. P. Kleggetveit, B. Namer, T. Helås, O. Obreja, M. Schmelz, and E. Jørum, "Double spikes to single electrical stimulation correlates to spontaneous activity of nociceptors in painful neuropathy patients," *Pain*, vol. 153, no. 2, pp. 391–398, 2012.

[34] I. P. Kleggetveit, B. Namer, R. Schmidt, T. Helås, M. Rückel, K. Orstavik, M. Schmelz, and E. Jorum, "High spontaneous activity of C-nociceptors in painful polyneuropathy," *Pain*, vol. 153, no. 10, pp. 2040–2047, 2012.

[35] J. Serra, H. Bostock, R. Solà, J. Aleu, E. García, B. Cokic, X. Navarro, and C. Quiles, "Microneurographic identification of spontaneous activity in C-nociceptors in neuropathic pain states in humans and rats," *Pain*, vol. 153, no. 1, pp. 42–55, 2012.

[36] R. H. Gracely, S. A. Lynch, and G. J. Bennett, "Painful neuropathy: altered central processing maintained dynamically by peripheral input," *Pain*, vol. 51, no. 2, pp. 175–194, 1992.

[37] S. Haroutounian, L. Nikolajsen, T. F. Bendtsen, N. B. Finnerup, A. D. Kristensen, J. B. Hasselstrøm, and T. S. Jensen, "Primary afferent input critical for maintaining spontaneous pain in peripheral neuropathy," *Pain*, vol. 155, no. 7, pp. 1272–1279, 2014.

[38] L. M. Mendell and P. D. Wall, "Responses of single dorsal cord cells to peripheral cutaneous unmyelinated fibers," *Nature*, no. 4979, pp. 97–99, 1965.

[39] C. J. Woolf, "Evidence for a central component of post-injury pain hypersensitivity," *Nature*, vol. 306, no. December, 1983.

[40] A. Latremoliere and C. J. Woolf, "Central Sensitization: A Generator of Pain Hypersensitivity by Central Neural Plasticity," *The Journal of Pain*, vol. 10, no. 9, pp. 895–926, 2009.

[41] R. Baron, G. Hans, and A. H. Dickenson, "Peripheral input and its importance for central sensitization," *Annals of Neurology*, vol. 74, no. 5, pp. 630–636, 2013.

[42] A. M. Tan, Y. W. Chang, P. Zhao, B. C. Hains, and S. G. Waxman, "Rac1-regulated dendritic spine remodeling contributes to neuropathic pain after peripheral nerve injury," *Experimental Neurology*, vol. 232, no. 2, pp. 222–233, 2011.

[43] F. Y. Liu, X. X. Qu, J. Cai, F. T. Wang, G. G. Xing, and Y. Wan, "Electrophysiological properties of spinal wide dynamic range neurons in neuropathic pain rats following spinal nerve ligation," *Neuroscience Bulletin*, vol. 27, no. 1, pp. 1–8, 2011.

[44] Y. Ren, Y. Lu, L. Xiong, S. Zhou, Y. Gong, Y.-Y. Sun, H. Dong, N. Gu, R.-R. Ji, Y. Gao, and N. Xia, "A feed-forward spinal cord glycinergic neural circuit gates mechanical allodynia," *Journal of Clinical Investigation*, vol. 123, no. 9, pp. 4050–4062, 2013.

[45] M. L. Nichols, "Transmission of Chronic Nociception by Spinal Neurons Expressing the Substance P Receptor," *Science*, vol. 286, no. 5444, pp. 1558–1561, 1999.

[46] A. Dalal, M. Tata, G. Allègre, F. Gekiere, N. Bons, and D. Albe-Fessard, "Spontaneous activity of rat dorsal horn cells in spinal segments of sciatic projection following transection of sciatic nerve or of corresponding dorsal roots," *Neuroscience*, vol. 94, no. 1, pp. 217–228, 1999.

[47] R.-g. Xie, W.-g. Chu, S.-j. Hu, and C. Luo, "Characterization of Different Types of Excitability in Large Somatosensory Neurons and Its Plastic Changes in Pathological Pain States," *International Journal of Molecular Sciences*, vol. 19, no. 1, p. 161, 2018.

[48] S. S. Bedi, Q. Yang, R. J. Crook, J. Du, Z. Wu, H. M. Fishman, R. J. Grill, S. M. Carlton, and E. T. Walters, "Chronic Spontaneous Activity Generated in the Somata of Primary Nociceptors Is Associated with Pain-Related Behavior after Spinal Cord Injury," *Journal of Neuroscience*, vol. 30, no. 44, pp. 14 870–14 882, 2010.

[49] K. C. Kajander, S. Wakisaka, and G. J. Bennett, "Spontaneous discharge originates in the dorsal root ganglion at the onset of a painful peripheral neuropathy in the rat," *Neuroscience Letters*, vol. 138, no. 2, pp. 225–228, 1992.

[50] C.-n. Liu, P. D. Wall, E. Ben-dor, M. Michaelis, R. Amir, and M. Devor, "Tactile allodynia in the absence of C- ® ber activation : altered firing properties of DRG neurons following spinal nerve injury," *Pain*, vol. 85, pp. 503–521, 2000.

[51] X. Liu, S. Eschenfelder, K. H. Blenk, W. Jänig, and H. J. Häbler, "Spontaneous activity of axotomized afferent neurons after L5 spinal nerve injury in rats," *Pain*, vol. 84, no. 2-3, pp. 309–318, 2000.

[52] Y. Song, H.-m. Li, R.-g. Xie, Z.-f. Yue, X.-j. Song, S.-j. Hu, and J.-l. Xing, "Evoked bursting in injured A b dorsal root ganglion neurons : A mechanism underlying tactile allodynia," *Pain*, vol. 153, no. 3, pp. 657–665, 2012.

[53] S.-j. Hu and J.-l. Xing, "Dorsal root ganglion compression as an animal model of sciatica and low back pain An experimental model for chronic compression of dorsal root ganglion produced by intervertebral foramen stenosis in the rat," *Pain*, vol. 77, pp. 15–22, 1998.

[54] C. Ma, Y. Shu, Z. Zheng, Y. Chen, H. Yao, K. W. Greenquist, F. A. White, and R. H. LaMotte, "Similar Electrophysiological Changes in Axotomized and Neighboring Intact Dorsal Root Ganglion Neurons," *Journal of Neurophysiology*, vol. 89, no. 3, pp. 1588–1602, 2003.

[55] J. Serra, R. Sol, J. Aleu, C. Quiles, X. Navarro, and H. Bostock, "Double and triple spikes in C-nociceptors in neuropathic pain states: An additional peripheral mechanism of hyperalgesia," *Pain*, vol. 152, no. 2, pp. 343–353, 2011.

[56] J. Wang, M. Kawamata, and A. Namiki, "Changes in properties of spinal dorsal horn neurons and their sensitivity to morphine after spinal cord injury in the rat," *Anesthesiology*, vol. 102, no. 1, pp. 152–164, 2005.

[57] B. C. Hains, J. P. Klein, C. Y. Saab, M. J. Craner, J. a. Black, and S. G. Waxman, "Upregulation of sodium channel Nav1.3 and functional involvement in neuronal hyperexcitability associated with central neuropathic pain after spinal cord injury.," *The Journal of neuroscience : the official journal of the Society for Neuroscience*, vol. 23, no. 26, pp. 8881–8892, 2003.

[58] J. L. Watson, T. J. Hala, R. Putatunda, D. Sannie, and A. C. Lepore, "Persistent at-level thermal hyperalgesia and tactile allodynia accompany chronic neuronal and astrocyte activation in superficial dorsal horn following mouse cervical contusion spinal cord injury," *PLoS ONE*, vol. 9, no. 9, 2014.

[59] D. M. Ritter, B. M. Zemel, T. J. Hala, M. E. O'Leary, A. C. Lepore, and M. Covarrubias, "Dysregulation of kv3.4 channels in dorsal root Ganglia following spinal cord injury.," *The Journal of neuroscience : the official journal of the Society for Neuroscience*, vol. 35, no. 3, pp. 1260–73, 2015.

[60] Q Yang, Z Wu, J. K. Hadden, M. A. Odem, Y Zuo, R. J. Crook, J. A. Frost, and E. T. Walters, "Persistent pain after spinal cord injury is maintained by primary afferent activity," *J Neurosci*, vol. 34, no. 32, pp. 10 765–10 769, 2014.

[61] S. J. West, K. Bannister, A. H. Dickenson, and D. L. Bennett, "Circuitry and plasticity of the dorsal horn - Toward a better understanding of neuropathic pain," *Neuroscience*, vol. 300, pp. 254–275, 2015.

[62] T. Cameron, "Safety and efficacy of spinal cord stimulation for the treatment of chronic pain: a 20-year literature review," *Journal of Neurosurgery*, vol. 100, no. Spine 3, pp. 254–267, 2004.

[63] K Kumar, G Hunter, and D Demeria, "Spinal cord stimulation in treatment ofchronic benign pain: challenges in treatment planning and present status, a 22-year experience," *Neurosurgery*, vol. 58, no. 3, pp. 481–496, 2006.

[64] M. A. Moffitt, D. C. Lee, and K. Bradley, *Spinal Cord Stimulation: Engineering Approaches to Clinical and Physiological Challenges*. 2009, pp. 155–194.

[65] J. L. Parker, D. M. Karantonis, P. S. Single, M. Obradovic, and M. J. Cousins, "Compound action potentials recorded in the human spinal cord during neurostimulation for pain relief," *Pain*, vol. 153, no. 3, pp. 593–601, 2012.

[66] C Burton, "Dorsal column stimulation: optimization of application," *Surgical Neurology*, vol. 4, no. 1, pp. 171–179, 1975.

[67] R. B. North and G. L. Roark, "Spinal cord stimulation for chronic pain," *Neurosurgery Clinics of North America*, vol. 6, pp. 145–155, 1995.

[68] G Barolat, F Massaro, J He, S Zeme, and B Ketcik, "Mapping of sensory responses to epidural stimulation of the intraspinal neural structures in man," *Journal of Neurosurgery*, vol. 78, pp. 233–239, 1993.

[69] J Holsheimer, "Computational modelling of spinal cord stimulation and its contribution to therapeutic efficacy," *Spinal Cord*, vol. 36, pp. 531–540, 1998.

[70] Y Hosobuchi, J. E. Adams, and P. R. Weinstein, "Preliminary percutaneous dorsal column stimulation prior to permanent implantation," *Journal of Neurosurgery*, vol. 37, no. 2, pp. 242–245, 1972.

[71] D. De Ridder, S. Vanneste, M. Plazier, E. Van Der Loo, and T. Menovsky, "Burst spinal cord stimulation: Toward paresthesia-free pain suppression," *Neurosurgery*, vol. 66, no. 5, pp. 986–990, 2010.

[72] S. Muhammad, S. Roeske, S. R. Chaudhry, and T. M. Kinfe, "Burst or High-Frequency (10 kHz) Spinal Cord Stimulation in Failed Back Surgery Syndrome Patients With Predominant Back Pain: One Year Comparative Data," *Neuromodulation: Technology at the Neural Interface*, vol. 20, no. 7, pp. 661–667, 2017.

[73] L. Kapural, C. Yu, M. W. Doust, B. E. Gliner, D. M. Morgan, L. L. Brown, T. L. Yearwood, R. Bundschu, A. W. Burton, T. Yang, R. Benyamin, and A. H. Burgher, "Novel HF10 Therapy is Superior to Traditional Low-Frequency SCS," *Anesthesiology*, vol. 123, no. 4, pp. 851–860, 2015.

[74] D Abejon, E Reg, C. D. Pozo, R Contreras, and J Insausti, "Dual spinal cord stimulation for complex pain: preliminary study," *Neuromodulation*, vol. 8, pp. 105–111, 2005.

[75] K. M. Alo, V Redko, and J Charnov, "Four year follow-up of dual electrode spinal cord stimulation for chronic pain," *Neuromodulation*, vol. 5, pp. 79–88, 2002.

[76] J.-P. V. Butyen, "The performance and safety of an implantable spinal cord stimulation system in patients with chronic pain: a 5-year study," *Neuromodulation*, vol. 6, pp. 79–87, 2003.

[77] R. S. Taylor, M. J. Desai, P. Rigoard, and R. J. Taylor, "Predictors of pain relief following spinal cord stimulation in chronic back and leg pain and failed back surgery syndrome: a systematic review and meta-regression analysis.," *Pain practice : the official journal of World Institute of Pain*, vol. 14, no. 6, pp. 489–505, 2014.

[78] J. D. Cole, L. S. Lilis, and E. M. Sedgwick, "Intractable central pain in spinal cord injury is not relieved by spinal cord stimulation," *Paraplegia*, vol. 29, no. 3, pp. 167–172, 1991.

[79] B. Cioni, M. Meglio, L. Pentimalli, and M. Visocchi, "Spinal cord stimulation in the treatment of paraplegic pain," *Journal of Neurosurgery*, vol. 82, pp. 35–39, 1995.

[80] R Melzack and P. D. Wall, "Pain mechanisms: a new theory," *Science*, vol. 150, pp. 971–979, 1965.

[81] B. S. Nashold, G Somjen, and H Friedman, "Paresthesias and EEG potentials evoked by stimulation of dorsal funiculi in man," *Experimental Neurology*, vol. 36, pp. 273–287, 1972.

[82] U Lindblom and B. A. Meyerson, "Influence on touch, vibration, and cutaneous pain of dorsal column stimulation in man," *Pain*, vol. 1, pp. 257–270, 1975.

[83] C. N. Shealy, N Taslitz, J. T. Mortimer, and D. P. Becker, "Electrical inhibition of pain: Experimental evaluation," *Anesthesia and Analgesia*, vol. 46, pp. 299–305, 1967.

[84] B. Howell, S. P. Lad, W. M. Grill, and J. C. Glorioso, "Evaluation of intradural stimulation efficiency and selectivity in a computational model of spinal cord stimulation," *PLoS ONE*, vol. 9, no. 12, pp. 1–26, 2014.

[85] B. Coburn, "A Theoretical Study of Epidural Electrical Stimulation of the Spinal Cord-Part II: Effects on Long Myelinated Fibers," *IEEE Transactions on Biomedical Engineering*, vol. BME-32, no. 11, pp. 978–986, 1985.

[86] B. Coburn and W. K. Sin, "A Theoretical Study of Epidural Electrical Stimulation of the Spinal CordPart I: Finite Element Analysis of Stimulus Fields," *IEEE Transactions on Biomedical Engineering*, vol. BME-32, no. 11, pp. 971–977, 1985.

[87] J. Holsheimer, "Which neuronal elements are activated directly by spinal cord stimulation," *Neuromodulation*, vol. 5, no. 1, pp. 25–31, 2002.

[88] J. J. Struijk, J. Holsheimer, G. G. van der Heide, and H. B. K. Boom, "Recruitment of Dorsal Column Fibers in Spinal Cord Stimulation: Influence of Collateral Branching," *IEEE Transactions on Biomedical Engineering*, vol. 39, no. 9, pp. 903–912, 1992.

[89] J. J. Struijk, J. Holsheimer, and H. B. K. Boom, "Excitation of Dorsal Root Fibers in Spinal Cord Stimulation: A Theoretical Study," *IEEE Transactions on Biomedical Engineering*, vol. 40, no. 7, pp. 632–639, 1993.

[90] J. E. Arle, L. Mei, K. W. Carlson, and J. L. Shils, "High-Frequency Stimulation of Dorsal Column Axons: Potential Underlying Mechanism of Paresthesia-Free Neuropathic Pain Relief," *Neuromodulation: Technology at the Neural Interface*, vol. 19, no. 4, pp. 385–397, 2016.

[91] S. F. Lempka, C. C. McIntyre, K. L. Kilgore, and A. G. Machado, "Computational Analysis of Kilohertz Frequency Spinal Cord Stimulation for Chronic Pain Management," *Anesthesiology*, vol. 122, no. 6, pp. 1362–76, 2015.

[92] J. E. Arle, K. W. Carlson, L. Mei, N. Iftimia, and J. L. Shils, "Mechanism of dorsal column stimulation to treat neuropathic but not nociceptive pain: Analysis with a computational model," *Neuromodulation*, vol. 17, no. 7, 2014.

[93] T. C. Zhang, J. J. Janik, and W. M. Grill, "Modeling effects of spinal cord stimulation on wide-dynamic range dorsal horn neurons: influence of stimulation frequency and GABAergic inhibition.," *Journal of Neurophysiology*, vol. 112, no. 3, pp. 552–567, 2014.

[94] D. Lee, B. Hershey, K. Bradley, and T. Yearwood, "Predicted effects of pulse width programming in spinal cord stimulation: a mathematical modeling study.," *Med. Biol. Eng. Comput.*, vol. 49, no. 7, pp. 765–74, 2011.

[95] F. Yang, A. F. Carteret, P. W. Wacnik, C. Y. Chung, L. Xing, X. Dong, R. A. Meyer, S. N. Raja, and Y. Guan, "Bipolar spinal cord stimulation attenuates mechanical hypersensitivity at an intensity that activates a small portion of A-fiber afferents in spinal nerve-injured rats," *Neuroscience*, vol. 199, pp. 470–480, 2011.

[96] K. L. Sato, L. M. Johane, L. S. Sanada, and K. A. Sluka, "Spinal cord stimulation reduces mechanical hyperalgesia and glial cell activation in animals with neuropathic pain," *Anesthesia and Analgesia*, vol. 118, no. 2, pp. 464–472, 2014. arXiv: NIHMS150003.

[97] Z. Song, O. B. Ansah, B. A. Meyerson, A. Pertovaara, and B. Linderoth, "The rostroventromedial medulla is engaged in the effects of spinal cord stimulation in a rodent model of neuropathic pain," *Neuroscience*, vol. 247, pp. 134–144, 2013.

[98] Z. Song, O. B. Ansah, B. A. Meyerson, A. Pertovaara, and B. Linderoth, "Exploration of supraspinal mechanisms in effects of spinal cord stimulation: Role of the locus coeruleus," *Neuroscience*, vol. 253, pp. 426–434, 2013.

[99] J. Barchini, S. Tchachaghian, F. Shamaa, S. J. Jabbur, B. A. Meyerson, Z. Song, B. Linderoth, and N. E. Saadé, "Spinal segmental and supraspinal mechanisms underlying the pain-relieving effects of spinal cord stimulation: An experimental study in a rat model of neuropathy," *Neuroscience*, vol. 215, pp. 196–208, 2012.

[100] Z. Song, C. Ultenius, B. A. Meyerson, and B. Linderoth, "Pain relief by spinal cord stimulation involves serotonergic mechanisms: An experimental study in a rat model of mononeuropathy," *Pain*, vol. 147, no. 1-3, pp. 241–248, 2009.

[101] Z. Song, B. A. Meyerson, and B. Linderoth, "Spinal 5-HT receptors that contribute to the pain-relieving effects of spinal cord stimulation in a rat model of neuropathy," *Pain*, vol. 152, no. 7, pp. 1666–1673, 2011.

[102] R. Shechter, F. Yang, Q. Xu, Y.-K. Cheong, S.-Q. He, A. Sdrulla, A. F. Carteret, P. W. Wacnik, X. Dong, R. A. Meyer, S. N. Raja, and Y. Guan, "Conventional and Kilohertz-frequency Spinal Cord Stimulation Produces Intensity- and Frequency-dependent Inhibition of Mechanical Hypersensitivity in a Rat Model of Neuropathic Pain," *Anesthesiology*, vol. 119, no. 2, pp. 422–432, 2013.

[103] Z. Song, H. Viisanen, B. A. Meyerson, A. Pertovaara, and B. Linderoth, "Efficacy of Kilohertz-Frequency and Conventional Spinal Cord Stimulation in Rat Models of Different Pain Conditions," *Neuromodulation: Technology at the Neural Interface*, vol. 17, no. 3, pp. 226–235, 2014.

[104] K. P. Meuwissen, J. W. Gu, T. C. Zhang, and E. A. Joosten, "Conventional-SCS vs. Burst-SCS and the Behavioral Effect on Mechanical Hypersensitivity in a Rat Model of Chronic Neuropathic Pain: Effect of Amplitude," *Neuromodulation*, vol. 21, no. 1, pp. 19–30, 2018.

[105] N. E. Saadé, J Barchini, S Tchachaghian, F Chamaa, S. J. Jabbur, Z Song, B. A. Meyerson, and B Linderoth, "The role of the dorsolateral funiculi in the pain relieving effect of spinal cord stimulation: a study in a rat model of neuropathic pain," *Experimental Brain Research*, vol. 233, no. 4, pp. 1041–1052, 2015.

[106] N. D. Crosby, C. L. Weisshaar, J. R. Smith, M. E. Zeeman, M. D. Goodman-Keiser, and B. A. Winkelstein, "Burst and tonic spinal cord stimulation differentially activate gabaergic mechanisms to attenuate pain in a rat model of cervical radiculopathy," *IEEE Transactions on Biomedical Engineering*, vol. 62, no. 6, pp. 1604–1613, 2015.

[107] B. Yuan, D. Liu, and X. Liu, "Spinal cord stimulation exerts analgesia effects in chronic constriction injury rats via suppression of the TLR4/NF-κB pathway," *Neuroscience Letters*, vol. 581, pp. 63–68, 2014.

[108] C. El-Khoury, N. Hawwa, M. Baliki, S. F. Atweh, S. J. Jabbur, and N. E. Saadé, "Attenuation of neuropathic pain by segmental and supraspinal activation of the dorsal column system in awake rats," *Neuroscience*, vol. 112, no. 3, pp. 541–553, 2002.

[109] J. G. Cui, B. Linderoth, and B. A. Meyerson, "Effects of spinal cord stimulation on touch-evoked allodynia involve GABAergic mechanisms. An experimental study in the mononeuropathic rat," *Pain*, vol. 66, no. 2-3, pp. 287–295, 1996.

[110] V. Yakhnitsa, B. Linderoth, and B. A. Meyerson, "Spinal cord stimulation attenuates dorsal horn neuronal hyperexcitability in a rat model of mononeuropathy," *Pain*, vol. 79, no. 2-3, pp. 223–233, 1999.

[111] C.-O. Stiller, J.-G. Cui, W. T. O'Connor, E. Brodin, B. A. Meyerson, and B. Linderoth, "Release of [gamma]-Aminobutyric Acid in the Dorsal Horn and Suppression of Tactile Allodynia by Spinal Cord Stimulation in Mononeuropathic Rats," *Neurosurgery*, vol. 39, no. 2, pp. 367–375, 1996.

[112] H Baba, M Yoshimura, S Nishi, and K Shimoji, "Synaptic responses of substantia gelatinosa neurones to dorsal column stimulation in rat spinal cord in vitro.," *The Journal of physiology*, vol. 478, pp. 87–99, 1994.

[113] F. Yang, Q. Xu, Y. K. Cheong, R. Shechter, A. Sdrulla, S. Q. He, V. Tiwari, X. Dong, P. W. Wacnik, R. Meyer, S. N. Raja, and Y. Guan, "Comparison of intensity-dependent inhibition of spinal wide-dynamic range neurons by dorsal column and peripheral nerve stimulation in a rat model of neuropathic pain," *European Journal of Pain (United Kingdom)*, vol. 18, no. 7, pp. 978–988, 2014.

[114] T. C. Zhang, J. J. Janik, R. V. Peters, G. Chen, R.-R. R. Ji, and W. M. Grill, "Spinal Sensory Projection Neuron Responses to Spinal Cord Stimulation Are Mediated by Circuits Beyond Gate Control.," *Journal of Neurophysiology*, vol. 0281, no. 919, 2015.

[115] Z. Song, B. A. Meyerson, and B. Linderoth, "High-Frequency (1 kHz) Spinal Cord Stimulation-Is Pulse Shape Crucial for the Efficacy? A Pilot Study," *Neuromodulation: Technology at the Neural Interface*, vol. 18, no. 8, pp. 714–720, 2015.

[116] N. D. Crosby, J. J. Janik, and W. M. Grill, "Modulation of activity and conduction in single dorsal column axons by kilohertz-frequency spinal cord stimulation," *Journal of Neurophysiology*, vol. 117, no. 1, pp. 136–147, 2017.

[117] L. S. Lesperance, M. Lankarany, T. C. Zhang, R. Esteller, S. Ratté, and S. A. Prescott, "Artifactual hyperpolarization during extracellular electrical stimulation: Proposed mechanism of high-rate neuromodulation disproved," *Brain Stimulation*, vol. 11, no. 3, pp. 582–591, 2018.

[118] Z. Wu, L. Li, F. Xie, J. Du, Y. Zuo, J. A. Frost, S. M. Carlton, E. T. Walters, and Q. Yang, "Activation of KCNQ Channels Suppresses Spontaneous Activity in Dorsal Root Ganglion Neurons and Reduces Chronic Pain after Spinal Cord Injury," *Journal of Neurotrauma*, vol. 34, no. 6, pp. 1260–1270, 2017.

[119] J. H. Zheng, E. T. Walters, and X. J. Song, "Dissociation of dorsal root ganglion neurons induces hyperexcitability that is maintained by increased responsiveness to cAMP and cGMP," *Journal of Neurophysiology*, vol. 97, no. 1, pp. 15–25, 2007.

[120] L. Davoody, R. L. Quiton, J. M. Lucas, Y. Ji, A. Keller, and R. Masri, "Conditioned place preference reveals tonic pain in an animal model of central pain," *Journal of Pain*, vol. 12, no. 8, pp. 868–874, 2011.

[121] K. J. Sufka, "Conditioned place preference paradigm: a novel approach for analgesic drug assessment against chronic pain," *Pain*, vol. 58, pp. 355–366, 1994.

[122] C. J. Labuda and P. N. Fuchs, "A behavioral test paradigm to measure the aversive quality of inflammatory and neuropathic pain in rats," *Experimental Neurology*, vol. 163, no. 2, pp. 490–494, 2000.

[123] M. P. Jensen, A. T. Hirsh, I. R. Molton, and A. M. Bamer, "Sleep Problems in Individuals With Spinal Cord Injury: Frequency and Age Effects," *Rehabilitation Psychology*, vol. 54, pp. 323–331, 2010.

[124] R Castriotta, M Wilde, and S Sahay, "Sleep Disorders in Spinal Cord Injury," *Sleep and Neurorehabilitation*, vol. 7, 2012.

[125] S. L. Lavela, S. P. Burns, B Goldstein, S Miskevics, B Smith, and F. M. Weaver, "Dysfunctional sleep in persons with spinal cord injuries and disorders," *Spinal Cord*, vol. 50, pp. 682–685, 2012.

[126] O Altindag, H Karagullu, and A Gur, "Current Research Sleep Disturbances in Patients with Spinal Cord Injury," *Orthopedics & Muscular System: Current Research*, vol. 3, pp. 10–13, 2014.

[127] K. Z. Lee and H. C. Kuo, "Vagal Control of Breathing Pattern after Midcervical Contusion in Rats," *Journal of Neurotrauma*, vol. 34, pp. 734–745, 2017.

[128] D Komnenov, J. Z. Solarewicz, F Afzal, K. D. Nantwi, D. M. Kuhn, and J. H. Mateika, "Intermittent hypoxia promotes recovery of respiratory motor function

in spinal cord-injured mice depleted of serotonin in the central nervous system," *Journal of applied physiology*, pp. 545–557, 2018.

[129] K.-z. Lee, Y.-j. Huang, and I.-l. Tsai, "Respiratory motor outputs following unilateral midcervical spinal cord injury in the adult rat," *Journal of applied physiology*, pp. 395–405, 2018.

[130] H Kloefkorn, S Idlett, M Halder, B Goolsby, and S Hochman, "Spinal contusion injury induces long-lasting changes in home cage activity and respiration that correlate with spontaneous and evoked indices of neuropathic pain," *Experimental Biology Meeting*, vol. San Diego, 2018.

[131] B. J. Kerr and S David, "Pain behaviors after spinal cord contusion injury in two commonly used mouse strains," *Experimental Neurology*, vol. 206, no. 2, pp. 240–247, 2007.

[132] D Noble, M McKinnon, T Neblett, W Goolsby, and S Hochman, "Use of electric field sensors for recording respiration, heart rate, and stereotyped motor behaviors in the rodent home cage," *Journal of neuroscience methods*, vol. 277, pp. 88–100, 2017.

[133] D. J. Noble, K. K. Martin, S. Parvin, and S. M. Garraway, "Spontaneous and Stimulus-Evoked Respiratory Rate Elevation Corresponds to Development of Allodynia in Spinal Cord-Injured Rats," *Journal of Neurotrauma*, vol. 36, no. 12, pp. 1909–1922, 2019.

[134] H Kloefkorn, L Aiani, A Lakhani, S Nagesh, A Moss, W Goolsby, J Rehg, N Pedersen, and S Hochman, "Noninvasive Sleep Scoring in Mice using Electric Field Sensors.," *bioRxiv*, no. 794552, 2019.

[135] S. R. Chaplan, F. W. Bach, J. W. Pogrel, J. M. Chung, and T. L. Yaksh, "Quantitative assessment of tactile allodynia in the rat paw," *Journal of Neuroscience Methods*, vol. 53, pp. 55–63, 1994.

[136] E. T. Walters, "Nociceptors as chronic drivers of pain and hyperreflexia after spinal cord injury: an adaptive-maladaptive hyperfunctional state hypothesis," *Front Physiol*, vol. 3, p. 309, 2012.

[137] Q Yang, Z Wu, J Du, R Crook, S Carlton, and E Walters, "Opening of KCNQ/Kv7 channels blocks both spontaneous activity in small DRG neurons and signs of chronic pain after spinal cord injury," *Journal of Pain*, vol. 14, S54, 2013.

[138] G. Corder, B. Ahanonu, B. F. Grewe, D. Wang, M. J. Schnitzer, and G. Scherrer, "An amygdalar neural ensemble that encodes the unpleasantness of pain," *Science*, vol. 363, no. 6424, pp. 276–281, 2019.

[139] L. S. Duraku, M. Hossaini, S. Hoendervangers, L. L. Falke, S. Kambiz, V. C. Mudera, J. C. Holstege, E. T. Walbeehm, and T. J. Ruigrok, "Spatiotemporal dynamics of re-innervation and hyperinnervation patterns by uninjured CGRP fibers in the rat foot sole epidermis after nerve injury," *Molecular Pain*, vol. 8, pp. 1–13, 2012.

[140] B. Pan, H. Yu, G. J. Fischer, J. M. Kramer, and Q. H. Hogan, "Dorsal Root Ganglionic Field Stimulation Relieves Spontaneous and Induced Neuropathic Pain in Rats," *The Journal of Pain*, vol. 17, no. 12, pp. 1349–1358, 2016.

[141] J. Deuis, L. Dvorakova, and I Vetter, "Methods used to evaluate pain behaviors in rodents," *Frontiers in Molecular Neuroscience*, vol. 10, no. September, pp. 1–17, 2017.

[142] M. Piel, J. Kroin, A. Van Wijnen, R Kc, and H. Im, "Pain assessment in animal models of osteoarthritis," *Gene*, vol. 537, no. 2, pp. 184–188, 2014.

[143] D. Cho, J. Cheong, M. Yang, S. Hwang, J. Kim, and C. Kim, "The effect of minocycline on motor neuron recovery and neuropathic pain in a rat model of spinal cord injury," *J Korean Neurosurgery Society*, vol. 49, no. 2, pp. 83–91, 2011.

[144] K. a. Dunham, A Siriphorn, S Chompoopong, and C. Floyd, "Characterization of a graded cervical hemicontusion spinal cord injury model in adult male rats.," *J Neurotrauma*, vol. 27, no. November, pp. 2091–2106, 2010.

[145] C Pitzer, C La Porta, R. Treede, and A Tappe-Theodor, "Inflammatory and neuropathic pain conditions do not primarily evoke anxiety-like behaviours in C57BL/6 mice," *European Journal of Pain*, vol. 23, no. 2, pp. 285–306, 2019.

[146] A Tappe-theodor and R Kuner, "Studying ongoing and spontaneous pain in rodents challenges and opportunities," *European Journal of Neuroscience*, vol. 39, no. April, pp. 1881–1890, 2014.

[147] A Tappe-Theodor, T King, and M. Morgan, "Pros and Cons of Clinically Relevant Methods to Assess Pain in Rodents," *Neuroscience and Biobehavioral Reviews*, vol. 100, no. February, pp. 335–343, 2019.

[148] M Barrot, "Tests and models of nociception and pain in rodents," *Journal of Neuroscience*, vol. 211, pp. 39–50, 2012.

[149] P. Reeh, J Bayer, L Kocher, and H. Handwerker, "Sensitization of nociceptive cutaneous nerve fibers from the rat's tail by noxious mechanical stimulation," *Experimental Brain Research*, vol. 65, no. 3, pp. 505–512, 1987.

[150] M Michaelis, C Vogel, K. Blenk, A Arnarson, and W Jänig, "Inflammatory mediators sensitize acutely axotomized nerve fibers to mechanical stimulation in the rat," *Journal of Neuroscience*, vol. 18, no. 18, pp. 7581–7587, 1998.

[151] D. Vrinten and F. Hamers, "CatWalk automated quantitative gait analysis as a novel method to assess mechanical allodynia in the rat; a comparison with von Frey testing," *Pain*, vol. 102, no. 12, pp. 203–209, 2003.

[152] N Andrews, E Legg, D Lisak, and E. Al., "Spontaneous burrowing behaviour in the rat is reduced by peripheral nerve injury or inflammation associated pain," *European Journal of Pain*, vol. 16, no. 4, pp. 485–495, 2012.

[153] C Pitzer, R Kuner, and A Tappe-Theodor, "Voluntary and evoked behavioral correlates in neuropathic pain states under different social housing conditions," *Molecular Pain*, vol. 12, pp. 1–15, 2016.

[154] B. D. Dalm, C. G. Reddy, M. A. Howard, S Kang, and T. J. Brennan, "Conditioned place preference and spontaneous dorsal horn neuron activity in chronic constriction injury model in rats," *Pain*, vol. 156, no. 12, pp. 2562–2571, 2015.

[155] D. D. Fuller, K. Z. Lee, and N. J. Tester, "The impact of spinal cord injury on breathing during sleep," *Respiratory physiology & neurobiology*, vol. 188, pp. 344–354, 2013.

[156] C Norrbrink Budh, C Hultling, and T Lundeberg, "Quality of sleep in individuals with spinal cord injury: a comparison between patients with and without pain," *Spinal cord*, vol. 43, no. 85-95, 2005.

[157] A Sankari, A Bascom, S Oomman, and M. S. Badr, "Sleep Disordered Breathing in Chronic Spinal Cord Injury," *Journal of Clinical Sleep Medicine*, vol. 10, 2014.

[158] F Scheer, J Zeitzer, N Ayas, R Brown, C Czeisler, and S Shea, "Reduced sleep efficiency in cervical spinal cord injury ; association with abolished night time melatonin secretion," *Spinal Cord*, vol. 44, pp. 78–81, 2006.

[159] A. M. Esteves, M. T. Mello, C. F. Squarcini, C. L. Lancellotti, A Comparoni, and S Tufik, "Sleep patterns over 15-day period in rats with spinal cord injury," *Spinal Cord*, vol. 45, pp. 360–366, 2007.

[160] P Franken, A Malafosse, and M Tafti, "Genetic Determinants of Sleep Regulation in Inbred Mice," *Sleep*, vol. 22, no. 2, pp. 155–169, 1999.

[161] V Swarnkar, U. Abeyratne, C Hukins, and B Duce, "A state transition-based method for quantifying EEG sleep fragmentation," *Med. Biol. Eng. Comput.*, vol. 47, no. 10, pp. 1053–1061, 2009.

[162] C Nepomuceno, P. R. Fine, J. S. Richards, H Gowens, S. L. Stover, U Rantanuabol, and R Houston, "Pain in patients with spinal cord injury," *Arch Phys Med Rehabil*, vol. 60, pp. 605–609, 1979.

[163] P. J. Siddall and J. D. Loeser, "Pain following spinal cord injury," *Spinal Cord*, vol. 39, pp. 63–73, 2001.

[164] K. D. Anderson, "Targeting recovery: priorities of the spinal cord-injured population," *Journal of Neurotrauma*, vol. 21, pp. 1371–1383, 2004.

[165] M. M. Backonja and J Serra, "Pharmacologic management part 1: better-studied neuropathic pain diseases," *Pain Med*, vol. 1, no. S28-S47, 2004.

[166] M. M. Backonja and J Serra, "Pharmacologic management part 2: lesser-studied neuropathic pain diseases," *Pain Med*, vol. 1, S48–S59, 2004.

[167] E. R. Felix, Y Cruz-Almeida, and E. G. Widerstrom-Noga, "Chronic pain after spinal cord injury: what characteristics make some pains more disturbing than others," *J Rehabil Res Dev*, vol. 44, pp. 703–715, 2007.

[168] R. P. Yezierski, "Spinal Cord Injury Pain: Spinal and Supraspinal Mechanisms," *The Journal of Rehabilitation Research and Development*, vol. 46, no. 1, p. 95, 2009.

[169] N. A. Silva, N Sousa, R. L. Reis, and A. J. Salgado, "From basics to clinical: a comprehensive review on spinal cord injury," *Progress in Neurobiology*, vol. 114, pp. 25–57, 2014.

[170] Z. Z. Wu, Q Yang, R. J. Crook, R. G. O'Neil, and E. T. Walters, "TRPV1 channels make major contributions to behavioral hypersensitivity and spontaneous activity in nociceptors after spinal cord injury," *Pain*, vol. 154, pp. 2130–2141, 2013.

[171] R Urban, G Scherrer, E. H. Goulding, L. H. Tecott, and A. I. Basbaum, "Behavioral indices of ongoing pain are largely unchanged in male mice with tissue or nerve injury-induced mechanical hypersensitivity," *Pain*, vol. 152, pp. 990–1000, 2011.

[172] G Kelly, C Blake, C Power, D O'Keeffe, and B. M. Fullen, "The Association Between Chronic Low Back Pain and Sleep A Systematic Review," *Clinical Journal of Pain*, vol. 27, pp. 169–181, 2011.

[173] P Finan and M Smith, "The Association of Sleep and Pain: An Update and a Path Forward.," *The Journal of Pain*, vol. 14, pp. 1539–1552, 2013.

[174] P. A. Boakye, C Olechowski, S Rashiq, M. J. Verrier, B Kerr, M Witmans, G Baker, A Joyce, and B. D. Dick, "A Critical Review of Neurobiological Factors Involved

in the Interactions Between Chronic Pain, Depression, and Sleep Disruption," *The Clinical Journal of Pain*, vol. 32, pp. 327–336, 2016.

[175] R Wodarski, S Schuh-Hofer, D. A. Yurek, K. A. Wafford, G Gilmour, R. D. Treede, and J. D. Kennedy, "Development and pharmacological characterization of a model of sleep disruption-induced hypersensitivity in the rat," *European Journal of Pain*, vol. 19, pp. 554–566, 2015.

[176] H Wei, W Zhao, Y.-x. Wang, and A Pertovaara, "Pain-related behavior following REM sleep deprivation in the rat : Influence of peripheral nerve injury , spinal glutamatergic receptors and nitric oxide," *Brain Research*, vol. 8, pp. 105–112, 2007.

[177] E. E. Benarroch, "The central autonomic network- functional organization, dysfunction and perspective," *Mayo Clin Proc*, vol. 68, no. 10, pp. 988–1001, 1993.

[178] P. D. Wall, M. Lidierth, and P. Hillman, "Brief and prolonged effects of Lissauer tract stimulation on dorsal horn cells," *Pain*, vol. 83, no. 3, pp. 579–589, 1999.

[179] J. A. Turner, J. D. Loeser, R. A. Deyo, and S. B. Sanders, "Spinal cord stimulation for patients with failed back surgery syndrome or complex regional pain syndrome: a systematic review of effectiveness and complications," *Pain*, vol. 108, pp. 137–147, 2004.

[180] L. M. Mendell, "Constructing and deconstructing the gate theory of pain.," *Pain*, vol. 155, pp. 210–216, 2014.

[181] Y Guan, P. W. Wacnik, F Yang, A. F. Carteret, C. Y. Chung, R. A. Meyer, S. N. Raja, and SN., "Spinal cord stimulation-induced analgesia: electrical stimulation of dorsal column and dorsal roots attenuates dorsal horn neuronal excitability in neuropathic rats," *Anesthesiology*, vol. 113, pp. 1392–1405, 2010.

[182] S Idlett, M Halder, M Sawchuk, J Quevedo, W Gu, M Moffitt, and S Hochman, "Relating dorsal column stimulation to the recruitment and modulation of sensory signaling in the isolated in vitro adult mouse spinal cord," *Society for Neuroscience*, vol. San Diego, 2016.

[183] S Idlett, M Sawchuk, T Zhang, N Brill, W Gu, and S Hochman, "Computational model-driven stimulation parameters for clinically-analogous SCS in mouse: are postsynaptic dorsal column tract cells recruited first?" *Internation Neuromodulation Society 13th World Congress*, vol. Edinburgh, 2017.

[184] S Idlett, M Halder, T Zhang, J. Quevedo, N Brill, W Gu, M Moffitt, and S Hochman, "Assessment of axonal recruitment using model-guided preclinical spinal cord stimulation in the ex vivo adult mouse spinal cord," *Journal of Neurophysiology*, 2019.

[185] C. Watson, G. Paxinos, G. Kayalioglu, and C. Heise, *Atlas of the Rat Spinal Cord*. Elsevier Ltd, pp. 238–306.

[186] V Sankarasubramanian, J. R. Buitenweg, J Holsheimer, and P Veltink, "Electrode alignment of transverse tripoles using a percutaneous triple-lead approach in spinal cord stimulation," *J Neural Eng*, vol. 8, 2011.

[187] N. A. Pelot, B. J. Thio, and W. M. Grill, "Modeling current sources for neural stimulation in COMSOL," *Front Comput Neurosci*, vol. 12, p. 40, 2018.

[188] C. A. Bossetti, M. J. Birdno, and W. M. Grill, "Analysis of the quasi-static approximation for calculating potentials generated by neural stimulation," *J Neural Eng*, vol. 5, pp. 44–53, 2007.

[189] I Hammar, P Krutki, H Drzymala-Celichowska, E Nilsson, and E Jankowska, "A trans-spinal loop between neurones in the reticular formation and in the cerebellum," *Journal of Physiology*, vol. 589, pp. 653–665, 2011.

[190] C. C. McIntyre and W. M. Grill, "Excitation of central nervous system neurons by nonuniform electric fields," *Biophys J*, vol. 76, pp. 878–888, 1999.

[191] J. B. Ranck, "Which elements are excited in electrical stimulation of mammalian central nervous system: a review," *Brain research*, vol. 98, pp. 417–440, 1975.

[192] F Rattay, "Analysis of the electrical excitation of CNS neurons," *IEEE Transactions on Biomedical Engineering*, vol. 45, pp. 766–772, 1998.

[193] P. J. Waddell, S. N. Lawson, and P. W. McCarthy, "Conduction Velocity Changes Along the Processes of Rate Primary Sensory Neurons," *Neuroscience*, vol. 30, no. 3, pp. 577–584, 1989.

[194] S Canbay, B Gurer, M Bozkurt, A Comert, Y Izci, and M. K. Baskaya, "Anatomical relationship and positions of the lumbar and sacral segments of the spinal cord according to the vertebral bodies and the spinal roots," *Clin Anat*, vol. 27, pp. 227–233, 2014.

[195] S Mandadi, P Hong, M. A. Tran, J. M. Bráz, P Colarusso, A. I. Basbaum, and P. J. Whelan, "Identification of multisegmental nociceptive afferents that modulate locomotor circuits in the neonatal mouse spinal cord," *J Comp Neurol*, vol. 521, pp. 2870–2887, 2013.

[196] T. L. Yearwood, B Hershey, K Bradley, and D Lee, "Pulse width programming in spinal cord stimulation: a clinical study," *Pain Physician*, vol. 13, pp. 321–335, 2010.

[197] M. R. Dimitrijevic, J Faganel, P. C. Sharkey, and A. M. Sherwood, "Study of sensation and muscle twitch responses to spinal cord stimulation," *Int Rehabil Med*, vol. 2, pp. 76–81, 1980.

[198] J. B. Hursh, "Conduction velocity and diameter of nerve fibers," *Am J Physiol*, vol. 127, pp. 131–139, 1939.

[199] D. R. McNeal, "Analysis of a model for excitation of myelinated nerve," *IEEE Transactions on Biomedical Engineering*, vol. 23, pp. 329–337, 1976.

[200] C Hildebrand and S Skoglund, "Calibre spectra of some fibre tracts in the feline central nervous system during postnatal development," *Acta Physiol Scand Suppl*, vol. 364, pp. 5–41, 1971.

[201] Y. C. Hwang, E. J. Hinsman, and O. F. Roesel, "Caliber spectra of fibers in the fasciculus gracilis of the cat cervical spinal cord: a quantitative electron microscopic study," *J Comp Neurol*, vol. 162, pp. 195–203, 1975.

[202] A. R. Light and E. R. Perl, "Spinal termination of functionally identified primary afferent neurons with slowly conducting myelinated fibers," *Journal of Comparative Neurology*, vol. 186, no. 2, pp. 133–150, 1979.

[203] S McHanwell and T. J. Biscoe, "The localization of motoneurons supplying the hindlimb muscles of the mouse," *Philos Trans R Soc Lond B Biol Sci*, vol. 293, pp. 477–508, 1981.

[204] P Rudomin and R. F. Schmidt, "Presynaptic inhibition in the vertebrate spinal cord revisited," *Experimental Brain Research*, vol. 129, pp. 1–37, 1999.

[205] W. D. Willis, *Dorsal root potentials and dorsal root reflexes: A double-edged sword*, 1999.

[206] J. C. Eccles, W Kozak, and F Magni, "Dorsal root reflexes of muscle group I afferent fibres," *Journal of Physiology*, vol. 159, pp. 128–146, 1961.

[207] A. J. Fink, K. R. Croce, Z. J. Huang, L. F. Abbott, T. M. Jessell, and E Azim, "Presynaptic inhibition of spinal sensory feedback ensures smooth movement," *Nature*, vol. 509, pp. 43–48, 2014.

[208] R Witschi, P Punnakkal, J Paul, J. S. Walczak, F Cervero, J. M. Fritschy, R Kuner, R Keist, U Rudolph, and H. U. Zeilhofer, "Presynaptic alpha2-GABAA receptors in primary afferent depolarization and spinal pain control," *Journal of Neuroscience*, vol. 31, pp. 8134–8142, 2011.

[209] P Shortland and P. D. Wall, "Long-range afferents in the rat spinal cord. II. Arborizations that penetrate grey matter," *Philos Trans R Soc Lond B Biol Sci*, vol. 337, pp. 445–455, 1992.

[210] D Angaut-Petit, "The dorsal column system: II. Functional properties and bulbar relay of the postsynaptic fibres of the cat's fasciculus gracilis," *Experimental Brain Research*, vol. 22, pp. 471–493, 1975.

[211] A. G. Brown and R. E. Fyffe, "Form and function of dorsal horn neurones with axons ascending the dorsal columns in cat," *Journal of Physiology*, vol. 321, pp. 31–47, 1981.

[212] G. J. Giesler and K. D. Cliffer, "Postsynaptic dorsal column pathway of the rat. II. Evidence against an important role in nociception," *Brain research*, vol. 326, pp. 347–356, 1985.

[213] E Jankowska, J Rastad, and P Zarzecki, "Segmental and supraspinal input to cells of origin of non-primary fibres in the feline dorsal columns," *Journal of Physiology*, vol. 290, pp. 185–200, 1979.

[214] A. G. Brown, P. B. Brown, R. E. Fyffe, and L. M. Pubols, "Receptive field organization and response properties of spinal neurones with axons ascending the dorsal columns in the cat," *Journal of Physiology*, vol. 337, pp. 575–588, 1983.

[215] R. Noble and J. S. Riddell, "Descending influences on the cutaneous receptive fields on postsynaptic dorsal column neurons in the cat," *Journal of Physiology*, no. 408, pp. 167–183, 1989.

[216] K Kumar, R Nath, and G. M. Wyant, "Treatment of chronic pain by epidural spinal cord stimulation: a 10-year experience," *Journal of Neurosurgery*, vol. 75, pp. 402–407, 1991.

[217] J. F. Ditunno, J. W. Little, A Tessler, and A. S. Burns, "Spinal shock revisited: a four-phase model," *Spinal Cord*, vol. 42, pp. 383–395, 2004.

[218] A. François, S. A. Low, E. I. Sypek, A. J. Christensen, C. Sotoudeh, K. T. Beier, C. Ramakrishnan, K. D. Ritola, R. Sharif-Naeini, K. Deisseroth, S. L. Delp, R. C. Malenka, L. Luo, A. W. Hantman, and G. Scherrer, "A Brainstem-Spinal Cord Inhibitory Circuit for Mechanical Pain Modulation by GABA and Enkephalins," *Neuron*, vol. 93, no. 4, 822–839.e6, 2017.

[219] R. E. Study and M. G. Kral, "Spontaneous action potential activity in isolated dorsal root ganglion neurons from rats with a painful neuropathy," *Pain*, vol. 65, no. 2-3, pp. 235–242, 1996.

[220] C. N. Shealy, J. T. Mortimer, and J. B. Reswick, "Electrical inhibition of pain by stimulation of the dorsal columns: Preliminary clinical report," *Anesthesia and Analgesia*, vol. 46, pp. 489–491, 1967.

[221] B. Y. M. Yoshimura and T. Jessell, "Amino Acid-Mediated EPSPs at Primary Afferent Synapses with Substantia Gelatinosa Neurons in the Rat Spinal Cord," *Journal of Physiology*, vol. 430, pp. 315–335, 1990.

[222] H. J. Luhmann, V. I. Dzhala, and Y. Ben-Ari, "Generation and propagation of 4-AP-induced epileptiform activity in neonatal intact limbic structures in vitro," *European Journal of Neuroscience*, vol. 12, no. 8, pp. 2757–2768, 2000.

[223] R. Ruscheweyh and J. Sandkühler, "Epileptiform activity in rat spinal dorsal horn in vitro has common features with neuropathic pain," *Pain*, vol. 105, no. 1-2, pp. 327–338, 2003.

[224] B. M. Zemel, D. M. Ritter, M. Covarrubias, and T. Muqeem, "A-Type KV Channels in Dorsal Root Ganglion Neurons: Diversity, Function, and Dysfunction," *Frontiers in Molecular Neuroscience*, vol. 11, no. August, pp. 1–17, 2018.

[225] K. J. Smith, P. A. Felts, and G. R. John, "Effects of 4-aminopyridine on demyelinated axons, synapses and muscle tension," *Brain*, vol. 123, no. 1, pp. 171–184, 2000.

[226] M Dragunow and R Faull, "The use of c-fos as a metabolic marker in neuronal pathway tracing," *Journal of Neuroscience Methods*, vol. 29, no. 3, pp. 261–265, 1989.

[227] L. Zhang, E. Morgan, J. Bagust, and R. G. Williams, "C-Fos Expression in Isolated Rat Spinal Cord," *Journal of Neuroscience Methods*, vol. 79, no. 1, pp. 105–113, 1998.

[228] S. P. H. Alexander, W. A. Catterall, E. Kelly, N. Marrion, J. A. Peters, H. E. Benson, E. Faccenda, A. J. Pawson, J. L. Sharman, C. Southan, J. A. Davies, and CGTP Collaborators, "The concise guide to PHARMACOLOGY 2015/16 : Voltage-gated ion channels CatSper and Two-Pore channels," *British journal of pharmacology*, vol. 172, pp. 5904–5941, 2015.

[229] B. Rudy, A. Chow, D. Lau, Y. Amarillo, A. Ozaita, M. Saganich, H. Moreno, M. S. Nadal, R. Hernandez-Pineda, A. Hernandez-Cruz, A. Erisir, C. Leonard, and E. Vega-Saenz De Miera, "Contributions of Kv3 channels to neuronal excitability," *Annals of the New York Academy of Sciences*, vol. 868, pp. 304–343, 1999.

[230] W. Sun, D. Smith, S. Bryn, R. Borgens, and R. Shi, "N-(4-pyridyl) methyl carbamate inhibits fast potassium currents in guinea pig dorsal root ganglion cells," *Journal of the Neurological Sciences*, vol. 277, no. 1-2, pp. 114–118, 2009.

[231] G. Taccola and A. Nistri, "Characteristics of the electrical oscillations evoked by 4-aminopyridine on dorsal root fibers and their relation to fictive locomotor patterns in the rat spinal cord in vitro," *Neuroscience*, vol. 132, no. 4, pp. 1187–1197, 2005.

[232] C. M. Bowe, J. D. Kocsis, E. F. Targ, and S. G. Waxman, "Physiological effects of 4aminopyridine on demyelinated mammalian motor and sensory fibers," *Annals of Neurology*, vol. 22, no. 2, pp. 264–268, 1987.

[233] G. Lees, "The effects of anticonvulsants on 4-aminopyridine-induced bursting: In vitro studies on rat peripheral nerve and dorsal roots," *British Journal of Pharmacology*, vol. 117, no. 3, pp. 573–579, 1996.

[234] A. E. Watts and J. G. R. Jefferys, "Effects of carbamazepine and baclofen on 4-aminopyridine-induced epileptic activity in rat hippocampal slices," *British Journal of Pharmacology*, vol. 108, no. 3, pp. 819–823, 1993.

[235] C. W. Kay, D. Ursu, E. Sher, and A. E. King, "The role of Cx36 and Cx43 in 4-aminopyridine-induced rhythmic activity in the spinal nociceptive dorsal horn: an electrophysiological study invitro," *Physiological Reports*, vol. 4, no. 14, pp. 1–10, 2016.

[236] R. Dubuc and S. Rossignol, "The effects of 4-aminopyridine on the cat spinal cord: rhythmic antidromic discharges recorded from the dorsal roots," *Brain Research*, vol. 491, no. 2, pp. 335–348, 1989.

[237] C Kirchhoff, J. D. Leah, S Jung, and P. W. Reeh, "Excitation of cutaneous sensory nerve endings in the rat by 4-aminopyridine and tetraethylammonium," *Journal of Neurophysiology*, vol. 67, no. 1, pp. 125–131, 1992.

[238] M. Devor, "Potassium channels moderate ectopic excitability of nerve-end neuromas in rats," *Neuroscience Letters*, vol. 40, no. 2, pp. 181–186, 1983.

[239] M. Truin, P. Van Venrooij, V. Duysens, R. Deumens, M. Van Kleef, and E. A. Joosten, "Spinal cord stimulation in a mouse chronic neuropathic pain model," *Neuromodulation*, vol. 10, no. 4, pp. 358–362, 2007.

[240] H. Huang, M. S. Kuzirian, X. Cai, L. M. Snyder, J. Cohen, D. H. Kaplan, and S. E. Ross, "Generation of a NK1R-CreER knockin mouse strain to study cells involved in Neurokinin 1 Receptor signaling," *Genesis*, vol. 54, no. 11, pp. 593–601, 2016.

[241] R. Fernandez Rojas, X. Huang, and K. L. Ou, "A Machine Learning Approach for the Identification of a Biomarker of Human Pain using fNIRS," *Scientific Reports*, vol. 9, no. 1, pp. 1–12, 2019.

[242] M. A. Yücel, C. M. Aasted, M. P. Petkov, D. Borsook, D. A. Boas, and L. Becerra, "Specificity of Hemodynamic Brain Responses to Painful Stimuli: A functional near-infrared spectroscopy study," *Scientific Reports*, vol. 5, pp. 1–9, 2015.

[243] U. Lee, M. Kim, K. Lee, C. M. Kaplan, D. J. Clauw, S. Kim, G. A. Mashour, and R. E. Harris, "Functional Brain Network Mechanism of Hypersensitivity in Chronic Pain," *Scientific Reports*, vol. 8, no. 1, pp. 1–11, 2018.

[244] E. Gentile, A. Brunetti, K. Ricci, M. Delussi, V. Bevilacqua, and M. de Tommaso, "Mutual interaction between motor cortex activation and pain in fibromyalgia: EEG-fNIRS study," *PLoS ONE*, vol. 15, no. 1, pp. 1–24, 2020.